Physics of Complex Systems

—

Biophysics

Martin Lenz

September 16, 2021

Foreword

Living systems are messy: they are typically very complex machines fine tuned by evolution, with very little of the regularity or uniformity we are used to in statistical mechanics. Does that mean that the whole enterprise of biophysics is doomed? Is developing theories for living systems hopeless and should you stay away from it? This is probably true for some problems, but maybe not for all. Over the last decades, physics has been instrumental in making sense of many complexities in biological systems, just like it has in making sense of the movements of planets or emission spectra of atoms in the past. What is clear is that unlike these fields, biophysics does not have a consensus framework comparable to Newton's laws of Schrödinger's equations. This doesn't make it the prettiest field to learn, but perhaps it is the ideal situation to be doing research: who knows, *you* could be the originator of that new paradigm.

These considerations will have two consequences for this course: (1) while we will focus on some topics related to the soft matter physics and statistical mechanics of the inner components of the cell, you should be aware that this is far from an exhaustive representation of biophysics. (2) in addition to seven main lectures and three tutorials, this course will consist in what I have come to refer to as "modeling projects", which I think are closer to some aspects of the work of a researcher in biophysics. The idea is the following: you will work in groups of 3 to 5 students, and I will meet three times with each group throughout the semester to discuss your progress. Each group will be presented with a piece of experimental data. You will work in teams throughout the semester to make sense of it, extract a physical picture through mathematical or computational modeling. There will be no question, no "right answer"; only your own insights and imagination. At the end of the project each group will have to write a sort of mini research article formulating and advancing (not necessarily solving) a question thanks to the data, and on which you will be evaluated.

The following chapters are most conveniently read in the order proposed, and the tutorials studied at the location where they are introduced. Useful coursework material and a mandatory warm-up exercise are to be found on my teaching webpage.

Contents

Chapter 1

The facts of Life

This chapter is quite atypical compared to the rest of the course. It is not really about physics, but rather constitutes a crash course in cell and molecular biology that is meant to give you a bit of elementary context for our subsequent discussions, as well as for the modeling projects. The next lectures will be much less descriptive.

Here we start with an overview of the basic molecules constituting a cell (Sec. 1.1), namely DNA (and variants thereof), proteins, fats and sugars. We then explore their relationships: DNA acts as a blueprint for proteins (Sec. 1.2). These proteins arrange themselves into complex three-dimensional machines required to perform most of the cell's functions (Sec. 1.3). Some of these proteins in turn exert a feedback on DNA (Sec. 1.4), while others interact with fat and sugar molecules to organize the cell (Sec. 1.5). Finally we will deve deeper into that cell architecture and introduce arguably its main architect, the cytoskeleton (1.6). In an attempt to convey a big picture without overwhelming the neophyte with terminology and caveats, many aspects of this quick orientation tour are oversimplified; for more accuracy consult *e.g.*, Ref. [1]. This chapter borrows several visuals and ideas from Refs. [2, 3].

1.1 The molecules of Life

Life, to the difference of many instances of inanimate matter, largely relies on large macromolecules. The basic ingredients are only a handful of elements (mainly carbon, oxygen, hydrogen and nitrogen), which allows for a relatively easy interconversion between different types of maloecules while guaranteeing an enormous versatility through sheer combinatorics. There are four main types of molecules:

Two information-rich molecule types

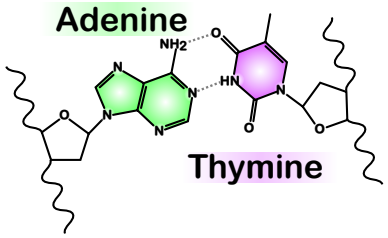

Nucleic acids (DNA and RNA) are made of 4 well-known nucleotides (A, T, G, C in the case of DNA) complementary in pairs. The illustration (adapted from Wikipedia) shows the geometry of the H-bonds that binds the A-T "base pair" as dashed lines. The squiggly lines materialize the sugar backbone that binds each nucleotide with the next one along the chain.

The complementary binding of two chains, or "strands" of DNA through these bonds results in the well-known double-stranded structure of DNA, which spontaneously twists itself into the even more famous double helix. The sequence of base pairs along a DNA molecule is meaningful and contains information which is translated into the structures of other molecules inside the cell, as we will see.

Proteins are sequences of amino acids, namely molecules with the structure illustrated here. Here R_1 and R_2 stand for one of 20 different chemical groups known as "residues" (illustrated in Fig. 1.1), implying that there are 20 possible different amino acids (in humans). Amino acids bind to each other through the formation of a "peptide bond", illustrated here, which removes one OH group plus one H atom from their structure to form a water molecule. This operation is repeated many times in a sequential manner, resulting in long, flexible chains known as "(poly)peptides" or "proteins" comprised of anywhere from a few tens to several hundreds of amino acids. Through its residue, each amino acid interacts physically and chemically with other amino acids as well as with the outside world. When combined in clever ways, these varied interactions allow proteins to act as molecular machines that do most of the interesting stuff that happens in the cell.

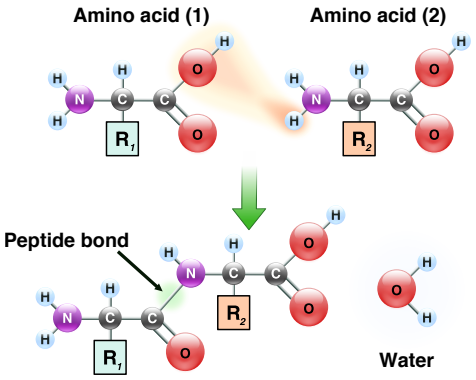

Two information-poor molecule types

Lipids are structurally similar to molecules of soap, with a water-loving polar head and a water-hating (oil-loving) tail section. In lipids, this hydrophobic section of the molecule is formed by two hydrocarbon chains. When put in water (most of the cell is made of water), these tails tuck away together and form two-dimensional membranes, as illustrated here. These membranes are very tough, as poking in a hole in them would imply exposing the hydrophobic tails to the water, which has a high (free-)energetic cost. Such membranes are thus used by the cells as versatile barriers. Most notably, all cells are enclosed by an outer membrane which makes sure that its components do not leak out.

Carbohydrates (sugars, starch and cellulose) are small molecules or polymers thereof, and are essentially made of atoms of C, H, O. They are much more simple and repetitive in structure than our information-rich molecules, and are typically used as an energy reserve or as structural elements.

Bottom line: a rough schematic of the cell

As a first approximation, you may think of a cell is a lipid envelope containing a collection of proteins and nucleic acids in a solution of water and salt, and surrounded by a protective scaffold of carbohydrates. Keep in mind however that this delimitation of roles is an extreme caricature which we will go back upon.

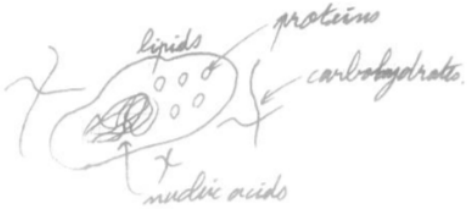

Ala, Val, Ile, Met, Leu, Phe, Trp, Cys, Tyr: hydrophobic
Gly, Asn, Ser, Thr, Glu, His, Pro, Arg, Gln, Asp, Lys: polar

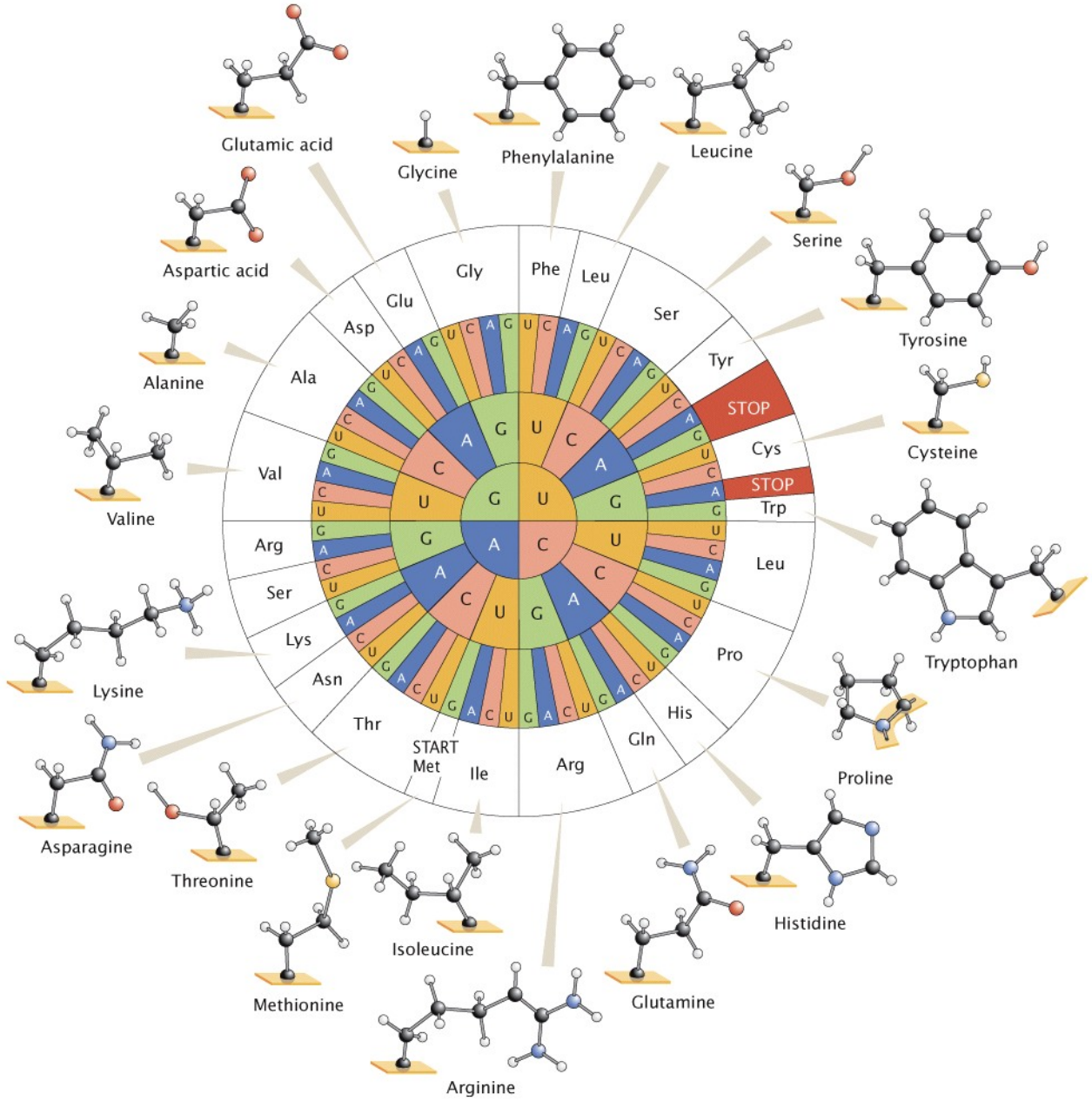

Figure 1.4 Physical Biology of the Cell, 2ed. (© Garland Science 2013)

Figure 1.1: The different residues and associated "codons", the three-base-pairs DNA sequences that code for each of them.

1.2 The central dogma of molecular biology

The central dogma of molecular biology is an explanation of the flow of genetic information within a biological system. It states that the genetic information is stored in nucleic acids, and is expressed physically and chemically as proteins according to the following process:

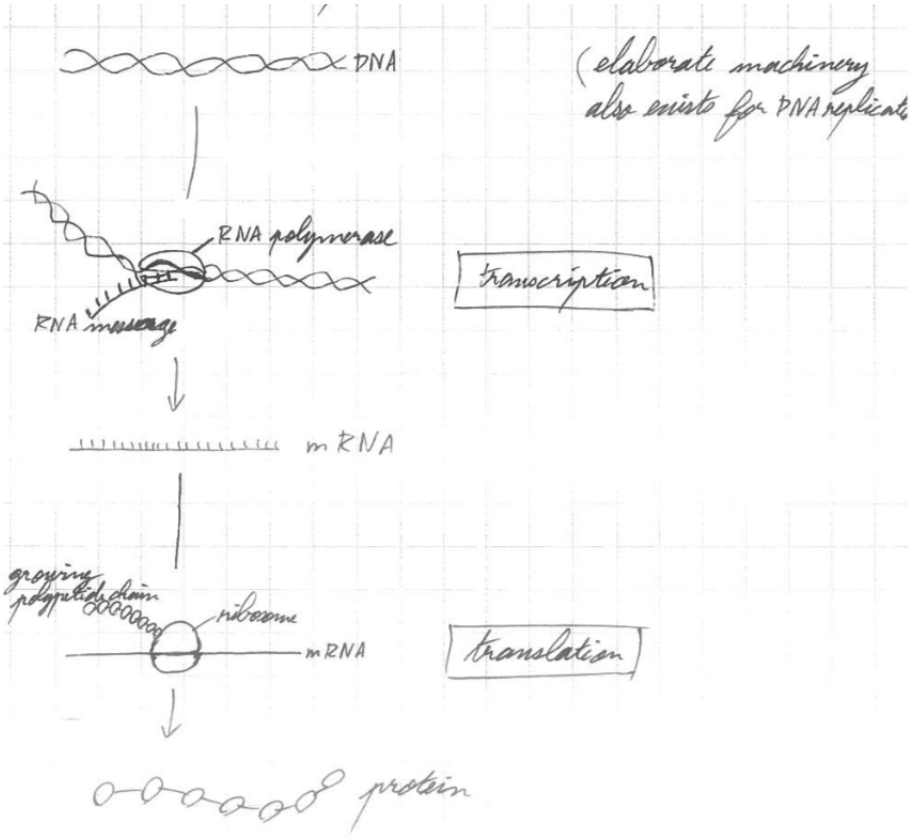

During this process, the sequence carried by the DNA molecule gets "transcribed" into a complementary messenger RNA (mRNA) sequence. RNA has a very similar structure to DNA, but remains single-stranded instead of forming helical double strands. Transcription is performed by a complicated protein machinery known as the RNA polymerase. In eukaryotes (*i.e.*, cells that have a nucleus; humans and yeast do but bacteria don't), this shorter mRNA molecule is exported out of the nucleus of the cell.

The mRNA is then captured by a ribosome – yet another complicated piece of protein-based machinery – which reads the sequence of RNA bases in groups of three known as "codons". If one were to think of the nucleic acid sequence as a language, the codons would be its words (Fig. 1.2). Remarkably, the ribosome "speaks" both this language and the language of proteins, and is able to translate the former into the latter according to the dictionary provided in Fig. 1.1. To read this dictionary, pick the first letter of your codon in the inner circle, then the second from the second circle and finally the third from the next. Accordingly, the codon UCA codes for Serine. Note the redundancy between certain codons, and the fact that in RNA the amino acid T (thymine) is replaced by U (uracil). Additionally, the codon AUG has a special role in addition to coding for methionine. It is indeed known as the "start codon", and represents the point at which the ribosome starts to read the mRNA molecule, codon by codon, recruiting the correct amino acids from the solution and binding them together into a protein by forming peptide bonds. This process continues until the ribosome reaches one of the stop codons (UAA, UAG or UGA), at which point the ribosome detaches and the protein is finished. The resulting sequence of amino acids is known as the protein's "primary structure".

To a first approximation, the DNA sequence subdivided into genes, each coding for one protein. When the cell decides it wants to produce the protein in question, the gene is transcribed into a single RNA molecule (or multiple copies thereof), each of which is translated into a single protein (or multiple copies thereof). As with most of the statements made in this chapter, things are more complicated in practice, even though we choose to keep things simple for now. For instance, 76% of human DNA is actually *not* a gene. These sections of our genome used to be called "junk DNA", a rather dismissive term that has gradually been replaced by the more circumspect "non-coding DNA" as we discover that even DNA that is not part of a gene can still perform useful, if still somewhat mysterious, functions.

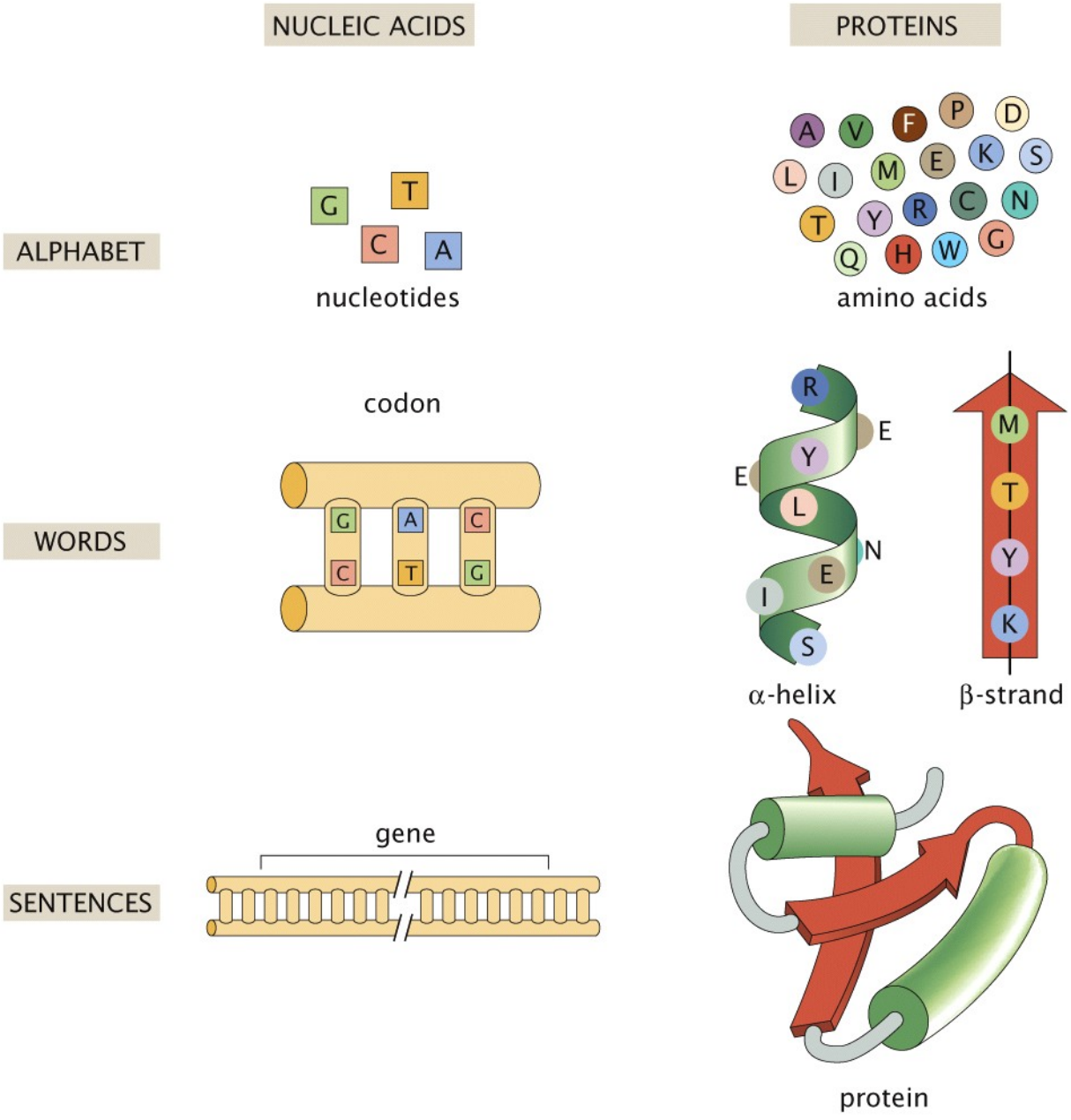

Figure 1.2 Physical Biology of the Cell, 2ed. (© Garland Science 2013)

Figure 1.2: The cell contains two information-rich molecule types, each of which has its own "language" structured into words and sentences. We discuss the role of each of those throughout this chapter.

1.3 Protein folding

The ability of a protein to perform its function is largely linked to its spatial structure; anticipating on Sec. 1.6 and the following chapters, some are for instance shaped like little walkers that flex their legs to step on special protein tracks. In some other cases their function is mainly biochemical, and crucially depends on the steric accessibility of a binding site. As a result, a crucial (and highly nontrivial) question is to know how to go from a protein's sequence to its structure. Although the details of this question are still the object of active research (and, perhaps amusingly, a biennal worldwide challenge), there are a few useful rules of thumb which we review in this section.

Proteins are essentially compact, *i.e.*, they typically do not contain large voids. Accordingly, their radius is roughly proportional to the length of their genome to the power 1/3.

While different residues have different charges and interactions with one another, a first useful approach is to parse them into two categories: those that are polar, and those that are hydrophobic (listed in the top left corner of Fig. 1.1). To illustrate how such interactions may influence the folding of the proteins, consider the case of a simplified protein with 6 amino acids folding on a square lattice in two dimensions. There are three possible comppact folds (up to rotations and inversions): Depending on the amino acid sequence, the energy of each structure will be different.

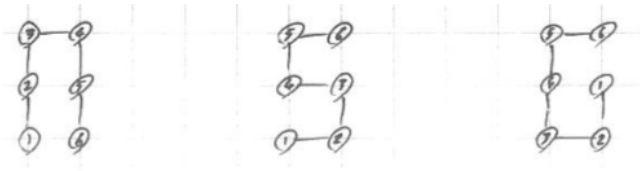

Here are the energies associated with two example sequences, where we represent polar and hydrophobic residues with black and white circles respectively. We moreover assume that an interface between two residues of the some type contributes 0 to the energy while a mismatch contributes an energy ϵ, and indicate the energy and associated Boltzmann weight: While the first example yields three degenerate ground states, the second has a clear ground

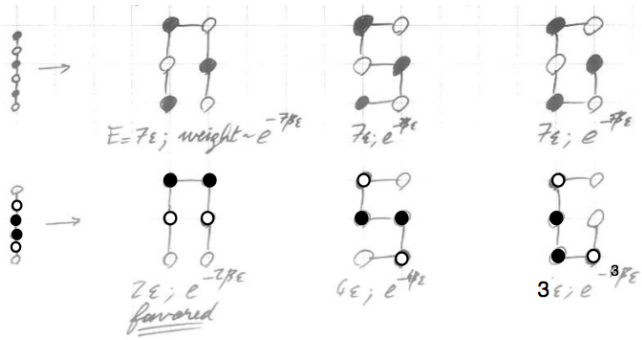

state, and thus tends to fold to a well-defined structure. Empirically, the protein sequences selected by evolution tend to be of the latter type and favor a unique ground state.

Whether or not the protein can easily reach its ground state is a nontrivial question however, as the state space of large proteins is enormous. Imagine a polymer similar to the one discussed above, but with 100 amino acids and on a 3D cubic lattice. In a first, very rough approximation each bond of the polymer can point in any of the six directions of the lattice, implying a number of possible configurations of the order of $6^{100} \simeq 6.5 \times 10^{77}$. Assuming – very optimistically – that the protein explores one configuration every 10^{-15} s, we deduce that probing all the available configurations would take it 2×10^{55} years, *i.e.*, 10^{45} times the age of the universe. This argument, known as Levinthal's paradox, implies that proteins cannot find their ground state simply by exploring their state space at random. Instead, successful proteins have a sequence that not only give rise to a stable folded state, but also guide the protein from its initial unfolded state towards it. Among the many mechanisms involved, two at least are widespread and easy to understand:

- In correctly folded proteins polar residues tend to be on the outside, and hydrophobic ones on the inside.
- Proteins do not fold at once, but tend to fold simple local substructures first, which then rearrange over longer length and time scales. The most basic example are the ubiquitous α helices and β strands illustrated in Fig. 1.2. These basic structures are often referred to as the protein's "secondary structure", and are still apparent in its "ternary structure", *i.e.*, its folded geometry (Fig. 1.2).

A final implication of these kinetic considerations is that while small peptides typically end up folding in their ground state, this is often not the case of larger proteins.

1.4 Gene regulation

It's nice to know how proteins are produced; but how does the cell know when to produce the right protein for the right job? The answer is again related to the action of proteins. One way of controlling gene expression is through "transcriptional regulation". A historic and simple example is the lac operon in *Escherichia coli*[1]: a region of its genome that acts as a genetic network where some genes/proteins control the transcription of others.

The basic context of this story is the following: *E. coli* feeds on different types of sugar, including glucose, which is easy to metabolize, and lactose, whose metabolism requires a specialized protein machinery. The components of this machinery offers new examples of the diverse roles played by proteins in the cell:

- lacZ: an enzyme that catalyzes (*i.e.*, speeds up the chemical reaction of) lactose breakdown.
- lacY: a pore-forming proteins that pokes holes in the membrane to let lactose into the cell
- lacA: a transacetylase, which performs a chemical modification (acetylation) of the sugar that enables its processing.

These proteins are expensive to produce, and should only be manufactured when lactose is present and glucose absent. The cell has ways to sense these sugars (using – would you have guessed it – proteins), which imply that two proteins are present or absent from the cellular medium depending on the conditions:

- lac repressor is present when lactose is absent
- CAP is present when glucose is absent.

These two proteins bind to the *E. coli* DNA in the vicinity of the location where the RNA polymerase initiates the transcription of the lac operon genes (the analog of a start codon for RNA polymerase). As schematized below, lac repressor prevents the RNA polymerize from binding, while CAP is required for its binding. As a result, transcription occurs only in the situation where glucose is absent (denoted by "− glucose") and lactose is present (denoted by "+ lactose").

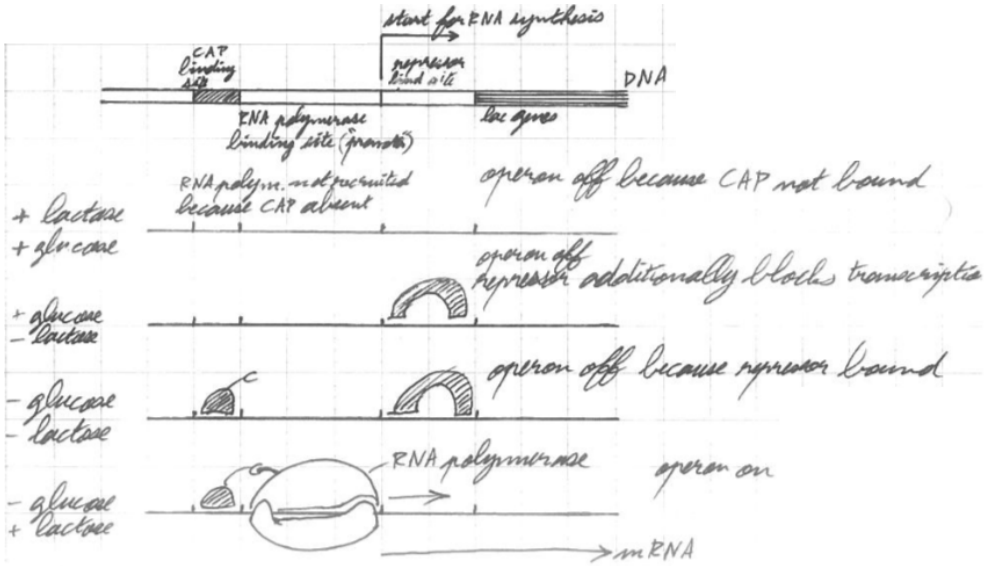

While the previous section showed us the basic nature of the influence of DNA on proteins, here we see that there are also mechanisms by which proteins provide a feedback. One may thus view protein expression in a cell as one big complicated dynamical system whose variables are the concentrations of different proteins. In such a picture cellular states are attractors of the dynamical system, be they fixed points, oscillating limit cycles or even more complicated structures.

[1]The apparent obsession of biologists for *E. coli*, a bacteria found in our gut, may at first surprise the physicist. Its justification is not that this specific bacterion is particularly fundamental, but rather that through years of study the community has developed very effective tools and resources to study it, giving it the status of "model organism". This arguably makes *E. coli* the easiest bacterion to study in practice, and thus a good testing ground for new ideas which investigators often argue (rightly or wrongly) are more generally valid for all bacteria, or even for all cells. Other model organisms include the brewer's yeast *Saccharomyces cerevisiae* (∼ the easiest eukaryote to study) and the fruit fly *Drosophila melanogaster* (∼ the easiest animal to study).

1.5 The organization of the cell

Our new-found understanding of the components and basic mechanisms of the cell allows us to usefully revisit the crude picture presented at the end of Sec. 1.1. We thus introduce perhaps the most fundamental distinction in biology, namely that between prokaryotes, *i.e.*, cells whose genome is not enclosed in a nucleus, and eukaryotes, where it is.

Figure 1.3 shows the differences in the level of organizations of the different cells using three examples of model organisms: *E. coli* and *S. cerevisiae*, which we have previously encountered, as well as HeLa cells[2], a type of human cancer cells which, unlike most human cells, keeps on dividing forever. By almost any reasonable biological measure, be it the internal structure of the cell, genetic similarity or position in the family tree of all living beings, the brewer's yeast is much closer to humans than to bacteria. Note that while the fibroblast and HeLa cells presented here happen have a similar morphology, there is a huge variability in the appearance of different cell types within our bodies.

Here are a few important differences between prokaryotes and eukayotes:

prokaryotes	**eukaryotes**
Cytoplasm (the medium inside the cell membrane) is well-mixed.	Cytoplasm is highly structured by membrane compartments.
mRNA can be translated by ribosomes close to where it was transcribed.	mRNA needs to be exported outside of the nucleus prior to translation.
Translation happens everywhere.	Translation happens preferentially at the endoplasmic reticulum.
Following translation, proteins diffuse away.	Following translation, proteins are often addressed to a specific location inside the cell and transported there.

While the objects described until now sounded pretty biochemical, the first distinction introduced here gives us a sense that geometry, spatial organization and mechanics also matter to the cell. One spectacular example of this idea is the cytoskeleton, a network of protein filaments that is a the same time the scaffold that gives the cell its mechanical properties and the engine that drives it.

1.6 Introduction to the cytoskeleton

Watch this video to familiarize yourselves with this system, to which we will come back on multiple occasions during the course.

[2]The cell's name derives from that of Henrietta Lacks, a 31-year-old African-American cervical cancer patient. The original tumor cells were taken a few months before her death in 1951 without her knowledge or consent, which was common practice at the time. Her life and the cell line are the subject of a best selling book, "The Immortal Life of Henrietta Lacks", whose author Rebecca Skloot estimates that 50 million tons of Ms. Lacks' cells have been grown in the lab from the original specimen.

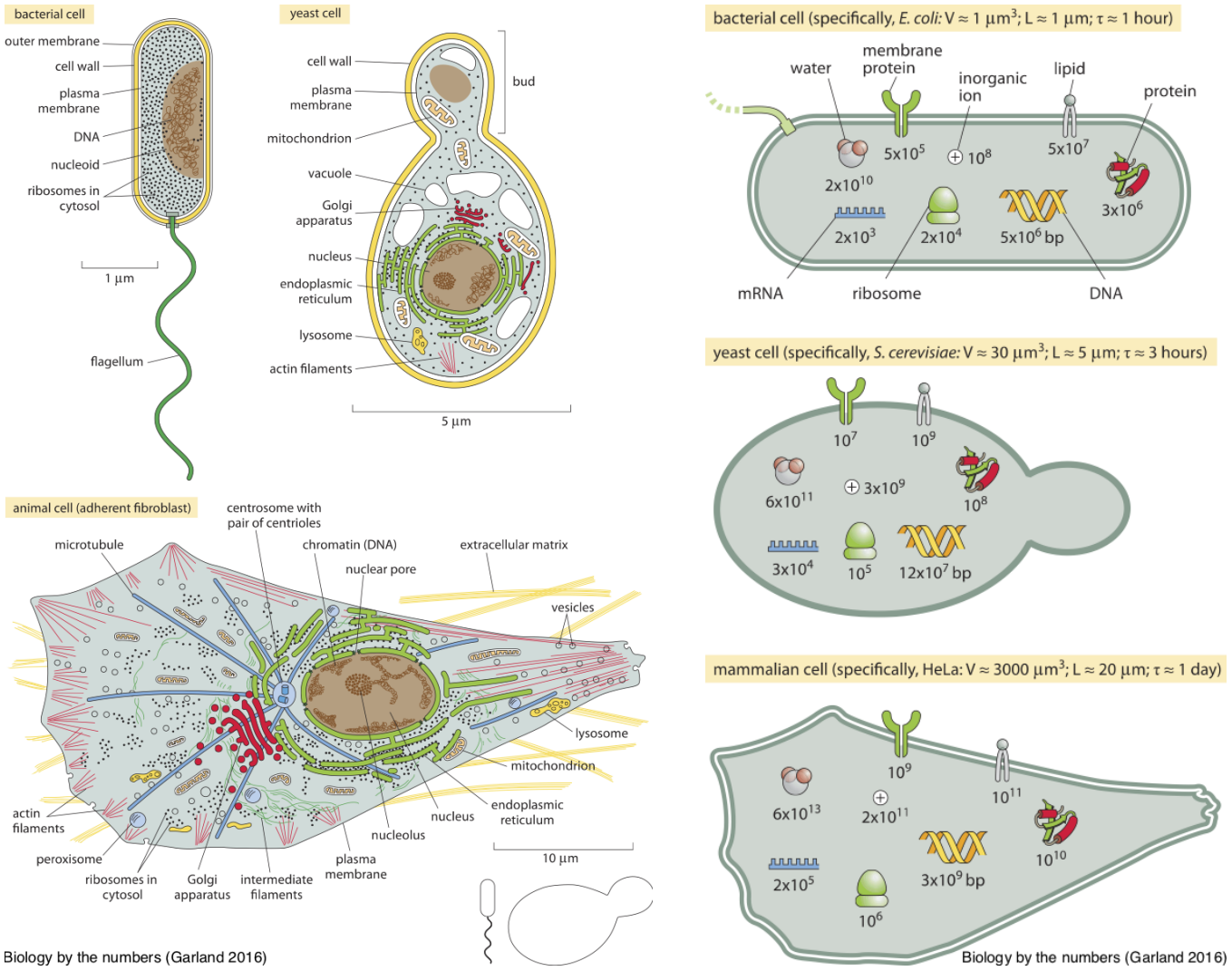

Figure 1.3: Functional schematics (*left*) and orders of magnitude (*right*) pertaining to one prokaryote (*E. coli*) and two eukaryotes (yeast cell and fast-moving human cells). The outline of the bacterion and yeast cell next to the scale bar at the bottom give a sense of scale. All compartments represented are delimited by a lipidic cell membrane, sometimes reinforced by a carbohydrate or a protein scaffold. On the right-hand-side, V is the typical volume of the cell, L its length and τ its division times. The numbers displayed inside the cells are molecule counts, except for DNA (total number of base pairs).

What's next

The rest of the course explores mechanical and statistical aspects related to the four basic molecular types presented in Sec. 1.1. In so doing, it details the connection between microscopic statistical models and larger-scale field theories, and insists on the usefulness of symmetry considerations in tackling extremely complex systems.

In tutorial 1, we discuss the elasticity of a single biopolymer subjected to thermal fluctuations, be it DNA, a carbohydrate polymer or protein filaments such as those found in the cytoskeleton. Chapter 2 then discusses how to relate this filament-level elasticity to the mechanical properties of large random networks made of these filaments. Chapter 3 then introduces the basic formalism of linear elasticity required to treat these networks as continuum media. Tutorial 2 then serves as a training in using these tools, resolves some paradoxes about network elasticity and illustrates how network mechanics results in the effective transmission of motor-generated forces in the cytoskeleton. The course then takes a new turn in chapter 4, where we go beyond the passive mechanics of cells and explore how motors drive them out of equilibrium at the microscopic level. This macroscopic information is then incorporated in large-scale, "active matter" theories of the cellular medium in chapter 5, which reuse some of our linear elasticity tools and augments them with some new active terms, thus giving rise to new original collective behaviors. Finally, chapter 6 elaborates the theory of lipid membrane mechanics, and tutorial 3 discusses the interaction of the membrane with the cytoskeleton.

Appendices

Optional training exercises

Use the Internet to answer the following questions:

1. What is the most abundant protein in the human body? What is it good for? Buy gelatin in the supermarket and hydrate it per the instructions on the packaging. Play with it. Why did I just ask you to do that?
2. How does the RNA polymerase know where to start transcription?
3. How did Bulgarian dissident writer Georgi Markov die (from a molecular point of view)?
4. Download and play the videogame "Foldit".
5. Where does the name "operon" come from?

Learning goals for this chapter

- Be able to enumerate the basic types of molecules present in cells and the differences between them
- Be able to explain the central dogma of cell biology
- Be able to explain why proteins cannot rely on equilibrium statistics for their folding, and quote two tricks they use to cicumvent that issue.
- Be able to explain how the cell "decides" to produce a protein or not
- Be able to quote at least 5 different functions that proteins can perform in the cell
- Be able to describe the basic differences between procaryotes and eukaryotes
- Be able to explain the treadmilling dynamics of actin and some of its basic mechanical properties
- Be able to describe how a molecular motor generates force and motion
- Be able to explain how striated muscle works.

Tutorial 1: Entropic elasticity of a semiflexible filament

Physics of Complex Systems M2 – Biophysics

Long thin filaments are ubiquitous in the cell, be they DNA molecules, structural elements of the cytoskeleton made out of proteins or carbohydrates such as polysaccharides used for energy storage or selected for their material properties (*e.g.*, cellulose or chitin). In many cases, the mechanical response of these objects is crucial for their biological function, and is strongly influenced by thermal fluctuations.

Here we consider the response of a somewhat rigid polymer, *e.g.*, a DNA filament to a longitudinal pulling or pushing force [see Fig. 1, as well as the classic reference Marko & Siggia, *Macromolecules* **28**, 8759 (1995)]. This response is dominated by a spring-like elasticity that originates in the straightening out of its transverse fluctuations, as discussed in the following. We thus look for the force-extension relation of that nonlinear spring. While physically related, the three sections can be tackled independently.

1 Force-extension relation

We consider an almost rectilinear polymer lying along the z direction, and denote its small lateral displacement along the transverse directions x and y by $\mathbf{r}_\perp = \{x(z), y(z)\}$. In this representation, the energy of the polymer is primarily due to its bending stiffness, and thus depends on its local curvature $|\partial_z^2 \mathbf{r}_\perp| = \sqrt{(\partial_z^2 x)^2 + (\partial_z^2 y)^2}$. As further discussed in Sec. 3, the resulting bending energy reads

$$E_b = \int_0^S \left\{ \frac{k_B T \ell_p}{2} \left[\left(\partial_z^2 x\right)^2 + \left(\partial_z^2 y\right)^2 \right] \right\} \mathrm{d}z, \tag{1}$$

where ℓ_p is a constant known as the persistence length and the total length S of the filament is also constant. The action of the outside tensile force F pictured in Fig. 1 results in an additional energy

$$E_t = \int_0^S \left\{ \frac{F}{2} \left[(\partial_z x)^2 + (\partial_z y)^2 \right] \right\} \mathrm{d}z \tag{2}$$

Assuming that the filament is attached such that $\mathbf{r}_\perp(0) = \mathbf{r}_\perp(S) = \mathbf{0}$, we use the Fourier decomposition

$$\mathbf{r}_\perp(z) = \sum_{n=1}^{+\infty} \tilde{\mathbf{r}}_n \sin\left(\frac{n\pi z}{S}\right) \qquad \text{with} \qquad \tilde{\mathbf{r}}_n = \tilde{x}_n \hat{\mathbf{x}} + \tilde{y}_n \hat{\mathbf{y}}. \tag{3}$$

1.1 Write the total energy $E = E_b + E_t$ as a function of the Fourier components $\tilde{x}_n$ and $\tilde{y}_n$, making sure to perform the integrations over z to simplify the result.

1.2 Using the equipartition theorem, write the equilibrium thermal averages $\langle \tilde{x}_n \rangle$ and $\langle \tilde{x}_n^2 \rangle$.

1.3 As will be discussed in Sec. 3, the end-to-end length of the filament is given by

$$L = \int_0^S \sqrt{1 - \left[(\partial_s x)^2 + (\partial_s y)^2 \right]}\, \mathrm{d}s \simeq S - \frac{1}{2} \int_0^S \left[(\partial_z x)^2 + (\partial_z y)^2 \right] \mathrm{d}z \tag{4}$$

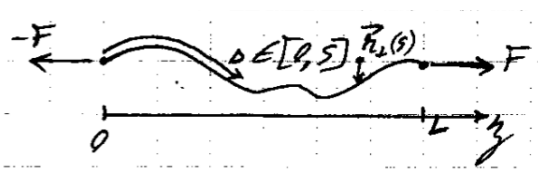

Figure 1: Parametrization of the filament. Here fluctuations take place in both the x and y directions.

to lowest order in the filament slope. Conclude from that that

$$\langle L\rangle \simeq S - \frac{S^2}{\pi^2 \ell_p} \sum_{n=1}^{+\infty} \frac{1}{n^2+\phi}, \tag{5}$$

where ϕ is the force F up to a normalization to be specified.

1.4 Prove that for $\zeta \geq 0$

$$\sum_{n=-\infty}^{+\infty} \frac{e^{in\zeta}}{n^2+\phi} = \frac{\pi}{\sqrt{\phi}} \left[\frac{e^{\zeta\sqrt{\phi}}}{e^{2\pi\sqrt{\phi}}-1} + \frac{e^{-\zeta\sqrt{\phi}}}{1-e^{-2\pi\sqrt{\phi}}} \right]. \tag{6}$$

1.5 Deduce from this the filament's force-extension relationship:

$$\langle L\rangle \simeq S - \frac{S^2}{\ell_p} \frac{\pi\sqrt{\phi}\coth(\pi\sqrt{\phi}) - 1}{2\pi^2\phi} \tag{7}$$

2 Discussion of the mechanical properties

2.1 What is the physical meaning of the persistence length ℓ_p? For DNA, $\ell_p \simeq 50\,\mathrm{nm}$. For actin, $\ell_p \simeq 10\,\mu\mathrm{m}$.

2.2 Draw the small-slope force-extension relationship of Eq. (7). What is the typical stiffness of the filament in the linear response regime? Its divergence denotes the buckling of the filament. What force is required to achieve this buckling? How large is it for a typical actin filament with $S \simeq 400\,\mathrm{nm}$? How does it compare to the typical molecular motor force $\approx 1\,\mathrm{pN}$? How much filament compression do you expect under such a force?

2.3 What happens beyond buckling? Give the scaling of the buckled filament's rigidity. Compare this situation with bending the filament with a transverse force.

3 Energy of a filament

We now study the foundation of the energies introduced in Sec. 1. We consider an inextensible filament with constant total arclength S, but whose end-to-end length L fluctuates (Fig. 1).

3.1 The molecular bonds between the monomers constituting the filament tend to keep it straight, and the local energy of the filament depends only on its local shape. Thus the filament bending energy can be expressed as

$$E_b = \int_0^S f[c(s)]\,\mathrm{d}s, \tag{8}$$

where $c(s)$ is the curvature of the filament at the location characterized by the arclength s and f is an unknown function. Expand f for a weakly deformed filament to obtain an explicit form for the bending energy as a function of $c(s)$ up to an unknown multiplicative constant. This so-called "worm-like chain model" is a staple of the study of biological semiflexible polymers.

3.2 For a curve defined by its position vector $\mathbf{r}(s)$, the curvature $c(s)$, tangent unit vector $\hat{\mathbf{t}}(s)$ and normal unit vector $\hat{\mathbf{n}}(s)$ are defined through

$$\hat{\mathbf{t}} = \partial_s \mathbf{r}; \qquad c\hat{\mathbf{n}} = \partial_s \hat{\mathbf{t}}. \tag{9}$$

Writing $\mathbf{r}(s) = \mathbf{r}_\perp(s) + z(s)\hat{\mathbf{z}}$, where $\mathbf{r}_\perp$ is a vector contained within the xy, show that to lowest order in the filament deviation from a straight line E_b is given by Eq. (1).

3.3 Prove Eq. (4).

3.4 Using this result and assuming the filament is being pulled at both ends by a force $\mathbf{F} = \pm F\hat{\mathbf{z}}$ as in Fig. 1, demonstrate that the energy E_t associated with the tension of the filament is given by Eq. (2).

Chapter 2

From filaments to gels: effective medium theory

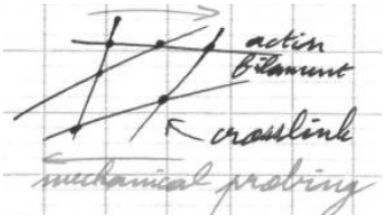

While tutorial 1 gave us an idea of the tensile strength of a single bond in a cytoskeletal network, the relationship between this quantity and the overall modulus of the gel is not obvious in a random network. Here we discuss the requirements for the gel to be rigid at all (Sec. 2.1), then introduce the most basic version of a widely used mean-field method to answer this question (Sec. 2.2). We will see that the modulus of the gel strongly depends on the connectivity of the network, leading to a paradox for crosslinked filament gels: since their filaments are bound to each other by crosslinks whose coordination is equal to 4, our theory predicts that they should not be rigid at all, in contradiction with experiments. Sec. 2.3 resolves this conundrum by revealing additional physical effects at play in the rigidity of fiber networks.

2.1 Maxwell's constraint-counting argument

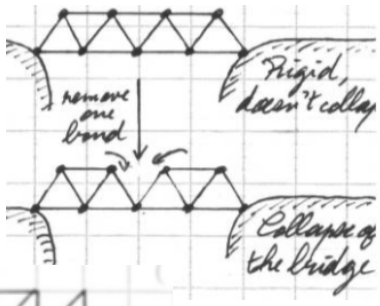

Consider an arbitrary mechanical frame made of stiff springs connected at certain vertices in dimension d. Is it rigid? One can think of this as of a bridge spanning a gorge: if too many beams (bonds between vertices) are removed, the bridge loses its rigidity and collapses.

More generally, if I grab two points in a large frame made of vertices and springs I can ask whether I will be free to move them with respect to each other without compressing any spring:

What is the critical connectivity? The simplest argument [4] consists in counting constraints in a frame with n_s springs and n_v vertices. We define:

N_f the number of degrees of freedom in the system

N_c the number of constraints imposed by the stiff springs.

If $N_c > N_f$ the frame is rigid (neglecting trivial global rotations and translations in the $N \to \infty$ limit), and

$$N_f = d \times n_v \tag{2.1a}$$

$$N_c = n_s. \tag{2.1b}$$

Defining $\langle z \rangle$ as the average connectivity of the vertices, each vertex is associated with $\langle z \rangle/2$ springs and

$$\frac{\langle z \rangle}{2} n_v = n_s. \tag{2.2}$$

Therefore

$$\begin{aligned} \text{rigidity} &\Leftrightarrow N_c > N_f \\ &\Leftrightarrow \frac{\langle z \rangle}{2} n_v > d n_v \\ &\Leftrightarrow \langle z \rangle > 2d \end{aligned} \tag{2.3}$$

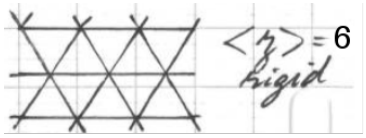

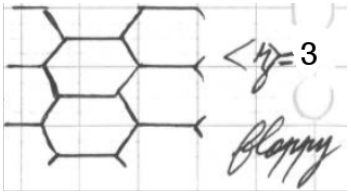

Thus the critical connectivity in $d = 2$ is 4, and in $d = 3$ it is 6. Note that this *rigidity percolation threshold* is distinct from and higher than the ordinary *connectivity percolation threshold*. For instance, the $\langle z \rangle = 3$ honeycomb lattice in the illustration percolates in the sense of connectivity percolation (one can walk along the bonds of the network from one side to the other), but not in the sense of rigidity percolation (one can shear the network without changing the length of any of its bonds).

2.2 Effective medium theory for a simple network

Beyond the simple constraint counting argument, can we predict what the modulus of sa gel will be for a given coordination? Here we present a simple mean-field method [5] that yields quantitatively excellent results for simple spring networks and is widely used even beyond those simple situations. It consists in approximating a randomly depleted network (here a triangular network where bonds have been removed at random) with a regular one (here a regular triangular network where each bond has a spring constant α_m):

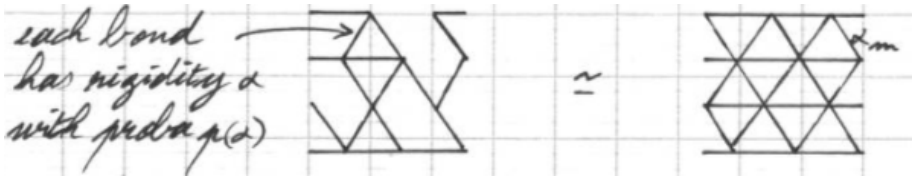

here all bonds in either networks have a rest length equal to one. Our goal in this section is to compute the effective-medium rigidity α_m in order for the regular network to provide the best possible approximation of the elasticity of the depleted network. This requires a self-consistent calculation, as explained below.

Note: in practice we will consider that the probability distribution $p(\alpha)$ for the bonds of the depleted network is such that:

$$\begin{aligned} &\alpha = 1 \text{ with probability } p \\ &\alpha = 0 \text{ with probability } 1 - p \end{aligned}$$

corresponding to the idea that each bond is either present of absent (the method described here indeed also applies to network where the rigidity of each bond is a continuum random variable).

Formulating the self-consistency condition

We start from the equivalent regular network where each bond has a (as yet unknown) rigidity α_m. We uniformly stretch the network by a strain δu_m, meaning that all the lengths in the network are multiplied by a factor $(1 + \delta u_m)$. In particular, if we single out a single bond it stretches as shown in the illustration.

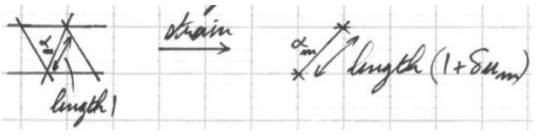

Now starting from this strained state (reproduced as situation A below), we imagine replacing *one* of the deterministic, bonds with rigidity α_m by a random bond of rigidity α drawn with the probability distribution $p(\alpha)$. This operation only concerns a single bond, and all other bond rigidities in the network remain equal to α_m. All bonds, both

deterministic and random, still have a rest length equal to one. As a result of the bond substitution, the deformation of the springs in the network changes. For instance, is the new bond is stiffer than α_m, then the distance between its two extremities will decrease (situation B below; note that the new distance is denoted $1 + \delta u$). If it is softer, that distance will increase. Our self-consistency condition, on which the rest of the calculation is based, consists in demanding that *on average, the change in length of the substituted bond must be equal to zero.*

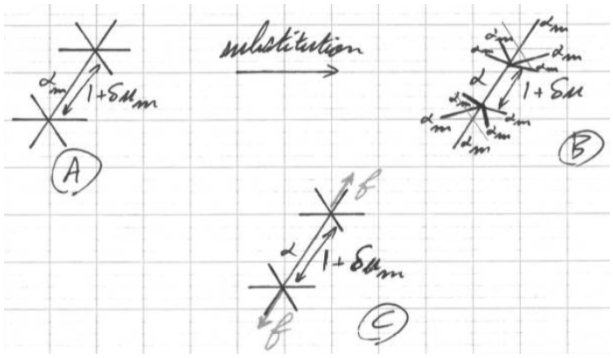

To compute the value of δu as a function of the rigidity α, we introduce the situation denoted as C in the schematic above. In this new situation, we exert an external force f on the substituted bond, and choose the value of this force precisely so that the length of the bond is exactly equal to δu_m. By comparing situations A and C, we see that the rest of the network (*i.e.*, the system formed by all springs except the central spring) has the same geometry in both situation. This implies that the force exerted on in situation A is equal to the force exerted on it in situation C. In the former case, this force is equal to the tension of the deterministic spring. In the latter, it is equal to the sum of the tension of the α-spring with the external force. As a result:

$$\alpha_m \delta u_m = f + \alpha \delta u_m, \tag{2.4}$$

which gives us a value for the force f.

We now compare situations B and C. The distance between the two extremities of the central spring is given by the balance of force between the bond of interest, the external force and the rest of the network. To linear order, the force exerted by the rest of the network is related to the displacement through an effective spring constant α'_m:

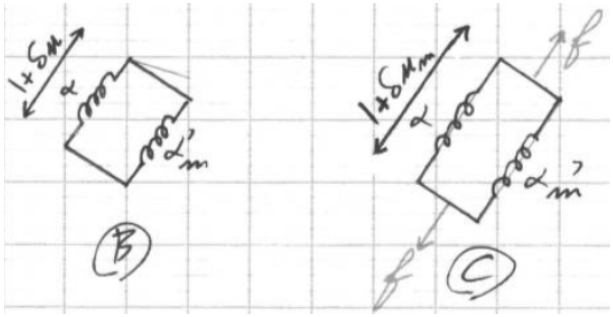

Comparing the difference in elongation between the two situations and recognizing that assembling the two springs α and α_m results in an overall spring constant $\alpha + \alpha_m$, this implies

$$f = (\alpha + \alpha'_m)(\delta u_m - \delta u). \tag{2.5}$$

Eliminating f from Eqs. (2.4) and (2.5), we obtain

$$\begin{aligned} (\alpha + \alpha'_m)(\delta u_m - \delta u) &= (\alpha_m - \alpha)\delta u_m \\ \Leftrightarrow \delta u_m - \delta u &= \frac{\alpha_m - \alpha}{\alpha'_m + \alpha}\delta u_m \end{aligned} \tag{2.6}$$

and therefore our self-consistency condition reads

$$\delta u_m = \langle \delta u \rangle \quad \Leftrightarrow \quad \left\langle \frac{\alpha_m - \alpha}{\alpha'_m + \alpha} \right\rangle = \int p(\alpha) \frac{\alpha_m - \alpha}{\alpha'_m + \alpha} \, \mathrm{d}\alpha, \tag{2.7}$$

which we must solve for α_m to conclude.

Elasticity of the surrounding medium

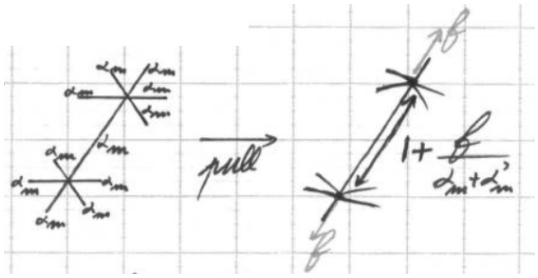

The last obstacle to solving Eq. (2.7) is to relate the effective spring constant α'_m of "the rest of the network" to the rigidity α_m of its constitutive springs. To begin with, let us reflect on the response of a full regular network of α_m (illustrated here). When the extremities of the central bond are pulled apart, the effective spring constant resisting the deformation is clearly $\alpha_m + \alpha'_m$.

This total effective spring constant must be proportional to α_m, since doubling the rigidity of every spring in the network can only double the rigidity of the network as a whole. We thus introduce a constant, dimensionless geometrical factor a^* defined by

$$\alpha_m + \alpha'_m = \frac{\alpha_m}{a^*}. \tag{2.8}$$

Since the network as a whole can only be stiffer than the central spring alone, we must have $a^* \in (0, 1)$.

While a^* can be computed from a direct calculation, here we spare ourselves the trouble of performing this calculation and use a shortcut that takes advantage of the Maxwell criterion derived in Sec. 2.1. We consider the probability distribution for a depleted network:

$$p(\alpha) = p\delta(\alpha - 1) + (1 - p)\delta(\alpha), \tag{2.9}$$

where δ stands for the Dirac distribution. Then

$$\left\langle \frac{\alpha_m - \alpha}{\alpha'_m + \alpha} \right\rangle = \left\langle \frac{\alpha_m - \alpha}{\alpha_m(1/a^* - 1) + \alpha} \right\rangle = p\frac{\alpha_m - \alpha}{\alpha_m(1/a^* - 1) + 1} + (1 - p)\frac{\alpha_m - \alpha}{\alpha_m(1/a^* - 1)}. \tag{2.10}$$

Per our self-consistent condition, this quantity must vanish. With a little arithmetic, this is easily shown to be equivalent to

$$\alpha_m = \frac{p - a^*}{1 - a^*}. \tag{2.11}$$

This is the result we were looking for, save for the fact that we still do not know the value of a^*. We however note that Eq. 2.11 only gives a physical (positive) rigidity for $p > a^*$, and that the predicted rigidity vanishes from $p = a^*$. This is directly reminiscent of our discussion of Sec. 2.1, whereby we expected a depleted network to have a finite modulus only if its average coordination $\langle z \rangle$ exceeded a certain threshold $2d$. In our example, $\langle z \rangle = z_{\max} p$ where $z_{\max} = 6$ is the maximum coordination of our triangular lattice. As a result, the critical bond presence probability p_c for rigidity percolation is given by

$$z_{\max} p_c = 2d \Rightarrow p_c = a^* = 2d/z_{\max}. \tag{2.12}$$

Note that the aforementioned full calculation of a^* yields the same result. At the end of the day, Eq. (2.11) thus yields the following profile for the effective spring constant of the network:

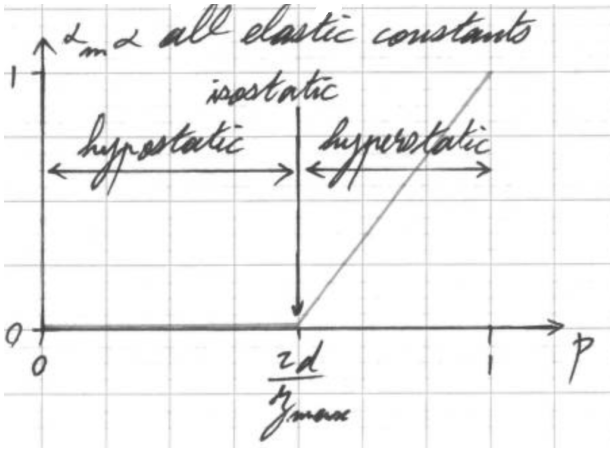

i.e., the effective spring constant is zero below the percolation threshold, then rises affinely to one above it. In the terminology of rigidity percolation, which concerns not only the physics of elastic networks but is also extensively used to describe granular packings and structural glasses, a system with exactly as many constraints as degrees of freedom is "isostatic". If it has fewer (more) constraints, then it is described as hypostatic (hyperstatic).

The effective spring constant α_m does not directly characterize the macroscopic elasticity of the network; that role falls to macroscopic elastic constants such as the Young's modulus, which we discuss in more detail in Chapter 3. As we will see in tutorial 2 however, such constants are all proportional to α_m, implying that our calculation is but one step away from a complete continuum theory of our random elastic network. Finally, it is worth noting that the mean-field approach described here is remarkably accurate when compared to numerical simulations or random networks, even in the vicinity of the Maxwell critical point. The reasons for this remarkable accuracy are not well understood.

2.3 Soft vs. hard networks

Let us now attempt to apply our new theory to an actin gel made of straight filaments bound two by two by crosslinking proteins, as schematized in the first illustration of this chapter. We model this system as a network of vertices (the crosslinking points) bound by springs: indeed, we showed in Tutorial 1 that actin segments held between two points acted as springs for small deformations, and studied the physical origin of this springiness as well as its magnitude. Under this model, we find ourselves with a three-dimensional spring network whose coordination is equal to 4. This implies a hypostatic network, and therefore a vanishing modulus.

This conclusion is worth contrasting with experimental results. As discussed in Tutorial 1, the predicted elastic modulus for a hyperstatic network made of entropic springs far exceeds those observed in experiments. This lends support to the idea that the entropic springiness of the filaments is not sufficient to stabilize an actin network due to insufficient connectivity. Nevertheless, the experimental modulus is not zero, suggesting that other stabilizing effects are at play. In this section, we discuss the nature of such possible stabilizing effects. Their specific application to the case of biopolymer networks is discussed in Tutorial 2.

What does being soft mean?

Let us consider the simple spring network (or "frame" in the engineering literature) in the illustration. This is a finite network with 4 springs and 4 vertices, making it easy to count its degrees of freedom and constraints:

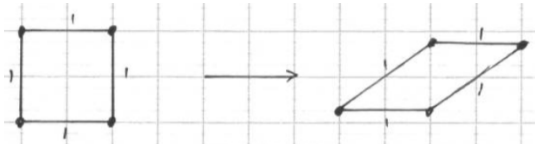

- 8 degrees of freedom (4 vertices with two degrees of freedom each)
- 4 constraints (the length of each 4 springs must remain equal to one)

As a result, the network has 4 remaining degrees of freedom that are not constrained. Of these three degrees of freedom, three are trivial in the sense that they do not deform the network. They consist in (1) translating the network in the x direction, (2) translating the network in the y direction and (3) rotating the frame. These trivial degrees of freedom should in principle also have been included in the discussion of Sec. 2.1, although their small number make them of little importance for large networks. This implies the existence of one non-trivial degree of freedom, whereby the network can be deformed without changing the length of any spring. This mode of deformation is known as a "soft mode" in the physics literature and a "mechanism" to engineers. More specifically, it is clear that even if the frame considered here is deformed with an angle of order one, the cost of this deformation in terms of spring energy will be exactly equal to zero. This is known as a "finite mechanism".

There is another type of mechanisms besides finite ones. Consider the contraption in the illustration, where two springs with rest length 1 are bound to two fixed plates with a distance of 2 between them. Moving the central point vertically changes the lengths of the springs by a large amount, and is therefore clearly not a mechanism. On the other hand, the situation is a little more subtle when moving is in the x direction. Indeed, as shown in the illustration in this case the length of each spring becomes $\ell = \sqrt{1+\delta x^2}$. As a result, the elastic energy of the system becomes (assuming the springs have a spring constant equal to unity):

$$E = 2 \times \frac{1}{2}(\ell - 1)^2 = \left(1 + \frac{\delta x^2}{2} - 1\right)^2 + \mathcal{O}(\delta x^6) = \frac{1}{4}\delta x^4 + \mathcal{O}(\delta x^6). \tag{2.13}$$

Therefore this deformation is not entirely free, but its cost is of order 4 in displacement, and therefore is free if considering only the linear response regime of the system. This type of mechanism is known as an "infinitesimal mechanism".

This second example calls for another comment. With two springs and one vertex in two dimensions, it clearly has two degrees of freedom and two constraints, suggesting that it should be rigid to linear order and not have a mechanism. That would indeed be the case if the two springs were at an angle in their resting state, as would for instance happen if the distance between the fixed plates was a little smaller than 2. Instead, the situation considered here is singular and does not work well with the simple constraint counting argument of Sec. 2.1. This is a useful reminder that this argument is only approximate, and can be put at a difficulty both in the type of singular situations presented here, as well as in cases where one region of a system is very connected while another is completely floppy, resulting in the coexistence of a large number of constraints and the existence of many soft modes. All these circumstances can be cleanly discussed using a slight sophistication of our constraint counting arguments [6].

Why are isostatic networks soft?

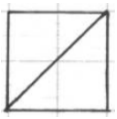

Let us go back to the square frame considered above. How can we make is rigid? The easiest solution is to add an additional spring, as illustrated here. Now the system has as many constraints as non-trivial degrees of freedom, and is therefore isostatic. In this situation, any deformation of the frame has a cost to harmonic order.

These considerations sound all well and good for a finite frame, but appear to clash with our findings on infinite networks. Indeed, we conclude at the end of Sec. 2.2 that an isostatic network has a vanishing modulus (this mean-field conclusion is additionally borne out by simulations and experiments). Where does the discrepancy come from? To shed light in this question, consider a square lattice of springs in two dimensions. With four half-springs per vertex (each spring is shared between two vertices) and two degrees of freedom per vertex, this system may appear to be isostatic. Yet it has several finite mechanisms, as shown here (the second type of deformation shown below is known as "shearing"):

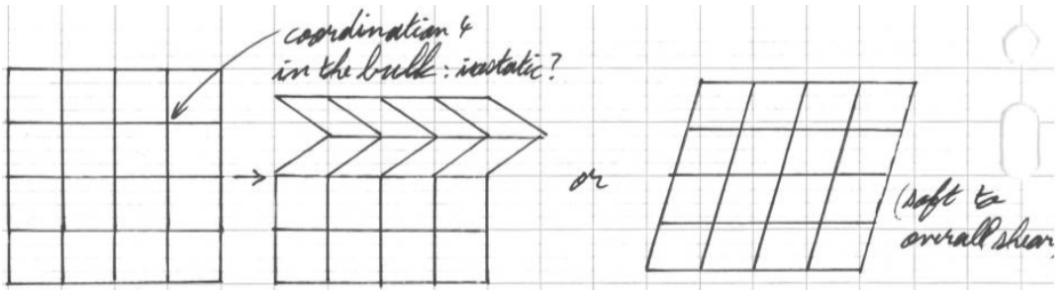

The existence of these mechanisms are due to the fact that our constraint counting argument in the bulk does not tell the whole story. Indeed, the coordination of the vertices at the boundary of the system is less than 4, making the system hypostatic overall. This slight, local undercoordination in the system is then turned into a macroscopic deformation through the appearance of a few collective soft modes whereby the displacements of the vertices are correlated over large distances.

The influence of these collective soft modes goes beyond slightly hypostatic systems. Section 2.2 thus shows that slightly *hyper*static networks also have a vanishing modulus. To understand this, consider randomly adding just enough diagonal springs to the square lattice discussed above so as to make it hyperstatic overall. This represents a number of springs of order $\sqrt{n_v}$ with n_v the number of vertices. Then attempt to deform the system macroscopically, *e.g.*, by shearing it as above. Given the small modification to the elasticity of the system, the pattern of deformation will be largely unchanged, but will now require deforming $\mathcal{O}(\sqrt{n_v})$ springs. As a result, the overall modulus of the frame is not rigorously zero anymore, but rather of order $1/\sqrt{n_v}$. This number does go to zero in the large-n_v limit, thus rationalizing the tendency of large isostatic system to have a vanishing modulus. The physics of similar delocalized soft modes is at the core of contemporary discussions of the physics of jamming [7].

Stabilizing soft modes through a bending rigidity

Having better understood the softness of hypo- and isostatic networks, we return to the question why biopolymer gels have a finite modulus. We thus note that modeling them as networks of springs leaves out one important point, namely their bending rigidity. Let us indeed consider a

biopolymer similar to those considered in Tutorial 1, and add a crosslink in its middle as illustrated. Because of the filament's bending stiffness, changing the angle θ between the three points materialized on the illustration has an energetic cost, which is completely ignored by the spring network model discussed up to this point.

To illustrate how this new physical ingredient can stiffen the soft modes of a fiber network and endow it with a finite modulus (a topic further discussed in Tutorial 2), we write that the energy of a bent configuration of the filament is $e_{\text{bending}} = \frac{\kappa}{2}\theta^2$, with κ an elastic constant proportional to the filament's bending stiffness. We now trap the filament between two walls as before and estimate the energy associated to a δx displacement:

$$E = \frac{\delta x^4}{4} + \frac{\kappa}{2}\theta^2 \simeq \frac{\delta x^4}{4} + \frac{\kappa}{2}\delta x^2. \tag{2.14}$$

Therefore, the previously soft mode how now acquired a stiffness (*i.e.*, an energy cost quadratic in the displacement) that is proportional to κ.

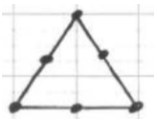

The addition of a bending rigidity can also be factored into an updated constraint counting argument. Consider the triangular frame of the illustration. If regarded as a spring network, it is clearly hypostatic. Now regard each side of the triangle as a biopolymer, which implies associating an energy cost $\frac{\kappa}{2}\theta^2$ to any angular deformation of each of the three vertices located in the middle of a side. The constraint counting now goes as follows:

- 12 degrees of freedom including 3 trivial ones
- 6 spring-like ("stretching") constraints
- 3 bending constraints (stemming from the three new quadratic penalty on angles)

As a result, the frame has as many constraints as non-trivial degrees of freedom. It is a finite isostatic network, and therefore rigid.

It is thus worth keeping in mind that the term of isostaticity and the associated value of the critical connectivity depends on the list of interactions considered (*e.g.*, stretching only *vs.* stretching+bending). For a detailed discussion of network stabilization through bending interactions and the associated rigidity transitions (which are believed to be analogous to critical points in second-order phase transitions), as well as other topics in fiber network elasticity, see Ref. [8]

Stabilizing soft modes through tension

Another way to stabilize soft modes is to endow the network with a pre-tension. Intuitively, this process is reminiscent to the physics of a party balloon. When the balloon is deflated, its tensionless skin can be bent and sheared without any effort. Once it is inflated however, the skin is very tense and any deformation of the balloon, even ones that do not change its volume, become energetically costly.

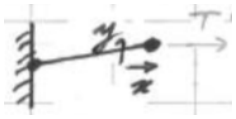

A simpler example of this stabilization is provided by the illustration, which has a single vertex bound to a fixed wall with a single spring. In the absence of any tension, this system has an obvious finite mechanism which consists in rotating the vertex around the attachment point. Let us now consider a system with a tension T manifested in the energy as

$$E = \frac{1}{2}(\ell - 1)^2 - Tx = \frac{1}{2}\left(\sqrt{(1+x)^2 + y^2} - 1\right)^2 - Tx, \tag{2.15}$$

where ℓ is the length of the spring and (x, y) are the coordinates of the vertex. Here the origin of the coordinates is taken for a horizontal spring of length 1. Expanding the length for small displacements:

$$\ell - 1 \simeq x + \frac{x^2 + y^2}{2} + \left(-\frac{1}{8}\right)x^2 \simeq x + \frac{y^2}{2}, \tag{2.16}$$

where we have included only the lowest-order terms in x and y. Inserting into the energy, we find:

$$E \simeq \frac{1}{2}\left(x + \frac{y^2}{2}\right)^2 - Tx. \tag{2.17}$$

Minimizing this energy with respect to x and y yields the equilibrium position of the vertex in the presence of tension, namely $x_{\rm eq} = T$, $y_{\rm eq} = 0$. We denote by $(\delta x, \delta y)$ the deviation from this position and expand for small δ:

$$\begin{aligned} E &= \frac{1}{2}\left(T + \delta x + \frac{\delta y^2}{2}\right)^2 - T(T + \delta x) \\ &\simeq -\frac{T}{2} + \frac{\delta x^2}{2} + \frac{T}{2}\delta y^2 \end{aligned} \tag{2.18}$$

Therefore in the presence of a tension in the x direction ($T \neq 0$), a quadratic term in δy^2 appears and stabilizes the system's initial soft mode in the y direction. At the formal level, this is exactly the same phenomenon that endows the simple pendulum with a harmonic restoring force, assuming x is the direction of gravity.

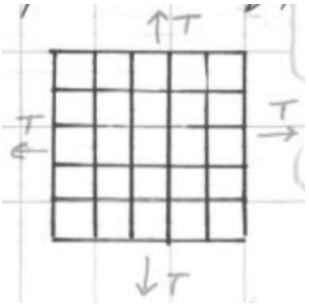

Let us now apply the insights gained from this example to the semi-realistic example of a stretched square lattice of the illustration. This configuration can be understood as a model for rubber elasticity. Indeed, in rubber flexible polymers (without bending rigidity) are crosslinked two by two during vulcanization. This results in an elastic network with coordination $\simeq 4$, and therefore ostensibly floppy. Clearly rubber is not really floppy in practice, as you can clearly verify by handling the tyres of your bicycle. Due to an externally imposed pre-tension, which originates in the steric and physico-chemical repulsion between monomers in the rubber case, each bond in the network has a pre-tension T. Now consider shearing the square lattice. Under this deformation, each vertical bond in the lattice undergoes a similar transformation as the single bond of our previous example. This rationalizes the stabilization of infinite networks by the application of prestress. For a detailed discussion of the general case, see Ref. [9].

Appendices

Optional Training exercises

1. Consider the uniform tilings of the Euclidean plane shown on this web page as spring networks. Which of those are hypostatic? isostatic? hyperstatic?
2. Repeat the exercise adding bending interactions between initially aligned points as if each straight line was a biopolymer.
3. Compute the effective elastic constant of a triangular, random spring network with $p(\alpha) = 1 + (\alpha - 1/2)x$ as a function of the parameter x.
4. Compute the equivalent of Eq. (2.14) in the absence of a bending rigidity ($\kappa = 0$) but when the constant spacing of the walls is $2 + \epsilon$ instead of 2. Explain how this stabilizes the soft mode through tension.
5. Consider a square frame similar to the one presented in the beginning of Sec. 2.3. Add a term $-PA$ to its elastic energy, where $P > 0$ is a constant (two-dimensional) pressure and A the area of the square. Show that this new term induces a pre-tension and stiffens the finite mechanism discussed in the text.

Learning goals for this chapter

- Be able to reconstruct Maxwell's argument and generalize it to a case where other interactions are present besides stretching (especially but not limited to cases where bending is present).
- With some guidance, be able to construct the effective medium theory of Sec. 2.2.
- Be able to apply it to a bond stiffness probability distribution beyond the specific example of Eq. (2.9).
- Be able to explain the difference between a finite and an infinitesimal mechanism.
- Be able why a finite isostatic frame has a finite modulus, while an infinite one has a vanishingly small modulus.
- Be able to compute the rigidity conferred to soft stretching modes by bending and/or tension in simple geometries.

Chapter 3

A crash course in elasticity theory

Chapter 2 has taught us that a depleted spring network is analogous to a full network of weaker springs; here we look at how these full networks, or any solid object, respond to large-scale stress and deformation. As we will explore in the next tutorial, this large-scale material description will also be useful to describe depleted networks with $z < 2d$ stabilized by bending interactions.

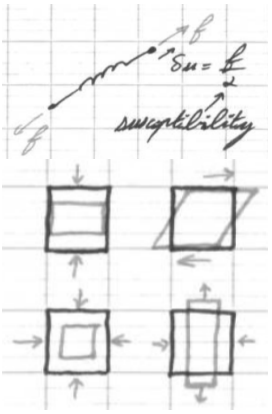

Our basic inspiration in characterizing a solid object comes from Hooke's law: applying a small force on a spring induces a small displacement proportional to the force. The proportionality constant is known as a spring constant, which is an example of a susceptibility. We want to apply the same idea to a cubic, solid piece of material.

Since the piece of material is three dimensional, instead of applying a force to it we apply a constant force per unit surface, which we might refer to as a pressure or a stress, and which we denote by σ. There is a complication however: unlike in the case of the one-dimensional spring, there are many ways of exerting a given σ on a cube: compressing it on the top and bottom, shearing it, compressing it isotropically, *etc.* As shown in the illustration, these different stressing protocols (indicated by arrows) may give rise to different types of deformation.

As a result of these multiple types of forces and deformations, our three-dimensional piece of material has not one, but many susceptibilities. Our aim in this chapter is to develop a formalism to write the stresses and deformations that are related by these susceptibilities (Sec. 3.1). The stresses must obey a force balance condition discussed in Sec. 3.2. Finally, we show in Sec. 3.3 that although one might naively expect that a piece of solid material may have up to 81 different susceptibilities, symmetry considerations imply that this number is much reduced, which provides us with a compact formulation of linear elasticity in dimensions larger than one.

3.1 Stress and strain

Here we introduce two quantities which respectively generalize the notions of force and displacement to an elastic material. This presentation follows that of paragraphs 1-5 and 7 of Ref. [10].

Stress

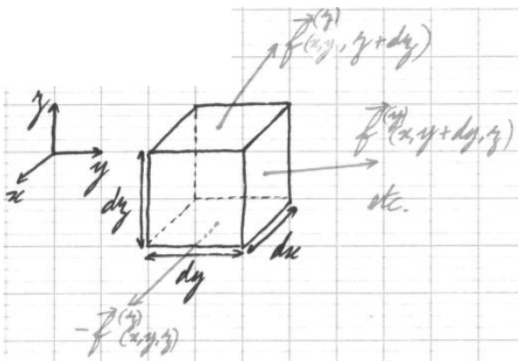

Consider cutting out a small cubic piece out of a material with dimensions $\mathrm{d}x$, $\mathrm{d}y$, $\mathrm{d}z$. What are the forces exerted on it by the rest of the material? There are several ways to answer this question. For instance, one may ask what force is exerted by the surroundings of the cube on its top face, with normal vector $\hat{\mathbf{z}}$. We denote this force as $\mathbf{f}^{(z)}$. It is a vector with three components $f_x^{(z)}$, $f_y^{(z)}$, $f_y^{(z)}$. Clearly this force depends on the altitude; therefore we denote the force exerted on the top face of the cube by $\mathbf{f}^{(z)}(x, y, z + \mathrm{d}z)$, while the force exerted *by* the cube on a hypothetical cube located below it is $\mathbf{f}^{(z)}(x, y, z)$. According to Newton's third law, the cube below thus exerts on the cube of interest a reciprocal force $-\mathbf{f}^{(z)}(x, y, z)$.

The same reasoning applies to the other faces of the cube, implying that we have three vector fields $\mathbf{f}^{(j)}$, where $j \in \{x, y, z\}$; equivalently we may say we have nine scalar fields $f_i^{(j)}$; but it turns out that the right way to think about the problem is to define a rank-2 tensor field through

$$\sigma_{ij}(\mathbf{r}) = \frac{f_i^{(j)}(\mathbf{r})}{\prod_{k \neq j} \mathrm{d}x_k}, \tag{3.1}$$

where $\mathbf{r}$ is the spatial position. According to this new notation, we can thus write, for instance:

$$\mathbf{f}^{(z)} = \mathrm{d}x\,\mathrm{d}y\,(\sigma_{xz}\hat{\mathbf{x}} + \sigma_{yz}\hat{\mathbf{y}} + \sigma_{zz}\hat{\mathbf{z}})\,, \tag{3.2}$$

making it clear that the component σ_{ij} is the force per unit surface exerted on face j in the direction i. This decomposition is made explicit below in the case of the top face of the cube:

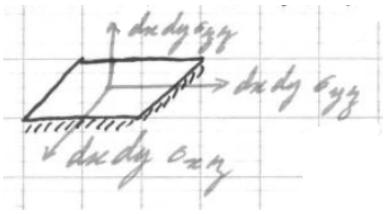

Here are a few examples of stress application geometries; all unspecified stress components are equal to zero:

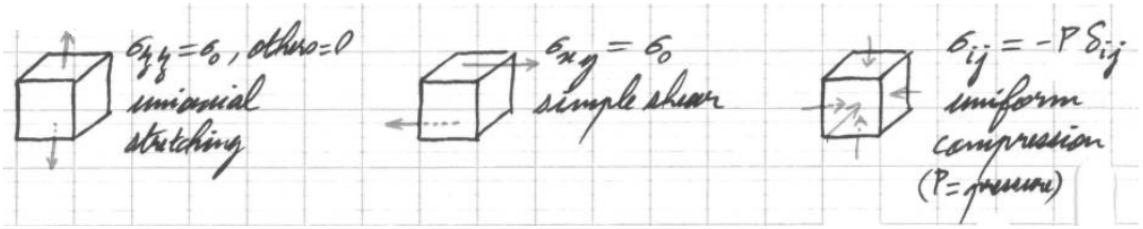

Here δ_{ij} is the Kroenecker symbol. Note the minus sign in front of P in the last case: a positive diagonal stress component $\sigma_{zz} > 0$ is associated with a material under tension, *i.e.*, subjected to a negative pressure.

Strain

Let us now look at how a cube deforms. Let $\mathbf{u}(x, y, z)$ be the displacement vector field of the material, which is materialized by the grey arrows in the schematic. A homogeneous diplacement $\mathbf{u} =$ constant does not distort the material, does not elicit any elastic stress and is thus irrelevant from the point of view of elasticity. By contrast, gradients of displacement, whereby one corner of the cube is being displaced by a different amount than the others, are crucial.

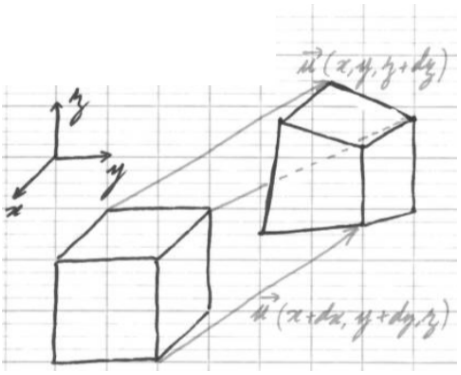

These considerations lead us to use as our primary characterization of the deformation the (linearized) strain tensor, which is build from the gradients of displacement:

$$\gamma_{ij} = \frac{1}{2}\left(\nabla_i u_j + \nabla_j u_i\right), \tag{3.3}$$

where $\nabla_i = \partial_i$ is the differentiation operator in direction i. More specifically, we define γ as the symmetrized displacement gradient tensor. We need not consider the antisymmetric part of the displacement gradient tensor in most cases, as it describes infinitesimal solid rotations of the medium, which do not induce any stresses.

Here are a few examples of two-dimensional deformations and the associated strain tensors:

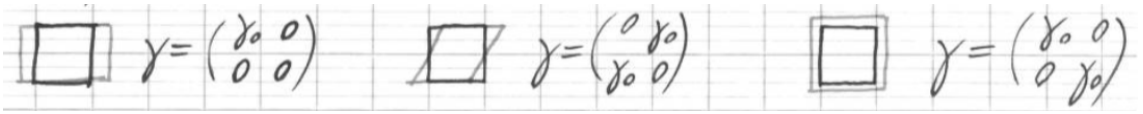

Note that the strain tensor is related to the change in volume of a small piece of material through

$$V_0 + \delta V = \det(I + \gamma) V_0, \tag{3.4}$$

where V_0 is the initial volume of the piece, δV the change and I the identity matrix.

3.2 Mechanical equilibrium

Consider the cube at the beginning of Sec. 3.1. The total force exerted on it by the rest of the material reads

$$\mathrm{d}\mathbf{f}_{\mathrm{material}} = \mathbf{f}^{(x)}(x+\mathrm{d}x,y,z) - \mathbf{f}^{(x)}(x,y,z) + \mathbf{f}^{(y)}(x,y+\mathrm{d}y,z) - \mathbf{f}^{(y)}(x,y,z) + \mathbf{f}^{(z)}(x,y,z+\mathrm{d}z) - \mathbf{f}^{(z)}(x,y,z) \quad (3.5)$$

In addition to these forces, we assume that the material is subjected to a force per unit volume $\mathbf{f}$, *e.g.*, a gravitational force. Applying force balance on the cube yields:

$$\mathrm{d}\mathbf{f}_{\mathrm{material}} + \mathbf{f}\,\mathrm{d}x\,\mathrm{d}y\,\mathrm{d}z = \mathbf{0}. \quad (3.6)$$

Combining Eqs. (3.1) and (3.5) to express the force balance condition Eq. (3.6) in term of the stress tensor, we find

$$\nabla_j \sigma_{ij} = -f_i, \quad (3.7)$$

which constitutes the force balance for our medium. Here and in the following we use the Einstein convention of summation over repeated indices. In practice, most elasticity problems boil down to using the (linear) relationship between σ and γ that we discuss in the next section, insert it in this force balance equation and solve for γ or for the displacement field $\mathbf{u}$ with appropriate boundary conditions (which, perhaps unexpectedly, is where the difficulty very often lies). We will do so in Tutorial 2.

In addition to force balance, we may consider torque balance on the cube of Sec. 3.1. This straightforwardly yields

$$\sigma_{ij} = \sigma_{ji} \quad (3.8)$$

Therefore σ and γ are both symmetric tensors.

3.3 Linear elasticity

As in Hooke's law, for small enough strain a linear relationship should exist between the components of σ_{ij} and γ_{kl}. In its most general form, this relationship reads

$$\sigma_{ij} = K_{ijkl}\gamma_{kl}, \tag{3.9}$$

where the elasticity tensor K_{ijkl} is constant (if the material is homogeneous) and of rank 4. Since each index in K_{ijkl} runs over three values x, y, z, the tensor has 81 entries in total for three-dimensional elasticity. Must we thus really specify 81 different elastic constants when characterizing a linear material? Fortunately not, as we discuss in this section.

Symmetry constraints

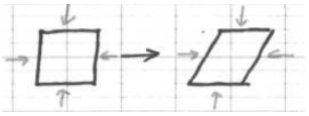

In an isotropic, achiral material, K_{ijkl} is considerably constrained by symmetry, and has only two independent elastic moduli at the end of the day. To get a feeling of the nature of these symmetry constraints, consider the illustration, where a square is compressed isotropically. Among all the components of K_{ijkl}, one describes the coupling between this compression geometry and a simple shear deformation. Looking at the picture however, it is clear that a piece of chiral material cannot deform in this way in response to uniform compression, as this would violate left-right symmetry. Thus the associated component of K_{ijkl} must vanish. The goal of this section is to systematically investigate all such simplifications to the elasticity tensor. Such symmetry considerations are useful in many contexts beyond linear elasticity, and chapters 5 and 6 both make use of them. To introduce the reader to the approach, here we provide a full derivation of K_{ijkl}.

We consider how K transforms under orthogonal transformations (*i.e.*, combinations of rotations and inversions) characterized by a change-of-basis tensor Q_{pi}; the orthogonality of the transformation implies

$$Q_{pi}Q_{pj} = \delta_{ij} \tag{3.10}$$

and the stress and strain, being proper tensors, transform in the following way:

$$\sigma'_{pq} = Q_{pi}Q_{qj}\sigma_{ij} \tag{3.11a}$$
$$\gamma'_{rs} = Q_{rk}Q_{sl}\gamma_{kl} \tag{3.11b}$$

where σ is the stress tensor in the old basis and σ' is the stress tensor in the new basis, and similarly for γ.

Since the material is isotropic, the relationship between the new tensors must be the same as between the old. Indeed, a material that has been rotated must respond in the same way as one that has not:

$$\sigma'_{pq} = K_{pqrs}\gamma'_{rs} \tag{3.12}$$

Note that there is *no* prime on K here: the rotated elasticiy tensor is the same as the unrotated one. Substituting Eqs. (3.11) yields

$$\begin{aligned} Q_{pi}Q_{pj}\sigma_{ij} &= K_{pqrs}\gamma'_{rs} \\ Q_{pi}Q_{pj}K_{ijkl}\gamma_{kl} &= K_{pqrs}\gamma'_{rs}. \end{aligned} \tag{3.13}$$

Combining Eqs. (3.10) and (3.11) yields $\gamma_{kl} = Q_{rk}Q_{sl}\gamma'_{rs}$, and so

$$Q_{pi}Q_{pj}Q_{rk}Q_{sl}K_{ijkl}\gamma'_{rs} = K_{pqrs}\gamma'_{rs}. \tag{3.14}$$

This equation is valid for any[1] strain tensor γ'_{rs}, implying that

$$K_{pqrs} = Q_{pi}Q_{pj}Q_{rk}Q_{sl}K_{ijkl} \tag{3.15}$$

for any orthogonal transformation Q. This condition can be expressed by saying that K is an isotropic tensor, which drastically constrains its form. We derive the most general form of a three-dimensional, rank-4 isotropic tensor in the next subsection.

[1] almost true

There are only three rank-4 isotropic tensors (reproduced from Ref. [11])

An isotropic tensor is one whose *components* are unchanged by rotation of the frame of reference. The trivial cases of this are the tensors of all orders whose components are all zero. All tensors of the zero[th] order are isotropic and there are no first order isotropic tensors. We have already met the only isotropic second order tensor, namely, δ_{ij}, but it is of interest to prove that it is the only one.

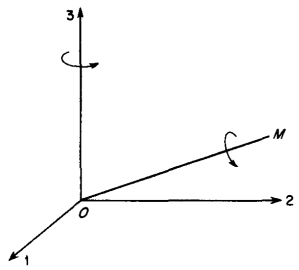

Fig. 2.6

Consider a general second order tensor A_{ij} and apply some particular rotations to it. The first of these is a rotation about a line equally inclined to all three coordinate axes, that is, with direction cosines all equal to $3^{-1/2}$. A rotation of 120° such as is shown in Fig. 2.6 can be made to carry the $O1$ axis into the $O3$ position, the $O2$ into the $O1$, and the $O3$ into the $O2$. Thus,

$$l_{31} = l_{12} = l_{23} = 1$$

and the other l_{ij} are zero. Hence, for example,

$$\bar{A}_{11} = A_{33} \quad \text{and} \quad \bar{A}_{23} = A_{12}.$$

However, if A is isotropic,

$$\bar{A}_{11} = A_{11} \quad \text{and} \quad \bar{A}_{23} = A_{23}$$

and so

$$\bar{A}_{11} = A_{11} = A_{33} \quad \text{and} \quad \bar{A}_{23} = A_{23} = A_{12}.$$

Applying this to each component in turn we see that

$$A_{11} = A_{22} = A_{33} \tag{2.7.1}$$

$$A_{23} = A_{32} = A_{31} = A_{13} = A_{12} = A_{21} \tag{2.7.2}$$

Now apply a rotation through a right angle about $O3$, so that $l_{12} = -l_{21} = l_{33} = 1$ and the other l_{ij} are zero. Then $\bar{A}_{12} = -A_{21}$ by the transformation and $\bar{A}_{12} = A_{12}$ by the requirement of isotropy. Thus by (2.7.2) $A_{12} = A_{21}$ and now $A_{12} = -A_{21}$ and the only way these can be simultaneously true is for them both to be zero. It follows that all the off diagonal components ($i \neq j$) are zero and all the diagonal ones are equal. Clearly a scalar multiple of an isotropic tensor is isotropic and so we may take $A_{ij} = \delta_{ij}$.

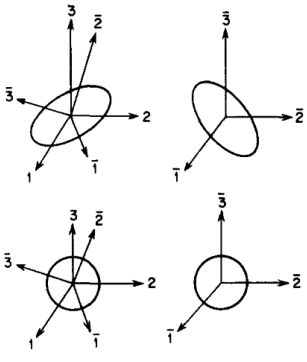
Fig. 2.7

The idea of isotropy for a second order tensor is connected with the geometrical figure of a sphere. We have noticed that $A_{ij}x_ix_j = 1$ is the equation of a quadric surface. The ellipsoid may be regarded as the typical quadric and clearly if its axes are unequal a rotation of the coordinate frame will require a different equation. A sphere, however, is invariant as a whole under rotation of axes and has the equation

$$x_1^2 + x_2^2 + x_3^2 = r^2.$$

This corresponds to the tensor $A_{ij} = \delta_{ij}/r^2$, so that isotropy is to be interpreted as geometrical invariance under rotation. (Cf. Fig. 2.7.)

Of tensors of the third order the only isotropic one is ϵ_{ijk}. We may see the isotropic character of this by writing $\bar{\epsilon}_{pqr} = \epsilon_{ijk}l_{ip}l_{jq}l_{kr}$ which is evidently the determinant

$$\bar{\epsilon}_{pqr} = \begin{vmatrix} l_{1p} & l_{1q} & l_{1r} \\ l_{2p} & l_{2q} & l_{2r} \\ l_{3p} & l_{3q} & l_{3r} \end{vmatrix}. \tag{2.7.3}$$

Now if any of the p, q, r are the same, this is a determinant with two identical columns and so vanishes. If $p = 1, q = 2, r = 3$, we know that this determinant is $+1$ so $\bar{\epsilon}_{123} = 1$. If p, q, r is an even permutation of 1, 2, 3 the sign of the determinant is unchanged, but if it is an odd permutation, $\bar{\epsilon}_{pqr} = -1$. However, this is just the definition of ϵ_{pqr} and so the components are unchanged by rotation.

The isotropic tensors of the fourth order are of some importance and there are three independent ones. It is clear that a product of isotropic tensors is isotropic so that we can immediately write down two such, namely, $\delta_{ij}\delta_{pq}$ and $\epsilon_{ijk}\epsilon_{kpq}$, but we need to work harder to find all the independent isotropic tensors. To outline the reasoning which is necessary to be sure we have all, it is convenient to divide the 81 components of a fourth order tensor T_{ijpq} into classes as follows.

Class	Character	Typical member
I	All suffixes the same	T_{1111}
II	Three suffixes the same	T_{1112}
III(i)	Suffixes the same in pairs	T_{1122}
(ii)		T_{1221}
(iii)		T_{1212}
IV	Only two suffixes the same	T_{1123}

(Since the suffixes must be equal to either 1, 2, or 3, it follows that at least two of them are the same.)

We now apply special rotations of the type shown in Fig. 2.6. These are listed in the table below by giving the nonzero l_{ij} of the transformation, and their effect on the typical member of each class is shown. We can write the transformation as an equality since the isotropic requirement is for the component to be unchanged. The second line is the effect of the transformation on another member of the class needed for the conclusion. Under class II, for example, we find $T_{1112} = T_{2223} = -T_{2221}$ and $T_{2223} = T_{2221}$ and the conclusion is that $T_{2221} = T_{2223} = 0$ and consequently all members of the class are zero. In the tensor representation of the class we put $\gamma_{ijpq} = 1$ if $i = j = p = q$ but zero otherwise. Then the representation of the subclasses of class III is given by a combination of Kronecker deltas and γ. For example, $\delta_{ij}\delta_{pq}$ will be 1 if $i = j$ and $p = q$, but the definition of the class excludes the possibility $i = j = p = q$ so that $\delta_{ij}\delta_{pq} - \gamma_{ijpq}$ represents it. Suppose then we make a linear combination of these and write

$$T_{ijpq} = a\delta_{ij}\delta_{pq} + b\delta_{ip}\delta_{jq} + c\delta_{iq}\delta_{jp} + (d - a - b - c)\gamma_{ijpq} \tag{2.7.4}$$

This certainly has isotropic properties under the rotations A, B, and C of the table but these are rather special since they leave a cube invariant as a whole. If we take a rotation that does not leave the cube invariant, for example, a rotation about $O3$ through an angle θ, then γ_{ijpq} is not invariant. Hence we must put $d = a + b + c$ and the general isotropic tensor can be written as a linear combination of the first three.

We observe that $\delta_{ij}\delta_{pq}$ is the product of two second order isotropic tensors and that the contracted product $\epsilon_{ijk}\epsilon_{kpq}$ is the difference of the other two. It is sometimes convenient to take the general isotropic tensor to be

$$T_{ijpq} = \lambda\delta_{ij}\delta_{pq} + \mu(\delta_{ip}\delta_{jq} + \delta_{iq}\delta_{jp}) + \nu(\delta_{ip}\delta_{jq} - \delta_{iq}\delta_{jp}) \tag{2.7.5}$$

The second term is symmetric with respect to the first and second or third and fourth indices and the third term is antisymmetric with respect to them.

Class	I	II	III(i)	III(ii)	III(iii)	IV
Operation A	Rotation about OM through 120°. $l_{12} = l_{31} = l_{23} = 1$.					
	$T_{1111} = T_{2222}$	$T_{1112} = T_{2223}$	$T_{1122} = T_{2233}$	$T_{1221} = T_{2332}$	$T_{1212} = T_{2323}$	$T_{1123} = T_{2231}$
Operation B	Rotation about $O3$ through 90°. $l_{12} = -l_{21} = l_{33} = 1$.					
	$T_{1111} = T_{2222}$	$T_{1112} = -T_{2221}$	$T_{1122} = T_{2211}$	$T_{1221} = T_{2112}$	$T_{1212} = T_{2121}$	$T_{1123} = -T_{2213}$
Operation C	Rotation to reverse the direction of OM. $l_{12} = l_{23} = l_{31} = -1$.					
	$T_{1111} = T_{3333}$	$T_{1112} = T_{3332}$ $T_{2223} = T_{2221}$	$T_{1122} = T_{3322}$	$T_{1221} = T_{3223}$	$T_{1212} = T_{3232}$	$T_{1123} = T_{3231}$ $T_{3231} = T_{2313}$
Conclusion	All equal	All zero	All equal	All equal	All equal	All zero
Representation	γ_{ijpq}		$\delta_{ij}\delta_{pq} - \gamma_{ijpq}$	$\delta_{iq}\delta_{jp} - \gamma_{iqjp}$	$\delta_{ip}\delta_{jq} - \gamma_{ipjq}$	

The two elastic moduli and their representations

We apply the result of the last subsection to the elasticity matrix K and start from the most general form for the isotropic, rank-4 tensor K:

$$K_{ijkl} = \lambda\delta_{ij}\delta_{kl} + \mu(\delta_{ik}\delta_{jl} + \delta_{il}\delta_{jk}) + \nu(\delta_{ik}\delta_{jl} - \delta_{il}\delta_{jk}), \tag{3.16}$$

Let us now consider using this form in Eq. (3.9). Since the strain tensor γ_{kl} is symmetric, the ν term in Eq. (3.16) will never contribute to the stress. As a result, the most general stress-strain relation for an isotropic, achiral three-dimensional medium reads

$$\sigma_{ij} = \lambda\gamma_{kk}\delta_{ij} + 2\mu\gamma_{ij}, \tag{3.17}$$

which involves only two elastic constants, as promised. The two coefficients λ and μ are known as the Lamé parameters of the material. While convenient when conducting calculations, λ does not have an immediate intuitive interpretation. As a result, two alternative, equivalent forms are often used instead of Eq. (3.17).

The first equivalent form is

$$\sigma_{ij} = K\gamma_{kk}\delta_{ij} + 2\mu\left(\gamma_{ij} - \frac{1}{d}\gamma_{kk}\delta_{ij}\right), \tag{3.18}$$

where d is the dimension of space, μ, the same quantity already encountered in Eq. (3.17), is known as the "shear modulus" and $K = \lambda + 2\mu/d$ is the "bulk modulus". To intuitively interpret these coefficients, consider the two following situations:

- Simple shear: $\nabla_y u_x = \Gamma$ and the other components of the deformation gradient tensor vanish. Then Eq. (3.18) yields

  $$\sigma_{xy} = \mu\Gamma. \tag{3.19}$$

  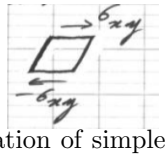

  Thus μ is simply the proportionality coefficient relating shear strain and shear stress in a situation of simple shear.

- Isotropic compression: $\nabla_x u_x = \nabla_y u_y = \ldots = \delta V/(dV_0)$, with the same definitions as in Eq. (3.4). Then $\sigma_{ij} = -P\delta_{ij}$, where the pressure P is given by

  $$P = -K\frac{\delta V}{V_0}, \tag{3.20}$$

  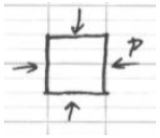

  i.e., K is the coefficient relating the relative volume change of the material to the pressure required to exact this change in the case of an isotropic, bulk deformation.

The second commonly used form of the stress-strain relation reads

$$\sigma_{ij} = \frac{E}{1+\nu}\left(\gamma_{ij} + \frac{\nu}{1-2\nu}\gamma_{kk}\delta_{ij}\right), \tag{3.21}$$

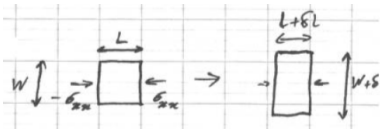

where E, the Young's modulus, is expressed in units of Pascals (force per unit surface, as is also the case for λ, μ and K) and ν is a dimensionless number known as the Poisson ratio. This form conveniently characterizes the axial compression of a material (see illustration for the notation), where σ_{xx} is the only non-vanishing component of the stress tensor. Then

$$\sigma_{xx} = E\frac{\delta L}{L} \tag{3.22a}$$

$$\frac{\delta W}{W} = -\nu\frac{\delta L}{L}, \tag{3.22b}$$

i.e., E is the coefficient relating the relative length change of the sample to the axial stress, and ν is the ratio of the relative change in width of the system relative to its relative change in length. The relative volume change in the sample is thus given by

$$\frac{\delta V}{V} = \left[1 - (d-1)\nu\right]\frac{\delta L}{L}, \tag{3.23}$$

implying that for $\nu = 1/(d-1)$ the material is incompressible. Surprisingly, the Poisson ratio of a material can be negative; it is then known as an "auxetic material". However mechanical stability requires that $\nu \in [-1, 1/(d-1)]$.

Appendices

Optional exercises

1. Prove that Eq. (3.4) is correct to lowest order in strain.
2. By applying torque balance on the cube of Sec. 3.1 establish Eq. (3.8).
3. Show that the unit tensor δ_{ij} is the only rank-2 isotropic tensor in three dimensions.
4. Show that there are two isotropic, rank-2 tensors in two dimensions, namely δ_{ij} and ϵ_{ij}, which has $\epsilon_{11} = \epsilon_{22} = 0$ and $\epsilon_{12} = -\epsilon_{21} = 1$. Note δ_{ij} is the only isotropic and achiral rank-2 2D tensor however.
5. Derive Eqs. (3.19), (3.20), (3.22a), (3.22b) and (3.23) from Eqs. (3.17), (3.18) and (3.21). Use these last three equations to express the pair (E, ν) as a function of (λ, μ) and (K, μ).
6. Check out these videos to find out what an auxetic material is (neither video makes me perfectly happy... let me know if you find better ones).
7. (difficult) What is the bending modulus of a bent plate? You can read paragraph 11 of Ref. [10] if you need help.

Learning goals for this chapter

- Be able to define the (linearized) stress and strain tensors.
- Be able to express the full stress and strain tensors for each of the little square illustrations of the chapter using any one of the three sets of elastic constants (λ, μ), (K, μ), (E, ν).
- Be able to state the force and torque balance conditions and prove them.
- Be able to state the stress-strain relations in terms of the sets of elastic constants (λ, μ) and (K, μ).
- Be able to explain the physical significance of the sets of elastic constants (K, μ) and (E, ν).
- Be able to apply symmetry considerations to constrain the form of an invariant tensor of rank up to three (being able to complete the corresponding optional exercises is a nice target in this respect).

Tutorial 2: Elasticity – stretching, bending and amplification

Physics of Complex Systems M2 – Biophysics

1 Linear response

Here we investigate the relationship between macroscopic linear elasticity theory and two possible underlying microscopic models.

1.1 Affine deformation of a hyperstatic network

Consider a triangular lattice of harmonic springs with stiffness α and rest length s in two dimensions. It behaves as an isotropic elastic solid on large length scales, and both its bulk and shear moduli can be expressed as functions of the stiffness α. Here we establish this relationship for the bulk modulus K.

1.1.1 Consider a deformation whereby the network is homogeneously and isotropically stretched, which results in a change of its volume V by δV. What is the form of the strain tensor γ associated with this deformation? Relate its components to δV.

1.1.2 Denoting by $r_i^{(a)}$ the initial position vector associated with vertex a, what is the displacement vector $u_i^{(a)}$ associated with the vertex following the deformation? Why is this type of deformation known as an "affine" deformation?

1.1.3 Write the work performed over the course of the deformation as a function of K and δV.

1.1.4 Write the microscopic expression for that same work, in terms of the spring stiffness α.

1.1.5 Deduce from this the relationship between K and α.

1.1.6 Generalizing this scaling to a hyperstatic 3D actin network of unspecified structure with bond length $s \simeq 400\,\mathrm{nm}$, what typical value do you expect for its bulk modulus?

1.2 Bending-dominated elasticity of a hypostatic network

We now introduce another lattice, illustrated in Fig. 1. Note that despite its rather large unit cell, all its vertices are equivalent.

1.2.1 Will stretching interactions be enough to stabilize this network? Why? Drawing inspiration from the middle and right-hand-side of Fig. 1, illustrate its floppy mode of isotropic deformation.

1.2.2 Consider an isotropic overall deformation of the network as in Sec. 1.1. One possible response of the network to this kind of deformation is an affine deformation. How does the cost of such a deformation scale with the bond stiffness α?

1.2.3 Let θ be the angle between two consecutive bonds in a deformed network, as indicated in the right-hand-side of Fig. 1. We consider a mode of overall isotropic deformation whereby all hinges bend by the same angle θ. What is the new area of the unit cell?

1.2.4 We now introduce a bending interaction by associating an energy $e = k_B T \ell_p \theta^2/2s$ with each hinge between two consecutive bonds of length s misaligned by θ. How does the energy per unit cell depend on θ?

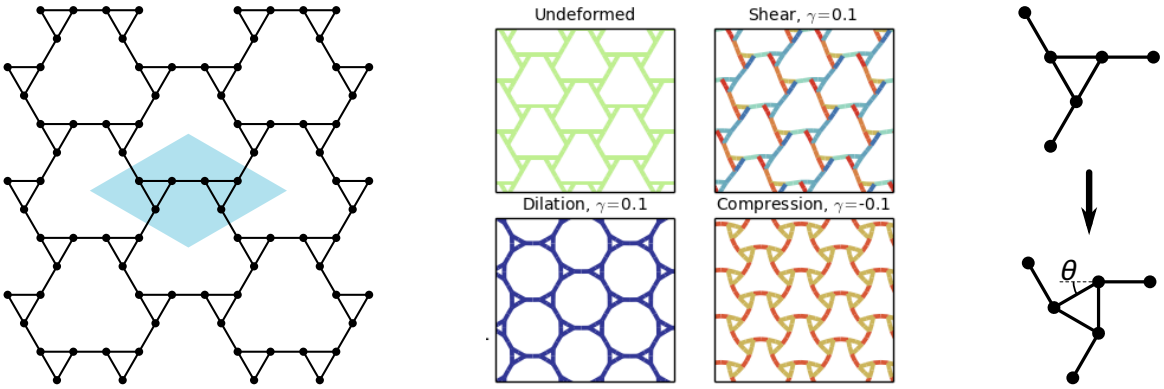

Figure 1: Simple bending-dominated lattice. *Left*: Ground-state structure with unit cell outlined in blue and vertices indicated by black circles. *Middle:* Numerically simulated deformations of a similar lattice. *Right:* Basic mode of network deformation considered here.

1.2.5 Assuming that the filaments constituting the network are much easier to bend than to stretch, how will the network deform in response to a uniform compression? Why is this known as a nonaffine deformation?

1.2.6 What is the bulk modulus of this network? Generalizing this scaling, what order of magnitude do you expect for the elastic moduli of an actin network?

1.3 Discussion

After examining these two examples, some conclusions are in order:

- Hypostatic networks avoid costly affine deformation by deforming along nonaffine soft modes.
- In the presence of a weak stabilizing interaction (*e.g.*, bending or prestress), these soft mode acquire a modulus without changing their spatial structure.
- The elasticity of hypostatic networks is nonaffine, yet linear at small deformations. In the case studied here it is bending-dominated (with a modulus $\propto k_B T \ell_p$ instead of $k_B T \ell_p^2$).

Although we computed bulk moduli because of the simplicity of the calculation involved, experimentalists virtually always report the shear moduli of their actin networks. Why?

2 Nonlinear response

2.1 Nonlinear bulk moduli

Beyond linear elasticity as explored in the main lectures, here we explore two possible microscopic causes for a nonlinear response at the material level.

2.1.1 *Constitutive nonlinearities.* Tutorial 1 showed us that a single bond in a network can respond nonlinearly to an applied force, for instance by buckling under compression and stiffening under extension. Using the force-extension relationship derived there, plot the pressure-volume relationship for the affinely deforming network of Sec. 1.1.

2.1.2 *Geometrical nonlinearities.* Plot the nonlinear pressure-volume relationship for the nonaffinely deforming network of Sec. 1.2. Discuss whether a nonlinear material response necessarily requires a material with an anharmonic Hamiltonian. If not, where does the nonlinearity come from?

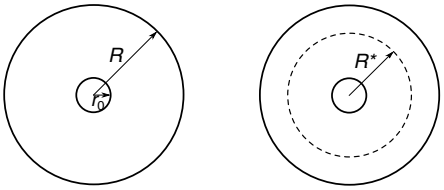

Figure 2: Geometry of our force transmission problem. *Left:* non-buckled case. *Right:* buckled case.

2.2 Active stress amplification by nonlinear materials

Contractile biological materials are typically composed of a fiber network with many actively contracting units embedded in it, be it molecular motors in the cytoskeleton or cells in an extracellular matrix. The contraction of the individual units induces a stress at the scale of the whole network, which is harnessed by the corresponding organism to perform a variety of functions. Here we assess how the elastic properties of the network affect this process of force generation in a very simplified spherical geometry. The force balance equation in this geometry reads

$$\frac{1}{r}\frac{\mathrm{d}}{\mathrm{d}r}\left(r\sigma_{rr}\right) - \frac{\sigma_{\theta\theta}}{r} = 0 \quad \text{in } d=2 \text{ dimensions} \tag{1a}$$

$$\frac{1}{r^2}\frac{\mathrm{d}}{\mathrm{d}r}\left(r^2\sigma_{rr}\right) - \frac{\sigma_{\theta\theta}+\sigma_{\phi\phi}}{r} = 0 \quad \text{in } d=3 \text{ dimensions} \tag{1b}$$

In addition, for a radial deformation $\mathbf{u}(r) = u(r)\hat{\mathbf{r}}$, the strain tensor in spherical coordinates is given by

$$\gamma = \begin{pmatrix} \partial_r u & 0 & 0 \\ 0 & u/r & 0 \\ 0 & 0 & u/r \end{pmatrix} \tag{2}$$

2.2.1 Rationalize the form of Eq. (1) by considering the balance of forces on a small $(\mathrm{d}r, \mathrm{d}\theta)$ element in two dimensions.

2.2.2 Solve the force balance equation for a linear elastic material and give the general form of the radial displacement $u(r)$ in a spherical geometry in $d = 2$, (then optionally generalize to arbitrary d).

2.2.3 We consider a localized active unit exerting a radial stress discontinuity in $r = r_0$:

$$\lim_{\epsilon\to 0}\left[\sigma_{rr}(r_0+\epsilon) - \sigma_{rr}(r_0-\epsilon)\right] = \sigma_0 \tag{3}$$

with $\sigma_0 > 0$. Denoting by $\mathbf{f}$ the body force density exerted by the active unit on the network, what is the force dipole $D = \int(\mathbf{r}\cdot\mathbf{f})\,\mathrm{d}V$ exerted by this active unit on the network?

2.2.4 Now working in $d = 2$ for simplicity, we assume a fixed boundary $u(R) = 0$ at a radius $r = R$ as illustrated in Fig. 2. Give the form of the stress tensor everywhere in the medium, distinguishing the $r < r_0$ region from the $r_0 < r < R$ region.

2.2.5 How is the stress dipole exerted by the medium on the fixed boundary related to the active force dipole? This is actually just a specific instance of a much more general relation [1].

2.2.6 We now consider a nonlinear material that can only sustain compressive stresses up to a certain threshold σ_b, then buckles. In the buckled state, the compressive stresses saturate to $-\sigma_b$, while the extensile stresses can be arbitrary large. Assuming the material buckles in a region $r < R^*$ and then behaves linearly for $r > R^*$, give the stress tensor everywhere in the system in the limit $\sigma_0 \gg \sigma_b \Rightarrow R^* \gg r_0$.

2.2.7 Determine R^*. In this new nonlinear case, how is the boundary stress related to the active force dipole? Explain this stress amplification qualitatively.

References

[1] Pierre Ronceray and Martin Lenz. Connecting local active forces to macroscopic stress in elastic media. *Soft Matter*, 11(8):1597–1605, January 2015.

Chapter 4

Molecular motors

The first tutorial and two previous chapters have described the mechanics of the cell as that of a passive material, bridging the gap between a microscopic characterization of individual filaments and a continuum medium approach of biopolymer gels. While these aspects are crucial to understand many cellular behaviors, the cell's most unique properties from the point of view of statistical mechanics stem from its out-of-equilibrium character. Indeed, the cell does not merely respond to outside forces; it expends energy to produce internal forces as well. To tackle these aspects, this chapter discusses microscopic models of two devices through which cells produce such forces. As we have seen in the second half of the second tutorial, these forces are transmitted to the macroscopic level by the same passive structures we have previously studied. In the next chapter, we will see that the resulting macroscopic stresses can be incorporated in fundamentally nonequilibrium theories of the cellular medium.

In Sec. 4.1, we study a mechanism through which biopolymers harness the chemical (free) energy that drives their polymerization to push against obstacles. Section 4.2 then presents the complementary mechanism through which cells exert pulling force thanks to specialized motor proteins that use the biopolymer as a track on which they walk.

4.1 The brownian ratchet

Actin and microtubules are very dynamic biopolymers, getting polymerized and depolymerized from either of their non-identical ends. They also get crosslinked, branched, cut and capped by specialized proteins. Here we present the most simplified model of the simplest manifestation of this intricate, incessant dynamics: the brownian ratchet, originally introduced in Ref. [12]. This model describes a filament that grows against an obstacle; since the filament polymerization is energetically favorable, the filament is able to push the obstacle even in the presence of an opposing force. We ask how the resulting pushing velocity depends on the value of the opposing force and on the surrounding actin concentration.

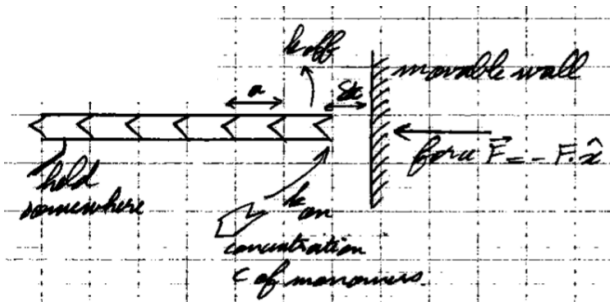

In the model illustrated here, the filament has two distinct ends: the "pointed end" on the left, and the "barbed end" on the right. The filament grows against a movable wall whose position fluctuates thermally. If the wall fluctuates too far to the left, it is blocked by the presence of the filament barbed end. It is moreover prevented from wandering too far to the right by a constant, externally applied leftwards force of amplitude F.

In many cell motility processes, the role of the wall is played by the membrane of the cell, a situation that we revisit in Tutorial 3. The left end of the filament is fixed and the filament itself is completely stiff. It is not completely stationary however, as individual monomers can be added or removed from its barbed end. The rate at which monomers are removed is constant and denoted as k_{off}. The monomer addition rule is more complex: denoting the size of an individual monomer by a, we assume that if the distance δx between the barbed end and the wall is smaller than a, then there is insufficient space for monomer addition and the addition rate is zero. On the other hand, if the wall is far enough not to hinder the polymerization process ($\delta x > a$), then the rate for adding a new monomer is proportional to the concentration c of monomeric actin in the surrounding solution, and denoted by $k_{\text{on}}c$.

Let us first consider the simple case where there is no wall, or equivalently where the force on the wall is so small that the wall is virtually always far away from the filament. In that case, the polymerization rate is $k_{\text{on}}c$ and the depolymerization rate k_{off}. Therefore the average number of monomers added per unit time is $k_{\text{on}}c - k_{\text{off}}$ and the

average change in filament length reads

$$\frac{\mathrm{d}\langle L\rangle}{\mathrm{d}t} = a(k_{\mathrm{on}}c - k_{\mathrm{off}}) = ak_{\mathrm{off}}\left(\frac{c}{c^*} - 1\right), \tag{4.1}$$

where we have defined $c^* = k_{\mathrm{off}}/k_{\mathrm{on}}$ the equilibrium concentration at which as many monomers are added from the filament as are removed on average. If the surrounding actin concentration is larger than c^*, the filament grows. If it is smaller, it shrinks.

Let us now consider the presence of a substantial outside pushing force F. The rate of monomer addition depends on $\mathcal{P}(\delta x \geqslant a)$, the probability that polymerization is allowed. Qualitatively, if the pushing force is large, the gap between filament and wall tends to be smaller, monomer addition is more difficult and polymerization slows down or reverses. Quantitatively, we estimate the probability $\mathcal{P}(\delta x \geqslant a)$ by assuming that the wall quickly reaches a state of thermal equilibrium, and therefore that the probability density for δx is given by the Boltzmann distribution:

$$p(\delta x) = \frac{F}{k_B T} e^{-F\delta x/k_B T}, \tag{4.2}$$

Where the normalization takes into account that δx can take any positive value but is never negative. As a result,

$$\mathcal{P}(\delta x > a) = \int_a^{+\infty} p(\delta x)\,\mathrm{d}(\delta x) = e^{-Fa/k_B T} \tag{4.3}$$

and therefore the polymerization rate at a given instant is

$$\begin{cases} k_{\mathrm{off}}\frac{c}{c^*} & \text{with probability } \mathcal{P}(\delta x \geqslant a) \\ 0 & \text{with probability } \mathcal{P}(\delta x < a) = 1 - \mathcal{P}(\delta x \geqslant a) \end{cases} \tag{4.4}$$

and so on average the polymerization velocity reads

$$v = \frac{\mathrm{d}\langle L\rangle}{\mathrm{d}t} = ak_{\mathrm{off}}\left(\frac{c}{c^*}e^{-Fa/k_B T} - 1\right). \tag{4.5}$$

Assuming that the surrounding actin concentration is larger than c^*, the velocity/force curve for the filament is therefore as in the illustration. As discussed before, an increase in the pushing force slows the filament growth, a prediction confirmed by experiments on collections of actin filaments. Whether the v vs. F curve is convex, as predicted here, or concave depends on the type of system used. In all cases however, there is a certain critical force $F_s = (k_B T/a)\ln(c/c^*)$ known as the "stall force" at which the pushing force of the filament exactly balances the outside force. Recalling that for an ideal solution, the chemical potential difference between an unbound monomer and a bound monomer is given by $\Delta\mu = k_B T \ln(c/c^*)$, we can make sense of the value of the stall force through the equality

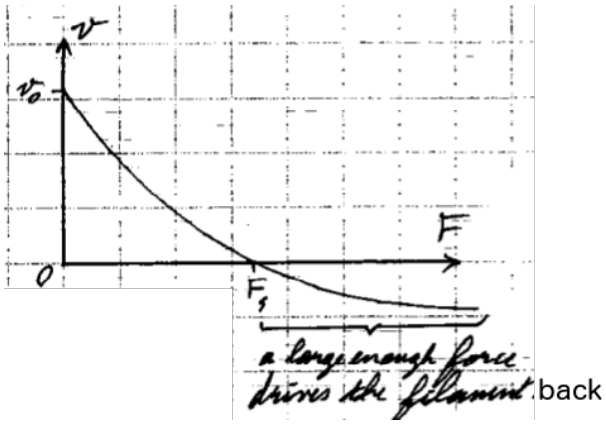

$$F_s a = \Delta\mu, \tag{4.6}$$

i.e., at the stall force, the mechanical work resulting from the addition of a monomer equals the chemical work provided by its polymerization. Note that the situation $F = F_s$ corresponds to the special case of a reversible dynamics; in general, $Fa \leqslant \Delta\mu$ for a growing filament. Due to their thermodynamic nature, these statements are clearly valid well beyond the specifics of the brownian ratchet model.

Overall, this example demonstrates that a polymerizing filament can function as a simple monothermal chemical engine. In contrast with *e.g.*, a Carnot engine, which takes heat from a high temperature heat reservoir and dumps it to a low temperature heat reservoir, a cyclic chemical engine takes particles (here actin monomers) from a high chemical potential particle reservoir and dumps them to a low chemical potential particle reservoir. The model presented here only describes the first half of this process, and we would need to supplement it with a model for actin depolymerization at the pointed end to obtain a fully *cyclic* engine. Such an engine would essentially recapitulate the "treadmilling" motion discussed in Sec. 1.6.

4.2 Motor proteins

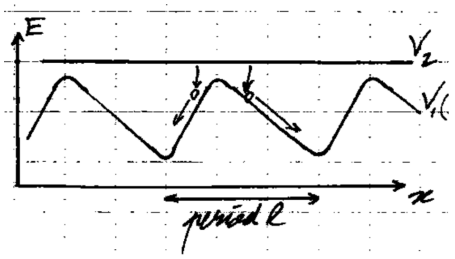

We now discuss perhaps the most iconic force-generating machinery of the cell, namely members of the myosin, kinesin and dynein superfamilies presented in Sec. 1.6. The motor heads of these proteins alternate between a filament-bound state where they strongly localize to dedicated binding sites, and an unbound state where their diffusion is largely unconstrained by the presence of the filament. A simple model could consist in representing the motor head as a particle evolving along a one-dimensional line with coordinate x and associating two potentials with each of these two states (see illustration).

Let us first present an oversimplified argument explaining the motion of the motor in this simple model. In the unbound state, the motor freely diffuses along the constant potential V_2, resulting in a spatially homogeneous density of motor heads. From that state, the motor head may bind either onto the steep left-leaning slope of $V_1(x)$ or to its gentle right-leaning-slope. In the former case, the motor slides left by a relatively small amount. In the latter, it slides to the right by a larger quantity. This imbalance implies that the motor tends to slide to the right more than to the left, and thus predicts a right-directed motor motion.

In this section we show that while it is partially correct, this schematic view is incomplete. Indeed, the details of how the system is driven out of equilibrium by the consumption of ATP matter a lot, and can actually in some cases induce a leftwards flow in the situation illustrated above. More specifically, we demonstrate that the steady-state motor flow along x can be directly expressed as a function of a signed quantity that describes how much the condition of detailed balance (which is associated with equilibrium statistics) is violated in the system.

Diffusion in an energy potential

In a first approach, we only consider the motion of our particle in the bound potential $V_1(x)$, forgetting for now about the unbound state associated with V_2. We denote its probability density function as a function of time $P(x,t)$, and discuss the evolution of this quantity.

The probability density function $P(x,t)$ evolves according to the Fokker-Planck equation. As a reminder, the Fokker-Planck equation can be understood by viewing $P(x,t)$ as a density of diffusing, non-interacting particles. The equation then plays the role of a mass conservation equation

$$\partial_t P(x,t) = -\partial_x J(x,t), \tag{4.7}$$

where the particle current $J(x,t)$ (known as the probability current in the language of the Fokker-Planck equation) has two contributions:

$$J = -D\partial_x P + P \times \mu F(x), \tag{4.8}$$

where the first term is a diffusion current similar as in Fick's law. The second term is a convective term and involves the mobility μ of a particle and the local force field $F = -\partial_x V_1$ induced on each particle by the external potential $V_1(x)$. In this language, the Fokker-Planck equation is a biased diffusion equation. Inserting Einstein's relation $D = \mu k_B T$ finally yields

$$\partial_t P = D\partial_x \left(\partial_x P + \frac{P}{k_B T} \partial_x V_1 \right). \tag{4.9}$$

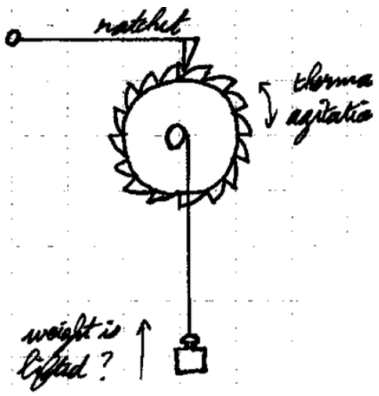

Before considering the full two-potential situation illustrated at the beginning of the present section, we wonder whether the single-potential dynamics of Eq. (4.9) allows for the existence of a steady-state, directed motor current as required for biological transport. This is actually equivalent to asking a famous textbook physics question, namely whether Feynman's ratchet can lift a weight. This imaginary asymmetric cogwheel, illustrated on the right, is subjected to thermal fluctuations but also equipped with a ratchet meant to block the thermal fluctuations that would have the wheel rotate clockwise, while allowing it to rotate in the opposite direction. If that trick worked (which it doesn't if the ratchet is at the same temperature as the wheel), the counterclockwise motion of the wheel could be used to perform work, for instance by lifting a weight.

Denoting by x the angle of the wheel and considering $V_1(x)$ as the gravitational energy of the ratchet, one can model this device using Fokker-Planck equation. Here we use this framework to

discuss the impossibility of steady-state directed motion in Feynman's ratchet. Indeed, a steady-state condition implies a constant probability density fonction $P(x)$. Combining the resulting condition $\partial_t P = 0$ with Eq. (4.7) implies $J(x,t) = J_0$, where J_0 is a constant. Inserting this condition in Eq. (4.8) yields

$$\begin{aligned}
\partial_x P(x) + \frac{P(x)}{k_B T}\partial_x V_1(x) &= -\frac{J_0}{D} \\
\partial_x[\ln P(x)] + \partial_x\left(\frac{V_1(x)}{k_B T}\right) &= -\frac{J_0}{P(x)D} \\
P(x) &= P_0 e^{-V_1(x)/k_B T} \times \exp\left[-\frac{J_0}{k_B T}\int^x \frac{\mathrm{d}x'}{P(x')}\right],
\end{aligned} \tag{4.10}$$

where P_0 is a constant. This last equality boils down to a Boltzmann distribution in the special case $J_0 = 0$.

To determine the value of J_0, we remark that in a periodic potential at steady-state the probability density function must also be periodic, implying

$$\frac{P(\ell)}{P(0)} = 1 \quad \Leftrightarrow \quad \exp\left[\frac{V_1(0) - V_1(\ell)}{k_B T}\right] \times \exp\left[-\frac{J_0}{k_B T}\int_0^\ell \frac{\mathrm{d}x'}{P(x')}\right] = 1 \tag{4.11}$$

The periodicity of V_1 implies that the first exponential equals one, and therefore that

$$\frac{J_0}{D}\int_0^\ell \frac{\mathrm{d}x}{P(x)} = 0 \tag{4.12}$$

Since P is always positive and finite almost everywhere, the integral is strictly positive, implying $J_0 = 0$. Thus the probability density distribution is an equilibrium one. This implies

$$J(x,t) = -D\partial_x P - \frac{D}{k_B T}P\partial_x V_1 = D\frac{\partial_x V_1}{k_B T}P_0 e^{-V_1/k_B T} - \frac{D}{k_B T}P_0 e^{-V_1/k_B T}\partial_x V_1 = 0, \tag{4.13}$$

i.e., at equilibrium the diffusive and convective currents exactly compensate, thus abolishing the possibility of a steady-state ratchet rotation/motor transport in a single potential.

Motor current

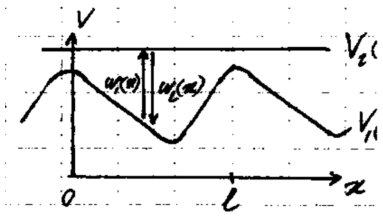

Having now established that our two-potential system, which is meant to represent the attachment-detachment dynamics of the molecular motor, is required for directed motion, we return to our original diagram, which we reproduce in the illustration. By convention, we moreover choose to set $x = 0$ in the location where the potential $V_1(x)$ has its maximum. We introduce the detachment rate $\omega_1(x)$, that is to say the probability per unit time that a particle located at position x in potential 1 switches to potential 2 (the particle remains at position x during the switch). We likewise define the attachment rate $\omega_2(x)$. This yields a system of coupled Fokker-Planck equations for the probability densities $P_1(x,t)$, $P_2(x,t)$ of being at position x at time t while in state 1 or 2 respectively:

$$\partial_t P_1(x,t) = -\partial_x J_1(x,t) - \omega_1(x)P_1(x,t) + \omega_2(x)P_2(x,t) \tag{4.14a}$$
$$\partial_t P_2(x,t) = -\partial_x J_2(x,t) + \omega_1(x)P_1(x,t) - \omega_2(x)P_2(x,t), \tag{4.14b}$$

where the probability currents are similar to the one discussed in Eq. (4.8):

$$J_1(x,t) = -D\partial_x P_1(x,t) - \frac{D}{k_B T}P_1(x,t)\partial_x V_1(x) \tag{4.15a}$$
$$J_2(x,t) = -D\partial_x P_2(x,t). \tag{4.15b}$$

Note that the convective current in the last equation vanishes due to the fact that V_2 is constant in our example.

Here we consider the stationary state $\partial_t P_1 = \partial_t P_2 = 0$, which describes the steady-state operation of the motor after many ATP hydrolysis cycles. In this regime, the system forgets the location of its initial condition and $P_1(x)$ as well as $P_2(x)$ are ℓ-periodic functions of space, as are $\omega_1(x)$, $\omega_2(x)$ and $V_1(x)$. The total motor current at location x is $J(x) = J_1(x) + J_2(x)$. This is our quantity of interest, since it describes the average rate at which motors move to

the right. Summing Eqs. (4.14a) and (4.14b) yields $\partial_x J = 0$, and therefore J is a constant. We can thus write:

$$\begin{aligned} J &= \frac{1}{\ell}\int_0^\ell J\,\mathrm{d}x \\ &= \frac{1}{\ell}\int_0^\ell J_1(x)\,\mathrm{d}x + \frac{1}{\ell}\int_0^\ell J_2(x)\,\mathrm{d}x \\ &= \frac{1}{\ell}\int_0^\ell J_1(x)\,\mathrm{d}x - \frac{D}{\ell}\int_0^\ell \partial_x P_2(x)\,\mathrm{d}x \\ &= \frac{1}{\ell}\int_0^\ell J_1(x)\,\mathrm{d}x - \frac{D}{\ell}[P_2(\ell) - P_2(0)], \end{aligned} \tag{4.16}$$

and due to P_2's periodicity, the last term vanishes, implying that we only need to compute $J_1(x)$ to obtain the value of J:

$$J = \frac{1}{\ell}\int_0^\ell J_1(x)\,\mathrm{d}x \tag{4.17}$$

We now ask whether P_1 and P_2 could be equilibrium probability distributions, *i.e.*, Boltzmann distributions. We specifically ask:

1. Do motors move if P_1 and P_2 are equilibrium distributions?
2. What are the conditions on ω_1, ω_2 for such an equilibrium to indeed be possible?

The equilibrium distributions discussed here are characterized by

$$P_1^{\mathrm{eq}}(x) \propto \exp\left[-\frac{V_1}{k_B T}\right] \tag{4.18a}$$

$$P_2^{\mathrm{eq}}(x) \propto \exp\left[-\frac{V_2}{k_B T}\right] = \text{constant here} \tag{4.18b}$$

Similar to the calculation leading to Eq. (4.13), inserting these two distributions into Eq. (4.15) yields $J_1^{\mathrm{eq}} = J_2^{\mathrm{eq}} = 0$, which answers our first question: if the system is allowed to go to equilibrium, then no net motor motion occurs. In addition, inserting these same distributions into Eq. (4.14) yields

$$\omega_1(x) P_1^{\mathrm{eq}}(x) = \omega_2(x) P_2^{\mathrm{eq}}(x) \tag{4.19}$$

This condition, known as "detailed balance" should be viewed as a requirement for a set of attachment and detachment rates to be compatible with equilibrium statistics. We can rephrase it as meaning that the system can only reach equilibrium if

$$\frac{\omega_1(x) e^{-V_1(x)/k_B T}}{\omega_2(x)} = \text{constant} \tag{4.20}$$

To understand the physical meaning of this condition, consider the illustration. The central circle highlights the position x in potential 1. There are six fluxes of probability into and out of this state: motors coming from and leaving from the left, motors coming from and leaving for position x in potential 2, and motors coming from and leaving from the right. The system is said to be at steady state when $P_1(x)$ does not depend on time, *i.e.* when the sum of the six probability fluxes is equal to zero. That condition is one of "global balance": the probability fluxes in and out of the state considered balance overall. The condition of detailed balance is more demanding. Indeed, it requires that the fluxes discussed above compensate not only globally, but two by two. Thus the flux coming in from potential 2 must exactly balance the flux going out to potential 2, which is precisely the condition expressed by Eq. (4.19). In addition the flux coming in from the left must exactly balance the flux coming out from the left, which is guaranteed by the Boltzmann form of P_1^{eq}, and similarly for the fluxes on the right. Looking at the illustration, this all means that the arrows must compensate not only globally, but in pairs.

In the presence of an outside energy source, in this case the continuous supply and consumption of ATP, the rates ω_1 and ω_2 governing the dynamics of the motor may violate detailed balance, which can result in motor motion. In the following discussion we choose to fix $\omega_2 =$ constant for simplicity, and quantify the violation of detailed balance through the function

$$\gamma(x) = \frac{\omega_1(x) e^{-V_1(x)/k_B T}}{\omega_2 \times \frac{1}{\ell}\int_0^\ell e^{-V_1(x)/k_B T}\,\mathrm{d}x}. \tag{4.21}$$

Clearly the equality of Eq. (4.20) is equivalent to the statement $\gamma(x) = \text{constant}$. Introducing the Fourier decomposition

$$\gamma(x) = \tilde{\gamma}_0 + \sum_{n=1}^{+\infty} \left[\tilde{\gamma}_n^c \cos\left(\frac{2\pi n x}{\ell}\right) + \tilde{\gamma}_n^s \sin\left(\frac{2\pi n x}{\ell}\right) \right], \tag{4.22}$$

this implies that detailed balance is satisfied if and only if all $\tilde{\gamma}_n^c$, $\tilde{\gamma}_n^s$ vanish. These coefficients thus quantify the "non-equilibrium-ness" of the system.

To compute the motor current as a function of the $\tilde{\gamma}_n^{c/s}$ terms, we consider the limit where the convection in V_1 is much faster than diffusion; this limit reflects the fast equilibration of the motor heads following binding in the numerical simulation movie presented in Sec. 1.6. This implies $\mu V_1 \gg D$, or equivalently $k_B T \ll V_1$, meaning that binding is much stronger than thermal agitation. In this limit, we propose a small-$k_B T$ expansion for P_1, namely:

$$P_1(x) = P_1^0(x) + k_B T\, \delta P_1(x) + \mathcal{O}(k_B T^2). \tag{4.23}$$

Inserting this expansion into Eqs. (4.14) and (4.15) to dominant order in $1/k_B T$, the motion in the potential dominates and the transitions with state 2 are negligible:

$$\partial_x P_1^0(x) + \frac{P_1^0}{k_B T} \partial_x V_1(x) = 0 \qquad \text{with} \qquad P_1^0 \ \ell\text{-periodic.} \tag{4.24}$$

This implies

$$P_1^0(x) = \frac{e^{-V_1(x)/k_B T}}{\int_0^\ell e^{-V_1(x')/k_B T}\, \mathrm{d}x'}, \tag{4.25}$$

where the integration constant was chosen in order for $P_1^0(x)$ to be normalized over one period of the potential. This expression means that the fast convection makes the system quickly settle into a quasi-equilibrium state. As discussed before, the leading term of Eq. (4.25) cannot give rise to any motor current, implying that information about the motor motion only emerges at the next order in $k_B T$:

$$\partial_x J_1 = -\omega_1(x) P_1^0(x) + \omega_2 P_2(x) = \omega_2 \left[P_2(x) - \frac{\gamma(x)}{\ell} \right] \tag{4.26a}$$

$$\partial_x J_2 = \omega_1(x) P_1^0(x) - \omega_2 P_2(x) = \omega_2 \left[\frac{\gamma(x)}{\ell} - P_2(x) \right] \tag{4.26b}$$

with

$$J_1(x) = -D\, \delta P_1(x)\, \partial_x V_1(x) \tag{4.27a}$$

$$J_2(x) = -D\, \partial_x P_2(x). \tag{4.27b}$$

Equation (4.27a) implies that $J_1(x)$ vanishes in $x = 0$ since $\partial_x V_1(0) = 0$. Thus using Eq. (4.26a) we have

$$\begin{aligned} J_1(x) &= \int_0^x \partial_x J_1(x')\, \mathrm{d}x' \\ &= \omega_2 \int_0^x \left[P_2(x') - \frac{\gamma(x')}{\ell} \right] \mathrm{d}x' \end{aligned} \tag{4.28}$$

We thus need to compute $P_2(x)$ to obtain $J_1(x)$, which we in turn need to compute J. Combining Eqs. (4.26b) and (4.27b) we obtain

$$\partial_x^2 P_2(x) - \frac{\omega_2}{D} P_2(x) = -\frac{\omega_2}{D\ell} \gamma(x). \tag{4.29}$$

Therefore, in Fourier space

$$P_2(x) = \frac{\tilde{\gamma}_0}{\ell} + \frac{1}{\ell} \sum_{n=1}^{+\infty} \frac{1}{1 + \frac{D}{\ell^2 \omega_2} (2\pi n)^2} \left[\tilde{\gamma}_n^c \cos\left(\frac{2\pi n x}{\ell}\right) + \tilde{\gamma}_n^s \sin\left(\frac{2\pi n x}{\ell}\right) \right]. \tag{4.30}$$

Inserting this into Eq. (4.28), we find

$$J_1(x) = \omega_2 \int_0^x \left\{ \sum_{n=1}^{+\infty} \frac{-\frac{D}{\ell^2 \omega_2} (2\pi n)^2}{1 + \frac{D}{\ell^2 \omega_2} (2\pi n)^2} \left[\tilde{\gamma}_n^c \cos\left(\frac{2\pi n x}{\ell}\right) + \tilde{\gamma}_n^s \sin\left(\frac{2\pi n x}{\ell}\right) \right] \right\} \frac{\mathrm{d}x}{\ell}. \tag{4.31}$$

Therefore, as expected $\tilde{\gamma}_0$ clearly does not contribute to the current. Finally, inserting this expression into Eq. (4.17) and integrating the cosines and sines twice yields

$$J = -\frac{D}{\ell^2} \sum_{n=1}^{+\infty} \frac{2\pi n \tilde{\gamma}_n^s}{1 + \frac{D}{\ell^2 \omega_2} (2\pi n)^2}. \tag{4.32}$$

This equation directly expresses the magnitude of the net motor motion as a function of the violation of the detailed balance condition (as expressed by the values of the detailed-balance-violating coefficients $\tilde{\gamma}_n^s$).

Qualitative discussion

Equation (4.32) expresses that two conditions are required to obtain a non-vanishing motor current:

- The existence of nonequilibrium transitions between states 1 and 2 (manifested by violations of the detailed balance condition)
- A left-right asymmetry favoring directional motion (manifested by non-zero values for the asymmetric coefficients $\tilde{\gamma}_n^s$ as opposed to the symmetrical $\tilde{\gamma}_n^c$).

Note that the sign of the asymmetry of $\tilde{\gamma}(x)$ is not necessarily the same as that of $V_1(x)$: thus depending on the details of the transition rates, motor motion in any given potential profile can be either right-directed or left-directed, contrary to the simplistic description given at the beginning of this chapter.

Concretely, if $\tilde{\gamma}_1^s < 0$ and all other Fourier coefficients of γ vanish, we have the picture illustrated below:

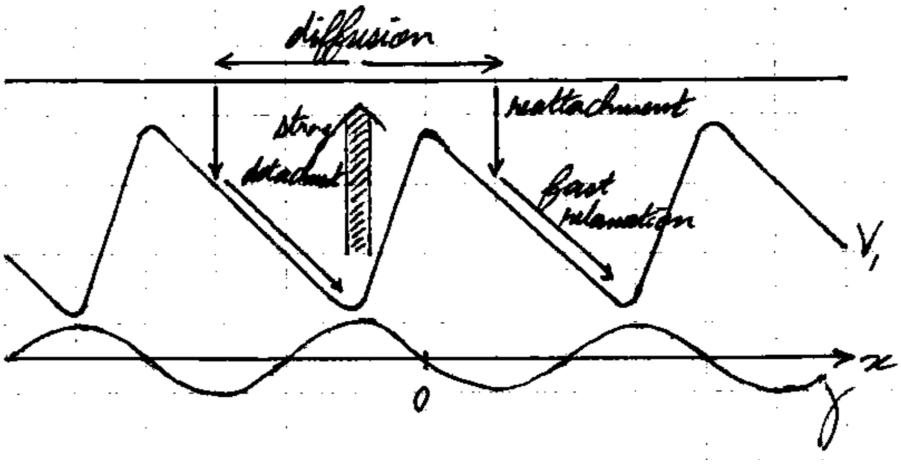

To understand this figure, picture a motor starting at the bottom of the well just to the left of $x = 0$. In this well, the value of γ is more than the average of γ, and therefore the detachment rate exceeds that value prescribed by detailed balance. As a result, there is a net flux of particles from the bottom of the well towards state 2, pictured by the thick arrow. Once in state 2, the particles diffuse symmetrically to the left and the right. They reattach after a certain typical time. This reattachment process is pictured by the downwards arrows, consistent with the fact that the particle flow is predominantly from state 2 towards state 1 in the regions where γ is low. Consider however the respective situations of a particle reattaching to the left and to the right of the central well. In the former case, the particle immediately slides back to its initial position. In the latter case, it moves to the bottom of the next well. Since the two trajectories are equally likely, the overall process results in a net rightwards motion of the particles.

Appendices

Optional exercises

1. Let us write the master equation for the probability to have n monomers in the filament in the Brownian ratchet model as $\partial_t p(n,t) = \bar{k}_{\rm on} p(n-1,t) + k_{\rm off} p(n+1,t) - (\bar{k}_{\rm on} + k_{\rm off}) p(n,t)$. While in the example studied in this chapter only $\bar{k}_{\rm on} = k_{\rm on} c \exp(-Fa/k_B T)$ depends on the force F, in the most general case both $\bar{k}_{\rm on}$ and $k_{\rm off}$ may be force dependent. Nevertheless these expression are constrained by the detailed balance condition. Express this constraint.
2. Rederive Eq. (4.6) from this constraint only.
3. Can the dynamics of our formulation of Feynman's ratchet give rise to a steady-state that violates detailed balance? Why?
4. What is the mean velocity of the motor considered in Sec. 4.2?
5. (requires a little work) Consider subjecting the motor described in Sec. 4.2 to an outside force f. How does the motor velocity depend on the applied force?
6. Derive the motor current/velocity as a function of V_1 only in the special case where ω_1 and ω_2 are both constants.

Learning goals for this chapter

- Be able to explain the mechanism through which a growing filament exerts a force on an obstacle.
- Be able to rederive the force-velocity relation of the brownian ratchet.
- Be able to compute the stall force of a growing filament from equilibrium arguments.
- Be able to reproduce our discussions of the single-potential Fokker-Planck equation without guidance, and to reproduce derivations similar to the two-potential discussion with some guidance.
- Be able to reconstitute and explain the model detailed in Eqs. (4.14) and Eqs. (4.15).
- Be able to explain the relationship between detailed balance and motor motion.
- Understand and be able to reconstitute the qualitative discussion at the end of Sec. 4.2.

Chapter 5

Active matter

In contrast with the microscopic models presented in chapters 2 and 4 and in the first two tutorials, many theoretical descriptions of living materials take place on macroscopic scales describing filaments, motors and sometimes collections of many cells not as individual entities, but as a continuum medium with inherent nonequilibrium activity. The microscopic causes of this activity are not specifically investigated in these models. Instead, they are introduced in the most general way allowed by symmetry, similar to the discussion of Sec. 3.3. Here we discuss this foundation in Sec. 5.1, then demonstrate some of the typical behaviors induced by these active terms, namely flow (in Sec. 5.2) and hydrodynamic instability (Sec. 5.3).

5.1 Hydrodynamic theories

Many active matter theories draw inspiration from so-called generalized hydrodynamics theories. Such theories, which comprise the Navier-Stokes equation, heat transport equations or those governing superfluidity or the hydrodynamics of liquid crystals, describe the flow or deformations of a continuum medium on long length and time scales. Such length scales must be longer than any molecular length scales in the system (*e.g.*, the typical distance between two proteins), and the time scales longer than any microscopic time scale (*e.g.*, the time required for a single molecular motor to take a step). The two limits are related. Indeed, as we consider the system's relaxation over larger and larger length scales L, some of the system's relaxation time scales (for instance the diffusion time L^2/D) become longer and longer, and thus end up dominating the system's long-time dynamics. Here we study the relaxation modes of the system over these so-called *hydrodynamic* time scales, *i.e.*, time scales that diverge as the system's size diverges. Remarkably, when considering these length and time scales, generalized hydrodynamics provides us with the equations of motion for the system based solely on symmetry considerations, as opposed to having to specify a microscopic model. In this sense, the derivation of a generalized hydrodynamic theory is close in spirit to the derivation of the linear elastic theory of Sec. 3.3.

To illustrate the steps involved in the derivation of such a theory, we consider the relaxation of an unspecified conserved quantity. Such a quantity is defined as one that is exchanged between neighboring regions of the system but never created or destroyed. For reasons that are laid out in the following, the relaxation of such a quantity is associated with a hydrodynamic time scale. Let us monitor the transport of such a quantity $\rho(x,t)$ in a one-dimensional system:

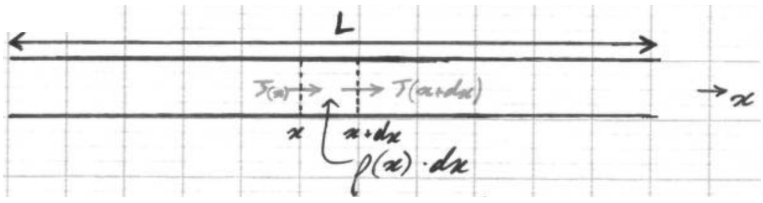

Because ρ is conserved, the amount of ρ contained in the box located between x and $x+\mathrm{d}x$ can only change by being exchanged with the neighboring regions. The rate of exchange is described by the position-dependent current $J(x,t)$, yielding:

$$\partial_t \left[\rho(x,t)\mathrm{d}x\right] = J(x,t) - J(x+\mathrm{d}x,t) \tag{5.1}$$

If we assume that the typical heterogeneities in the system occur over a length scale $\approx L$, then it follows that the currents $J(x,t)$ and $J(x+\mathrm{d}x,t)$ must be almost identical, with differences of order $\approx (\mathrm{d}x/L) \underset{L\to\infty}{\to} 0$. In the

continuum limit:

$$\partial_t \rho = -\partial_x J. \tag{5.2}$$

This constitutes a conservation equation: the time derivative of ρ is proportional to a gradient. Since typical variations in the system occur over a length scale L, we deduce that $\partial_x J \approx (J/L) \propto L^{-1} \underset{L\to\infty}{\to} 0$. Combining this result with Eq. (5.2), we find that the time derivative $\partial_t \rho$ goes to zero in the limit of large systems. In other words, the relaxation of ρ become very slow in this limit only by virtue of ρ being conserved, regardless of the microscopic nature of the quantity ρ. Indeed, one tenet of generalized hydrodynamics is that for each conserved quantity in the system there must be one hydrodynamic relaxation time scale.

The next step in building our hydrodynamic theory is to find an expression for J. We assume that the system is weakly perturbed from a homogeneous profile of ρ, namely $\rho(x,t) = \rho_0 + \delta\rho(x,t)$ with $\delta\rho$ small, and build the expression of J on general grounds regardless of any microscopic considerations. In our simple setting, J is entirely determined by the spatial profile of $\delta\rho$. Assuming as discussed above that gradients are small, we perform an expansion in powers of the gradient (remembering that each gradient is of order L^{-1}, and therefore small):

$$\begin{aligned} J = \alpha^{(0,0)} &+ \alpha^{(0,1)}\delta\rho + \alpha^{(0,2)}\delta\rho^2 + \alpha^{(0,3)}\delta\rho^3 + \dots \\ &+ \alpha^{(1,1)}\partial_x\delta\rho + \dots \\ &+ \alpha^{(2,1)}\partial_x^2\delta\rho + \dots \\ &+ \dots \end{aligned} \tag{5.3}$$

In this equation the first line groups the terms with zero gradients, the second those with one gradient etc.. Each line has several terms corresponding to a Taylor expansion in increasing powers of the small quantity $\delta\rho$. Thus the constant coefficient $\alpha^{(i,j)}$ is associated with a term with i gradients that is additionally of order j in $\delta\rho$. This double expansion in powers of the gradient *and* of the deviation from the reference state is a generic feature of hydrodynamic theories.

The evolution equation for $\delta\rho$ is obtained by inserting Eq. (5.3) into Eq. (5.2):

$$\begin{aligned} \partial_t\delta\rho = &- \alpha^{(0,1)}\partial_x\delta\rho - \alpha^{(0,2)}\partial_x(\delta\rho^2) - \dots \\ &- \alpha^{(1,1)}\partial_x^2\delta\rho - \dots \\ &- \dots \end{aligned} \tag{5.4}$$

Of the many terms of this equation, some violate the physical symmetries of the problem, implying that the associated α-coefficients are zero. Our diffusing system is thus left-right symmetric, implying that Eq. (5.4) must be invariant under the transformation $(\delta\rho, x, t) \to (\delta\rho', x', t')$, where

$$\delta\rho' = \delta\rho, \qquad x' = -x \qquad \text{and} \qquad t' = t. \tag{5.5}$$

In other words, the evolution equation for the reversed system characterized by the coordinates $(\delta\rho', x', t')$ must be exactly the same as Eq. (5.4), which describes the evolution in the original coordinate $(\delta\rho, x, t)$. This new equation thus reads

$$\partial_{t'}\delta\rho' = -\alpha^{(0,1)}\partial_{x'}\delta\rho' - \alpha^{(0,2)}\partial_{x'}[(\delta\rho')^2] - \alpha^{(1,1)}\partial_{x'}^2\delta\rho' - \dots \tag{5.6}$$

Using the change of variable Eq. (5.5) into this equation, we find

$$\partial_t\delta\rho = \alpha^{(0,1)}\partial_x\delta\rho + \alpha^{(0,2)}\partial_x[\delta\rho^2] - \alpha^{(1,1)}\partial_x^2\delta\rho - \dots, \tag{5.7}$$

and we subtract Eq. (5.7) from Eq. (5.4) to find

$$\forall\{\delta\rho(x)\} \qquad \partial_x\left[\alpha^{(0,1)}\delta\rho + \alpha^{(0,2)}(\delta\rho^2)\right] = 0, \tag{5.8}$$

which can only be achieved if $\alpha^{(0,1)} = 0$ and $\alpha^{(0,2)} = 0$.

To lowest remaining order in both ∂_x and $\delta\rho$, the remaining evolution equation is thus

$$\partial_t\rho = D\partial_x^2\rho, \tag{5.9}$$

where $D = -\alpha^{(1,1)}$. Of course Eq. (5.9) is nothing more than the simple diffusion equation, but is is worth noting that its form can be derived without any physical input beyond the specification of the symmetries of the system. We make an extensive use of these ideas in this chapters, and discuss how such equations differ in systems that are active *vs.* systems that are not.

5.2 Tumor necrotic core

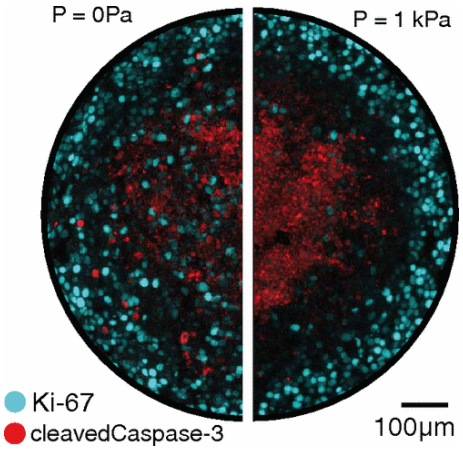

Since they do not make a reference to any specific microscopic physics, hydrodynamic theories can be applied to whole tissues made of cells as well as to the cytoskeleton. For our first, simplest model we thus model a cancerous tumor. Specifically, we discuss why a tumor that is not perfused with blood vessels can only reach a certain maximum size. The basic mechanism at play can be discerned by looking at the illustration, reproduced from Ref. [13], where the sites of cell divisions are marked in blue, while cell death is highlighted in red (the two sides of the figure correspond to tumors grown under different osmotic pressures). As diffusing food is more available to cells at the periphery than to those those on the inside, the tumor grows until the rate of cell death in its bulk balances the rate of cell birth at its surface. Then a nonequilibrum stationary state settles in, where cells that are born at the surface of the tumor flow inwards to replace their dead brethren and finally meet their fate in the central region, known as the "necrotic core" of the tumor. In a later stage of development, which we do not discuss here, the tumor tricks the body into growing new blood vessels to supply it with food throughout. This process, which allows it to grow further, is known as angiogenesis.

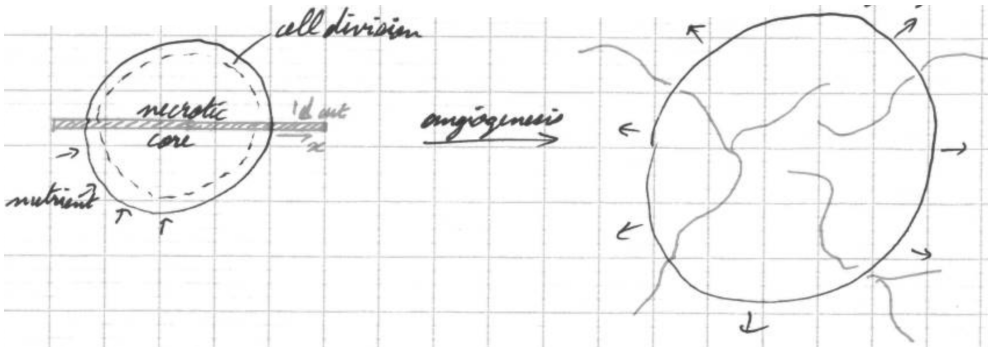

Here we model the steady-state balance between cell division and cell death that precedes angiogenesis. We consider a one-dimensional system, as illustrated on the left-hand-side of the figure above. While this simplification leaves out some of the geometry of the problem, it still allows us to illustrate the basic mechanism at play.

Building the theory

A full hydrodynamic description of our one-dimensional tissue must include its two conserved quantities: the cell density $\rho(x,t) = \rho_0 + \delta\rho(x,t)$, and the momentum density $p(x,t)$. The latter quantity is conserved if the bulk of the tumor is not subjected to any external forces. Indeed, Newton's second law means the exertion of a force from an object to another is equivalent to a transfer of momentum. Considering for a minute a tumor in dimension larger than one, the corresponding conservation equations read

$$\partial_t \delta\rho = -\nabla_i J_i \tag{5.10a}$$
$$\partial_t p_i = -\nabla_j(-\sigma_{ij}). \tag{5.10b}$$

Here the vector $\mathbf{J}$ is the mass current, as in Eq. (5.2). The momentum density $\mathbf{p}$ is also a vector, and therefore its current, which we denote by $(-\sigma)$ above, is a tensor of rank 2. More generally, the current associated with a conserved quantity has a tensorial rank that is one more than the rank of the conserved quantity. Recalling Newton's second law, we recognize that the left-hand-side of Eq. (5.10b) is simply the inertial term of Newton's second law[1], while we recognize from Eq. (3.7) that its right-hand side is the force per unit volume due to the stresses internal to the material. The conservation equation for the momentum density is thus nothing but the force balance equation, and the momentum current is the opposite of the stress tensor σ defined in Chapter 3.

Simplifying from this high-dimensional theory, we now specialize Eqs. (5.10) to their one-dimensional version, yielding

[1] This is not completely accurate as the current theory uses a Eulerian point of view. A more careful discussion would be required to properly take into account the associated convective terms. We however leave it aside here, as these terms are negligible in practice in our (overdamped) example.

$$\partial_t \delta\rho = -\partial_x J \tag{5.11a}$$
$$\partial_t p = \partial_x \sigma. \tag{5.11b}$$

The currents J and $-\sigma$ generically depend on $\delta\rho$ and p, and our next step is to explore this dependence. Had we considered the tumor as a three-dimensional elastic medium, the strain tensor γ would have played a role somewhat akin to that of a conserved quantity. Then the approach used in Eq. (5.3) would have prompted us to write the current (the stress tensor σ) as the most general expansion of the "conserved quantity" (the strain tensor γ). To linear order, this operation is rigorously identical to Eq. (3.9). To complete the demonstration that linear elasticity is but a special case of generalized hydrodynamics, we note that the symmetry considerations Eq. (3.16) are exactly parallel to those developed in Sec. (5.1), and to those that we are about to tackle in the case of the tumor. In one dimension however, these subtleties are unnecessary as the state of deformation of the medium is entirely characterized by its local density ρ. The most general expansion to linear order in $\delta\rho$ and p thus reads

$$J = \alpha_{\rho\rho}\delta\rho + \beta_{\rho\rho}\partial_x\delta\rho + \alpha_{\rho p}p + \beta_{\rho p}\partial_x p + \dots \tag{5.12a}$$
$$\sigma = \alpha_{p\rho}\delta\rho + \beta_{p\rho}\partial_x\delta\rho + \alpha_{pp}p + \beta_{pp}\partial_x p + \dots \tag{5.12b}$$

Note that while the $\alpha_{p\rho}$ term couples the stress to the density as is expected for a fluid with a finite compressibility, our more general hydrodynamic approach dictates that σ also depends on the velocity profile of the fluid through p (indeed $p = \rho v$). In other words, the so-called flux-force relations Eqs. 5.12 account for both elastic and viscous effects.

The next step in the hydrodynamic approach is to remove those couplings present in Eqs. 5.12 that violate the symmetries of the system. Specifically, the invariance under mirror symmetry $(x, \delta\rho, p) \to (-x, \delta\rho, -p)$ implies $\alpha_{\rho\rho} = 0$, $\beta_{\rho p} = 0$, $\beta_{p\rho} = 0$ and $\alpha_p p = 0$. Keeping only the remaining terms that are lowest order in gradient and defining $\chi = -\alpha_{p\rho}$, we insert the flux-force relations Eqs. (5.12) into the conservation equations Eqs. (5.11) to obtain

$$\partial_t \delta\rho = -\alpha_{\rho p}\partial_x p \tag{5.13a}$$
$$\partial_t p = -\partial_x(\chi\delta\rho). \tag{5.13b}$$

Since our tumor is not bound to a substrate, it also obeys another symmetry, namely Galilean invariance. The evolution equations in the inertial coordinates $x' = x - Ut$, $t' = t$, $\rho' = \rho$, $p' = p - \rho U$, where U is an arbitrary constant velocity, must thus be identical to Eqs. (5.13). In particular, mass conservation in the new coordinates reads

$$\partial_{t'}\delta\rho' = -\alpha_{\rho p}\partial_{x'}p' \Leftrightarrow \partial_t\delta\rho + U\partial_x\rho = -\alpha_{\rho p}\partial_x p + \alpha_{\rho p}U\partial_x\rho. \tag{5.14}$$

Subtracting this equation from Eq. (5.13a) yields $\alpha_{\rho p} = 1$. Defining the tissue pressure as $\mathcal{P} = \chi\delta\rho$ (pressure is defined up to a constant in this problem, allowing us to set $\mathcal{P} = 0$ when $\delta\rho = 0$), we thus find

$$\partial_t \delta\rho = -\partial_x p \tag{5.15a}$$
$$\partial_t p = -\partial_x \mathcal{P}. \tag{5.15b}$$

Equations (5.15) form the proper hydrodynamic theory for a tissue with conserved mass and momentum. It is identical to that for a *passive* (not active) one-dimensional, low-Reynolds number fluid with pressure (neglecting viscous effects, which are of higher order in gradient). To describe the active cell flow discussed above, we amend this description to include cell division and cell death, which introduces a nonequilibrium driving in the system. As a result of this modification, cell mass is no longer conserved. Our description is thus no longer strictly hydrodynamic but also includes time scales that scale as L^0 and thus become irrelevant in very large systems. This contrasts with the situation studied in the next section, where active terms are introduced in a way completely consistent with generalized hydrodynamics.

We assume that each cell divides with a constant rate k_{division} and undergoes apoptosis (programmed cell death) with a rate $k_{\text{apoptosis}}$. This results in an additional source term for the cell density:

$$(\partial_t\rho)^{\text{growth}} = k_{\text{division}}\rho - k_{\text{apoptosis}}\rho \tag{5.16}$$

Both these rates *a priori* depend on $\mathcal{P}$. Indeed, division may be more difficult in a crowded environment, or high mechanical stresses may favor cell death. We introduce the net cell birth rate $k(\mathcal{P}) = k_{\text{division}}(\mathcal{P}) - k_{\text{apoptosis}}(\mathcal{P})$. We furthermore assume the existence of a so-called homeostatic pressure, *i.e.*, a pressure at which division and apoptosis exactly compensate, leading to a cancellation of $k(\mathbf{P})$. Taylor expanding k for small deviations from this pressure as $k(\mathcal{P}) = -\kappa(\mathcal{P} - \mathcal{P}_h)$, we add the source term of Eq. (5.16) to Eqs. (5.15a) and write:

$$\partial_t\delta\rho = -\partial_x p + (\partial_t\rho)^{\text{growth}} = -\partial_x p - \kappa(\mathcal{P} - \mathcal{P}_h)\rho. \tag{5.17}$$

Therefore a stationary tumor state must obey

$$\partial_x p = -\kappa(\mathcal{P} - \mathcal{P}_h)\rho \tag{5.18a}$$

$$\partial_x \mathcal{P} = 0 \quad \text{with} \quad \mathcal{P} = \chi\delta\rho. \tag{5.18b}$$

Solving the tumor steady state

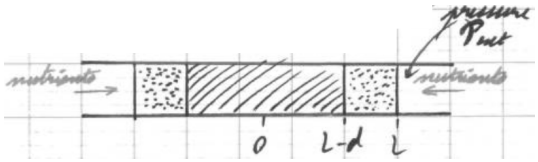

We consider a one-dimensional tumor with total length $2L$ spanning between $x = -L$ and $x = L$. The tumor is symmetric about $x = 0$, and so in the following we only consider the region of positive x. Nutrients diffuse into the tumor from its extremities. For simplicity we assume these nutrients diffuse into the tumor over a fixed distance d, implying that the outermost regions of the tumor (dotted in the illustration) are "well-fed", while the central region of the tumor (hatched) is "starved". This difference in supply of nutrients affects cell division and apoptosis, and so we assume that the two regions have different homeostatic pressures:

$$\mathcal{P}_h(x) = \begin{cases} \mathcal{P}_{h0} & \text{for } x < L - d \\ \mathcal{P}_{h0} + \Delta\mathcal{P}_h & \text{for } L - d < x < L \end{cases} \tag{5.19}$$

where $\Delta\mathcal{P}_h > 0$ characterizes the extent to which a well-fed tissue can grow against a larger opposing pressure than a starved one. We denote by $\mathcal{P}_{\text{ext}}$ the external pressure imposed by the tissue outside the tumor. According to Eq. (5.18b), stress balance on our system implies that the pressure is homogeneous, imposing $\mathcal{P} = \mathcal{P}_{\text{ext}}$ throughout. There are therefore three cases to consider. First, if $\mathcal{P}_{\text{ext}}$ is smaller than $\mathcal{P}_{h0}$, then both the well-fed and starved region of the tissue experience net growth, and therefore the tumor grows indefinitely. Second, if $\mathcal{P}_{\text{ext}} > \mathcal{P}_{h0} + \Delta\mathcal{P}_h$, both regions of the tumor always shrink and the tumor disappears. This is actually a frequent occurrence: most metastatic cells never succeed in growing into a full tumor after arresting into an organ. Third, if $\mathcal{P}_{h0} < \mathcal{P}_{\text{ext}} < \mathcal{P}_{h0} + \Delta\mathcal{P}_h$ then the well-fed region grows while the starved region shrinks, thus rendering a steady-state tumor possible. This is the situation encountered in the micrograph presented at the beginning of this section, and the one we focus on henceforth.

Considering only small variations of the tissue density for simplicity, we write $p = \rho v \simeq \rho_0 v$, where v is the local flow velocity, and expand Eq. (5.18a) to lowest order in $\delta\rho$ to find

$$\partial_x(\rho_0 v) = -\kappa(\mathcal{P}_{\text{ext}} - \mathcal{P}_h)\rho_0 \qquad \Leftrightarrow \qquad \partial_x v = -\kappa(\mathcal{P}_{\text{ext}} - \mathcal{P}_h). \tag{5.20}$$

In the starved region $0 < x < L - d$, this yields

$$\partial_x v = -\kappa(\mathcal{P}_{\text{ext}} - \mathcal{P}_{h0}) < 0 \qquad \Rightarrow \qquad v = -\kappa(\mathcal{P}_{\text{ext}} - \mathcal{P}_{h0})x, \tag{5.21}$$

where the integration constant is deduced from the symmetry-imposed boundary condition $v(0) = 0$. This velocity is negative, which manifests the dominance of apoptosis in the core of the tumor, which must be compensated by a constant influx of cells.

In the well-fed region $L - d < x < L$, we have

$$\partial_x v = -\kappa(\mathcal{P}_{\text{ext}} - \mathcal{P}_{h0} - \Delta\mathcal{P}_h) > 0 \qquad \Rightarrow \qquad v = -\kappa(\mathcal{P}_{\text{ext}} - \mathcal{P}_{h0})x + \kappa[x - (L - d)]\Delta\mathcal{P}_h, \tag{5.22}$$

where the integration constant is determined by imposing the continuity of the velocity in $x = L - d$.

To determine the size L of the steady-state tumor, we impose that its outer boundary is stationary, namely $v(L) = 0$. Imposing this condition in Eq. (5.22) yields

$$L = d\frac{\Delta\mathcal{P}_h}{\mathcal{P}_{\text{ext}} - \mathcal{P}_{h0}}. \tag{5.23}$$

Qualitatively, this equation shows that a better nutrient supply ($\Delta\mathcal{P}_h \nearrow$) makes the tumor grow, while an increasing pressure ($\mathcal{P}_{ext} \nearrow$) makes it shrink. More broadly, this example shows that active terms can induce steady-state flows in an otherwise simple fluid.

5.3 Instability in orientable fluids

Given the filamentous nature of the cytoskeleton, the patterns of local alignment of its constitutive fibers can play a major role in the forces that it exerts. To describe these effects, "active gel" theories have been developed by multiple authors over the past two decades to describe the emergence of collective cytoskeletal flows through the coupling between filament alignment and molecular-motor-induced active forces. Such flows are spectacularly manifested in the mesenchymal and amoeboidal modes of cell motility, which we illustrate below:

In both of these examples, the pattern of alignment and flow of the actin cytoskeleton (pictured by a collection of short black lines) drives the overall flow of the cellular medium, and ultimately the motion of the whole cell.

Here we consider a simple fluid cytoskeleton, which is appropriate if we aim to account for time scales much longer than the time required for its crosslinks to spontaneously detach; descriptions of the cytoskeleton as a solid are valid in the opposite limit. We consider a two-dimensional model on a substrate, reminiscent of the situation of the cell cortex (discussed in Sec. 1.6). We denote the two-dimensional position vector as $\mathbf{r}$, and assume that the system is invariant under both rotation and mirror symmetry.

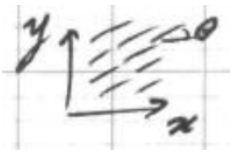

We characterize the local state of our fluid with two variables: the momentum density $\mathbf{p}(\mathbf{r},t)$ [or equivalently the local velocity $\mathbf{v}(\mathbf{r},t)$] and the local angle field $\theta(\mathbf{r},t)$. As shown in the illustration, the angle θ describes the local direction of alignment of the filaments relative to the x axis. While θ is not a conserved quantity *per se*, it must still be taken into account in a hydrodynamic theory. Indeed, the evolution equation for θ is of the form

$$\partial_t \theta = \dots \tag{5.24}$$

In general, the right-hand-side of this equation can depend on $\mathbf{v}$, θ and their derivatives. However, symmetry reveals that this dependence cannot involve a dependence in$\mathbf{v}$ or θ without derivatives. If it did, a homogeneous rotation would change the equations of motion, which is forbidden by isotropy. As a result θ depends only on gradients, and is therefore a hydrodynamic (slow-relaxing) variable in the same sense as the conserved quantity discussed in Eq. (5.1). Variables of this type are known as "broken-symmetry variables" and form the second class of variables that must be included in a hydrodynamic theory.

Building the model

In this section we present an alternative way of building active matter theories that does not emphasize the existence of conservation laws, but is based on similar symmetry considerations [14]. We thus use a gradient expansion and write the most general form for the evolution equation for θ:

$$\partial_t \theta = A_{ij} \nabla_i \nabla_j \theta + B_{ij} \nabla_i v_j, \tag{5.25}$$

where A_{ij} and B_{ij} are matrices of as yet unknown proportionality coefficients. Consistent with our previous discussion, this equation only includes gradient terms on its right-hand-side to respect isotropy and Galilean invariance. Additionally, the dependence in θ is only through terms that are second order in gradient, as first-order terms would violate the $\mathbf{r} \to -\mathbf{r}$ symmetry.

We now use two symmetries to restrict the range of possible coefficients A_{ij} and B_{ij}:

- We first consider the mirror symmetry with respect to the horizontal axis, namely under the operation $(\theta, x, y, v_x, v_y) \to (-\theta, x, -y, v_x, -v_y)$. To draw the consequences of this symmetry, one strategy consists in writing the evolution equation in the new coordinates θ', x' etc. similar to our approach in Eqs. (5.6) and (5.14), then compare the resulting equation to the original one. Here we instead employ a faster, equivalent one, which consists in considering which terms of Eq. (5.25) change sign under the transformation, and keep only the terms that pick up the same sign as the left-hand side. Since $\partial_t \theta \to -\partial_t \theta$, this implies that all terms on the right-hand-side which do not change sign much vanish. This yields:

$$A_{xy} = A_{yx} = 0 \quad \text{and} \quad B_{xx} = B_{yy} = 0. \tag{5.26}$$

- We next remark that going to a rotating frame, as if putting the system on a table spinning with a rotation rate Ω, should not change the form of the evolution equation. Such a transformation yields

$$x' = \cos(\Omega t)x - \sin(\Omega t)y \tag{5.27a}$$
$$y' = \sin(\Omega t)x + \cos(\Omega t)y \tag{5.27b}$$
$$v_x' = \cos(\Omega t)v_x - \sin(\Omega t)v_y - \Omega y' \tag{5.27c}$$
$$v_y' = \sin(\Omega t)v_x + \cos(\Omega t)v_y + \Omega x' \tag{5.27d}$$
$$\theta' = \theta + \Omega t. \tag{5.27e}$$

  We actually only need to consider the $t = 0$ case of this transformation, which leaves x and y invariant but yields

$$v_x' = v_x - \Omega y \tag{5.28a}$$
$$v_y' = v_y + \Omega x \tag{5.28b}$$
$$\partial_t\theta' = \partial_t\theta + \Omega. \tag{5.28c}$$

  Following the approach of Eqs. (5.6) and (5.14), we rewrite Eq. (5.4) for these new variables and use Eqs. (5.26) and (5.28) to find

$$\begin{aligned}\Omega + \partial_t\theta =& A_{xx}\nabla_x^2\theta + A_{yy}\nabla_y^2\theta \\ &+ B_{xy}\nabla_x(v_y + \Omega x) \\ &+ B_{yx}\nabla_y(v_x - \Omega_y).\end{aligned} \tag{5.29}$$

  Subtracting the original equation, this yields

$$\Omega = B_{xy}\Omega - B_{yx}\Omega \quad \Rightarrow \quad B_{xy} - B_{yx} = 1. \tag{5.30}$$

As a result of the application of these two symmetries, the general form of the θ evolution equation is

$$\partial_t\theta = A_{xx}\nabla_x^2\theta + A_{yy}\nabla_y^2\theta + \frac{1+\lambda}{2}\nabla_x v_y - \frac{1-\lambda}{2}\nabla_y v_x, \tag{5.31}$$

where A_{xx} and A_{yy} play the role of diffusion coefficients for the orientation field. If they are positive, they tend to make the orientation field more uniform, similar to the coupling constant of an XY model. This tendency for uniformity may in general depend on the value of θ. For instance, alignment may be faster in the direction parallel to the direction of alignment than perpendicular to it. In the following we disregard such effects and opt for a simplified model where $A_{xx} = A_{yy} = D$. Equation (5.31) involves another a priori unknown coefficient λ, which describes the behavior of the alignment vector in a shear flow. Depending on the sign of λ the particles may align parallel or perpendicular to the direction of shear, a preference that ultimately depends on the detailed shape of the particles. For the purposes of our simplified discussion we also ignore these effects, and set $\lambda = 0$ (no alignment). As a result of these simplifications, our angular evolution equation now reads

$$\partial_t\theta = D\Delta\theta + \frac{1}{2}\nabla_x v_y - \frac{1}{2}\nabla_y v_x. \tag{5.32}$$

We now consider the evolution equation for the second field describing our system, namely the momentum density $\mathbf{p}$. In contact with a substrate, the most general form for this equation to lowest admissible order in gradients is

$$\partial_t p_i = C_{ij}v_j + D_{ij}\nabla_j\theta, \tag{5.33}$$

where C_{ij} and D_{ij} are matrices of unknown coefficients.As discussed previously, this equation is the force balance equation of the system. The D_{ij} terms thus denote forces that depend on the configuration of the angle fields. Such forces violate time-reversal in a subtle way which we do not discuss here, and are therefore not allowed at equilibrium, and thus constitute the active terms which drive our system out of equilibrium. They involve a gradient, and as such they preserve the hydrodynamic character of $\mathbf{p}$. The C_{ij} terms have a more familiar origin: they are enabled by the presence of a substrate, which allows the system to break Galilean invariance and allows the existence of friction forces directly proportional to $\mathbf{v}$. Since these terms do not involve gradients, they deprive $\mathbf{p}$ of its hydrodynamic character. Had we chosen to derive our theory in the absence of a substrate, $\mathbf{p}$ would have retained its status as a conserved quantity and a hydrodynamic variable. We however retain the substrate in the following, leading to simpler calculations. Applying symmetries to Eq. (5.33) the same way we did Eq. (5.25), we find

$$\partial_t p_x = -\Gamma v_x - (\zeta_1 + \zeta_2)\nabla_y\theta \tag{5.34a}$$
$$\partial_t p_y = -\Gamma v_y - (\zeta_1 - \zeta_2)\nabla_x\theta, \tag{5.34b}$$

where we have simplified the generically anisotropic friction matrix to a single diffusion coefficient Γ in a similar way that we previously reduced matrix $\mathbf{A}$ to a single coefficient D. Equations. (5.34) however retain the full generality of the active θ-terms.

The active ζ terms describe active forces that stabilize or destabilize different perturbations to a homogeneously aligned state. Any such small perturbation can actually be decomposed into two basic types of deformations known as "splay", where the modulation of the direction of alignment is perpendicular to the alignment itself, and "bend", where it is parallel. As illustrated below, in a case where alignment is along the x direction, we can write the Fourier modes associated to either type of modulation as

$$\theta_{\text{splay}} = \theta_{\text{splay},0} \sin(qy) \tag{5.35a}$$

$$\theta_{\text{bend}} = \theta^b_{\text{bend},0} \sin(qx). \tag{5.35b}$$

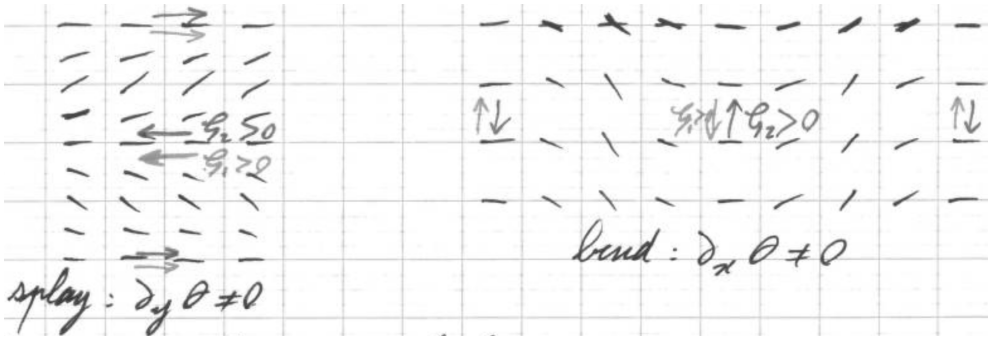

Noting that the second terms of the right-hand-sides of Eqs. (5.34) are respectively the x and y components of the active force density acting on the fluid, we find that the geometries illustrated above are respectively associated with the following active force densities:

$$\mathbf{f}_{\text{splay}} = -\zeta_1 q \cos(qy)\hat{\mathbf{x}} - \zeta_2 q \cos(qy)\hat{\mathbf{x}} \tag{5.36a}$$

$$\mathbf{f}_{\text{bend}} = -\zeta_1 q \cos(qx)\hat{\mathbf{y}} + \zeta_2 q \cos(qx)\hat{\mathbf{y}}. \tag{5.36b}$$

The arrows in the illustration above describe the direction of the fluid flow induced by each of these forces in the case of a positive ζ_1 and a positive ζ_2 (negative active coefficients are also allowed, resulting in forces in the opposite direction). This flow may tend to amplify the perturbation of the angle field, as in the case of $\zeta_1 > 0$ in the right-hand-side panel, or to make it smaller, as in the case of $\zeta_2 > 0$ in the same panel. While a positive ζ_2 is always uniformly stabilizing (and a negative one always destabilizing), ζ_1 always tends to destabilize either splay or bend deformations depending on its sign.

Stability analysis

We now consider a completely aligned state with $\theta_0(\mathbf{r}) = 0$, and discuss the evolution of a small perturbation $\delta\theta(\mathbf{r}, t)$ to that state. Considering an overdamped regime where the inertial terms $\partial_t \mathbf{p}$ of Eq. (5.34) are negligible, our equations of motion become in Fourier space

$$\partial_t \delta\tilde{\theta} = -Dq^2 \delta\tilde{\theta} + \frac{1}{2} i q_x \tilde{v}_y - \frac{1}{2} i q_y \tilde{v}_x \tag{5.37a}$$

$$\tilde{v}_x = -\frac{\zeta_1 + \zeta_2}{\Gamma} i q_y \delta\tilde{\theta} \tag{5.37b}$$

$$\tilde{v}_y = -\frac{\zeta_1 - \zeta_2}{\Gamma} i q_x \delta\tilde{\theta} \tag{5.37c}$$

where $\mathbf{q} = q_x\hat{\mathbf{x}} + q_y\hat{\mathbf{y}}$. Inserting Eqs. (5.37b) and (5.37c) into Eq. (5.37a), we find a closed-form equation for $\delta\tilde{\theta}$:

$$\partial_t \delta\tilde{\theta} = \underbrace{\left[-\left(D + \frac{\zeta_2}{2\Gamma} \right) q^2 + \frac{\zeta_1}{2\Gamma} \left(q_x^2 - q_y^2 \right) \right]}_{=\Lambda(\mathbf{q})} \delta\tilde{\theta}. \tag{5.38}$$

The solution of this equation simply reads

$$\delta\tilde{\theta}(\mathbf{q}, t) = \delta\tilde{\theta}(\mathbf{q}, t = 0) e^{\Lambda(\mathbf{q})t}, \tag{5.39}$$

where $\delta\tilde{\theta}(\mathbf{q}, t = 0)$ is the Fourier component of the initial perturbation associated with wavevector $\mathbf{q}$.

Equation (5.39) implies that all Fourier components with $\Lambda(\mathbf{q}) < 0$ tend to decay to zero, while those with a positive $\Lambda(\mathbf{q})$ diverge. The ordered state of the system is stable if *none* of the possible perturbations diverges, and unstable is *any* possible perturbation is divergent. Therefore stability requires $\forall \mathbf{q}\ \Lambda(\mathbf{q}) < 0$. Introducing the angle ϕ defined by $q_x = q\cos\phi$ and $q_y = q\sin\phi$, this is equivalent to demanding that the quantity

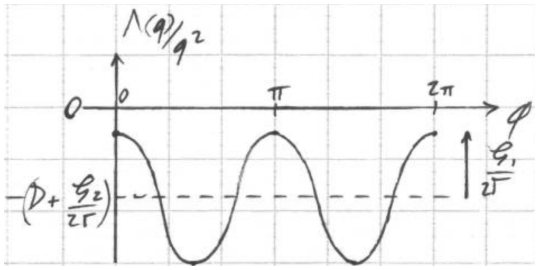

$$\frac{\Lambda(\mathbf{q})}{q^2} = -\left(D + \frac{\zeta_2}{2\Gamma}\right) + \frac{\zeta_1}{2\Gamma}\cos(2\phi) \tag{5.40}$$

is positive for all ϕ. This condition is presented graphically in the illustration, which makes it apparent that the active coefficient ζ_1 has an anisotropic effect. The system is stable if and only if the sinusoid always remains below zero, which is equivalent to the condition

$$\left|\frac{\zeta_1}{2\Gamma}\right| < D + \frac{\zeta_2}{2\Gamma}. \tag{5.41}$$

The resulting stability diagram for the system is shown below:

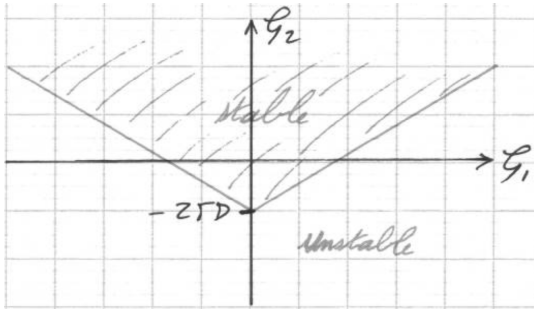

This diagram shows that nematic active systems are unstable in a wide range of parameters, which illustrates another oft-commented property of active systems. If the substrate is absent, additional symmetries impose $\zeta_2 = 0$, and the system is always unstable at large activity ($|\zeta_1| \to \infty$). This makes active nematic systems prone to a state of self-sustained flow that is observed experimentally and is associated with so-called "bacterial turbulence" and active microtubule systems (click links for videos), and could participate in cellular motion.

Appendices

Optional exercises

1. Find the steady-state radius of a three-dimensional tumor with spherical geometry.
2. Show using the invariance under a rotation of the system's axes of coordinates (*i.e.*, $x' = \cos\phi\, x - \sin\phi\, y$, $y' = \sin\phi\, x + \cos\phi\, y$ and $\theta' = \theta + \phi$ with ϕ a constant) that the right-hand-side of Eq. (5.24) can have neither terms that depend only on θ, nor terms directly proportional to the components of $\mathbf{v}$ without spatial derivatives.
3. Derive the symmetry results Eq. (5.26) with the approach of Eqs. (5.6) and (5.14).
4. Derive Eqs. (5.34) from Eq. (5.33) using symmetry considerations.
5. Compute the active force densities in the right-hand-side of Eqs. (5.34) to first order in ϵ for the two following distortions of the alignment field: $\theta = \epsilon \sin qx$ and $\theta = \epsilon \sin qy$. Associate each of these two configurations with either one of the panels of the figure that follows Eqs. (5.34) and use them to justify the directions of the arrows in that figure.
6. (difficult) Rederive Eqs. (5.34) in the absence of a substrate and in the presence of Galilean invariance. What is now the lowest order in gradient of the $\mathbf{v}$ terms on the right-hand-side? Show that $\zeta_2 = 0$ as discussed at the end of Sec. (5.3). Conclude on the stability of the momentum-conserving active fluid.

Learning goals for this chapter

- Be able to explain why hydrodynamic theories need only consider a small number of variables, namely conserved or broken symmetry variables.
- Be able to explain why a conserved quantity generally relaxes on hydrodynamic time scales.
- Be able to rederive a simple hydrodynamic theory (*e.g.*, that of Sec. 5.1) without help.
- Be able to write a generic small-gradient and small-deviation expansion, *e.g.*, for the current associated with a conserved quantity
- Be able to use the type of symmetries detailed in this chapter to simplify such an expression
- Be able to perform the stability analysis at the end of Sec. 5.3.
- Be able to explain why the stability of the system requires $\forall \mathbf{q}\ \Lambda(\mathbf{q}) < 0$.

Chapter 6

Membranes

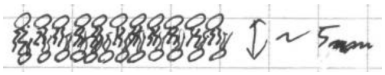

Membranes in cells are bilayers of phospholipids, with two hydrophobic tails and a hydrophillic head. They tuck their tails together away from the solvent to form impermeable membranes that are almost inextensible in their lateral direction. Within the plane of the membrane, lipids diffuse freely in most cases, making it a two-dimensional liquid. However out-of-plane deformations open gaps between the hydrophillic heads and expose the hydrophobic tails to the surrounding aqueous solvent, costing free energy. As a result such deformations are described by an elastic (free) energy, making biological membranes an interesting mixture of liquid and solid-like behavior.

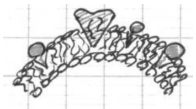

Different types of lipids may have different head-to-tail size ratios, and wedge-shaped proteins may insert into the membrane. Both of these effects may impart a curvature on the membrane, as shown in the illustration.

In this last chapter, we leave behind nucleic acids, proteins, and carbohydrates and consider the last of the four broad families of molecules introduced in Chapter 1, namely lipids and the membranes they form. In Sec. 6.1, we use symmetry considerations to derive a framework for the elasticity of these membranes. We then apply it to a few simple and experimentally relevant geometries in Sec. 6.2, including in situations involving curvature-inducing proteins. Tutorial 3 then extends these purely mechanical descriptions to introduce thermal fluctuations and consider a simple example of the ubiquitous interactions between membrane and cytoskeletal filaments.

6.1 Mechanical description

On length scales much larger than their thickness, membranes can be described as two-dimensional manifolds embedded in a fluid. Here we investigate their energy as a function of their shape.

Helfrich Hamiltonian

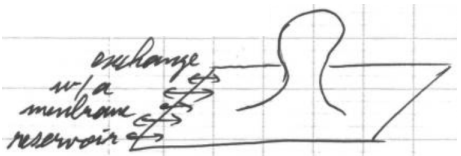

We consider a deforming patch of membrane, maybe one that evaginates to becomes a transport intermediate of the type of the vesicles shown in the movies of Sec. 1.6. This small patch is in contact with the rest of the cell's membrane, which acts as a membrane reservoir. As the membrane is almost unstretchable, changing the total area of membrane in the region we consider requires importing more membrane from this reservoir, much like a grand canonical gas must pay a chemical potential cost to import an additional particle from a chemical reservoir. This cost reads

$$H_\sigma = \sigma A, \tag{6.1}$$

where σ is the "membrane tension", *i.e.* the import cost of one unit of membrane area. This membrane tension has units of $\mathrm{J}\cdot\mathrm{m}^{-2}$, or equivalently of $\mathrm{N}\cdot\mathrm{m}^{-1}$. In cells it is of order $\sigma \simeq 10^{-4}\,\mathrm{N}\cdot\mathrm{m}^{-1}$. An alternative interpretation of its physical meaning is that σ is the force per unit length required to maintain the area of a membrane patch constant, much like the pressure is the force per unit surface that must be applied to a gas to keep its volume constant.

This area cost is not the only one involved in deforming the membrane. As discussed at the beginning of the chapter, bending the membrane also increases it energy. The local bending geometry of a membrane is characterized by its two principal radii of curvature R_1 and R_2, or equivalently by the associated curvatures $c_1 = 1/R_1$ and $c_2 = 1/R_2$. Optional exercise 2 at the end of this chapter discussed principal curvatures in more detail . For small curvatures, the free energy is of order 2 in the curvature and takes the following form, also known as the Helfrich Hamiltonian:

$$H_\kappa = \int \left[\frac{\kappa}{2}(c_1 + c_2)^2 + \frac{\kappa_G}{2} c_1 c_2\right] \mathrm{d}A, \tag{6.2}$$

where the integral runs over the area of the membrane. Here $C = c_1 + c_2$ is the total curvature of the membrane, and $C_G = c_1 c_2$ is its Gaussian curvature. As shown in the illustration, C_G is positive for a sphere, vanishes for a cylinder and is negative in a saddle geometry. The elastic constants κ and κ_G are known as the membrane's bending modulus and Gaussian curvature modulus. A reasonable order of magnitude for the former is $\kappa \simeq 20 k_B T$; the value and even the sign of the latter is much more debated, for reasons that become clearer below. The form of Eq. (6.2) stems from a symmetry argument, as further discussed in the following.

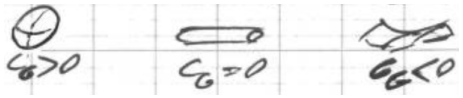

The Gauss-Bonnet theorem

Before we justify the form of Eq. (6.2), we briefly dwell on a mathematical property that has important implications in evaluating the membrane's energy. This theorem states that for a closed surface, the quantity

$$\oint C_G \, \mathrm{d}A = 2\pi\chi \tag{6.3}$$

is a *topological* invariant of the surface. In this equation, χ can be expressed as $\chi = 2 - 2g$, where g is the genus of the surface. As illustrated below, the genus can be understood as the number of handles of a closed surface:

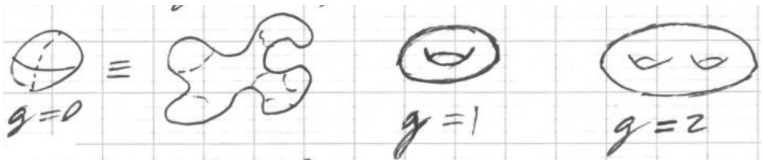

The leftmost panel of this figure shows two surfaces with genus 0, a sphere and a fingery structure. It emphasizes that the genus of a surface does not change as this structure is deformed as long as its surfaces do not cross or break: it is a topological quantity (more accurately, two homeomorphic manifolds have the same genus). The standard example of a surface with genus 1 is a donut, and each additional handle increases the genus of the surface.

For an open surface, $\oint C_G \, \mathrm{d}A$ is equal to a term computed at the boundary of the surface and involving its (geodesic) curvature. If the boundary is far away and not affected by the deformations of the membrane, this term can usually be considered constant.

Overall, as long as the genus of the membrane does not change and its boundary is far away, and assuming its Gaussian curvature modulus κ_G is constant over its surface, the Gauss-Bonnet theorem implies that the Gaussian curvature energy term of Eq. (6.2) is a constant. It can thus be disregarded when minimizing the energy of the surface.

The Monge gauge, and some symmetry considerations

For almost-planar membranes, it is convenient to parametrize the Helfrich Hamiltonian as a function of the vertical displacement $h(x, y)$ of the membrane away from the (x, y) plane, a representation known as the Monge gauge. The membrane energy takes the following form in general:

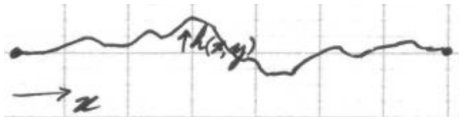

$$H = \iint f(h, \nabla_x h, \nabla_y h, \nabla_x \nabla_x h, \nabla_x \nabla_y h, \nabla_y \nabla_y h) \, \mathrm{d}x \, \mathrm{d}y, \tag{6.4}$$

where the form of the function f can be established either by expanding $H = H_\sigma + H_\kappa$ from Eqs. (6.1) and (6.2) for small h. Alternatively, it can be derived *de novo* from symmetry considerations. In the following we perform this derivation for the simple almost-flat membrane discussed here.

To establish the expression of the function f, we must first enforce the following symmetry constraints:

- H is invariant under an overall shift of h. Therefore H can only depend on h through its derivatives.
- H is invariant under the transformation $h \to -h$ because the membrane is up-down symmetric. Therefore the expansion of f in powers of h and its derivatives has only even powers.
- H is invariant under $(x, y) \to (-x, -y)$. Therefore the expansion only includes terms with even powers of ∇.

Finally, we only consider deformations over large length scales, *i.e.*, where the radius of curvature of the membrane is much larger than its thickness. As a result we perform an expansion in powers of ∇ and keep only the lowest-order terms. Given the constraints enumerated above, the double expansion in powers of h and of the gradient takes the form

$$H = \iint \left[a_{ij}(\nabla_i h)(\nabla_j h) + b_{ijkl}(\nabla_i \nabla_j h)(\nabla_k \nabla_l h)\right] \mathrm{d}x\, \mathrm{d}y. \tag{6.5}$$

In addition to the symmetries enumerated above, the Hamiltonian must be invariant under rotations in the (x, y) plane. As a result a_{ij} and b_{ijkl} have to be invariant under rotation. Recalling the results of chapter 3, we write the most general form for rank-two and rank-four two-dimensional isotropic tensors:

$$a_{ij} = a_1 \delta_{ij} + a_2 \epsilon_{ij} \tag{6.6a}$$

$$\begin{aligned} b_{ijkl} = {} & b_1 \delta_{ij}\delta_{kl} + b_2 \delta_{ij}\epsilon_{kl} + b_3 \epsilon_{ij}\delta_{kl} + b_4 \epsilon_{ij}\epsilon_{kl} \\ & + b_5 \delta_{ik}\delta_{jl} + b_6 \delta_{ik}\epsilon_{jl} + b_7 \epsilon_{ik}\delta_{jl} + b_8 \epsilon_{ik}\epsilon_{jl} \\ & + b_9 \delta_{il}\delta_{jk} + b_{10} \delta_{il}\epsilon_{jk} + b_{11} \epsilon_{il}\delta_{jk} + b_{12} \epsilon_{il}\epsilon_{jk}, \end{aligned} \tag{6.6b}$$

where

$$\delta = \begin{pmatrix} 1 & 0 \\ 0 & 1 \end{pmatrix} \qquad \text{and} \qquad \epsilon = \begin{pmatrix} 0 & 1 \\ -1 & 0 \end{pmatrix} \tag{6.7}$$

are the unit tensor and the fully antisymmetric tensor of rank 2, respectively. Here we deal with a two-dimensional problem, implying that there are two independent isotropic tensors of rank 2, namely δ and ϵ, in contrast with the three-dimensional case discussed in Chapter 3 (see optional exercise 3 of that chapter). The first corollary of this property is that Eq. (6.6a) has two terms. The second regards Eq. (6.6b). This equation is is similar to Eq. (3.16), in that it features all possible pairings of the four indices, one per line of its right-hand side. However while these pairings were only applied to δ in Eq. (3.16), here they must be applied to all possible combinations of δ and ϵ. Note that if the terms containing ϵ are omitted Eq. (6.6b) is equivalent to Eq. (3.16).

These complications are of little consequence for our broader discussion. Indeed, as when we insert the most general expressions of Eqs. (6.6) into Eq. (6.5), all instances of the antisymmetric tensor lead to a cancellation of terms, and term of order two in gradients reads

$$\iint a_1(\nabla_i h)(\nabla_i h)\, \mathrm{d}x\, \mathrm{d}y = \iint \frac{\sigma}{2}(\nabla h)^2\, \mathrm{d}x\, \mathrm{d}y, \tag{6.8}$$

where we have set $a = \sigma/2$. As the notation suggests, this terms is exactly the surface tension term of Eq. (6.1), as can be shown by writing the area element of the membrane as the Monge gauge

$$A = \iint \mathrm{d}A = \iint \sqrt{1 + (\nabla h)^2}\, \mathrm{d}x\, \mathrm{d}y \tag{6.9}$$

and expanding to order two in the small-slope ($|\nabla h| \ll 1$) limit. The term of order four in gradient features even more cancellation, yielding

$$\begin{aligned} & \iint \left[b_1(\nabla_i \nabla_i h)(\nabla_j \nabla_j h) + (b_2 + b_3)(\nabla_i \nabla_j h)(\nabla_i \nabla_j h)\right] \mathrm{d}x\, \mathrm{d}y \\ & \qquad = \text{boundary term} + \iint (b_1 + b_2 + b_3)(\nabla_i \nabla_i h)(\nabla_j \nabla_j h)\, \mathrm{d}x\, \mathrm{d}y = \text{boundary term} + \iint \frac{\kappa}{2} \Delta h^2\, \mathrm{d}x\, \mathrm{d}y. \end{aligned} \tag{6.10}$$

Here the first equality is obtained by integrating by part twice, and the second demonstrates the connection with Eq. (6.2) since the total curvature of the membrane $C = c_1 + c_2$ is equal to Δh to lowest order in h. Note that the Gaussian curvature term is hidden in the boundary term per the Gauss-Bonnet theorem, due to the fact that an almost-flat membrane clearly has a fixed topology.

Writing the Monge gauge membrane Hamiltonian for a perturbation of the form $h(\mathbf{r}) = \Re(h_0 e^{i\mathbf{q}\cdot\mathbf{r}})$ clearly shows that the Hamiltonian contains an intrinsic length scale:

$$H \propto \left(\frac{\kappa}{2} q^4 + \frac{\sigma}{2} q^2\right) |h_0|^2. \tag{6.11}$$

Clearly, for $q \gg \sqrt{\sigma/\kappa}$ (*i.e.* on small length scales) curvature dominates over tension, while for $q \ll \sqrt{\sigma/\kappa}$ (large length scales) tension dominates. In biological membranes, we typically have $\sqrt{\kappa/\sigma} \simeq$ 10-100 nm.

6.2 Noteworthy geometries

To gain a better intuition of the interplay between bending rigidity and tension, as well as their use in investigating membrane-protein interactions, we consider three configurations ubiquitous in the cell and in biophysical experiments.

Laplace law

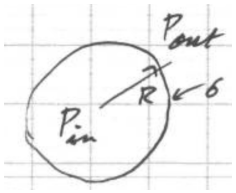

When a pressure (or osmotic pressure) difference $\Delta P = P_{\text{in}} - P_{\text{out}}$ is applied across a membrane, it adopts a spherical shape to establish a mechanical equilibrium. This is the same effect as the one responsible for the shape of soap bubbles. Considering a large bubble (radius $R \gg \sqrt{\kappa/\sigma}$), where only tension matters, the Laplace law gives the radius of the bubble. Its expression can be established by minimizing the energy of the bubble. Respectively denoting by V and A the volume and area of the bubble we get

$$E = -\Delta P \times V + \sigma A = -\frac{4\pi R^3}{3}\Delta P + 4\pi R^2. \tag{6.12}$$

Minimizing with respect to the bubble radius, we find $\Delta P R = 2\sigma$. Therefore the pressure difference is related to the membrane tension and total curvature $C = 2/R$ through

$$\Delta P = \sigma C. \tag{6.13}$$

Bare membrane tube

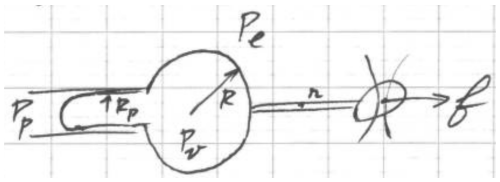

A handy and widely used geometry to determine the properties of a lipid membrane consists in forming a so-called giant unilamellar vesicle, a membrane sphere with a diameter of a few tens of micrometers. The operator then touches the vesicle with the tip of a thin, cylindrical glass micropipette with a radius R_p of the order of a few micrometers. They then start aspirating fluid through the micropipette. The vesicle is aspirated and partially pulled into the micropipette, and plugs it. Following this step, a mechanical equilibrium is reached where the membrane extends a stationary "tongue" into the pipette. The pressure P_e in the surrounding external medium and the pressure P_p in the pipette are held fixed (see the left hand side of the illustration). Once the vesicle is firmly held in the pipette, the operator moves a bead held in an optical tweezer (click for a description) into contact with the membrane. The bead is treated to stick to the membrane. As a result, when the operator subsequently moves it away from the vesicle, the membrane remains attached to it and a thin membrane tube or radius r and length L forms between the bead and the vesicle.

Here we explore the physics governing the radius of the tube, which results from a balance between the tension of the tube and its bending modulus. To understand where the tension comes from, we first look at the physics of the vesicle itself. Since this vesicle is much larger than $\sqrt{\kappa/\sigma}$, its shape can be accounted for by analyzing the balance between pressure and membrane tension only. To perform this analysis, we note that the considerations developed in the last section apply not only for a full spherical vesicle, but also to any membrane region subjected only to pressure and tension. We thus first apply them to the large spherical cap of radius R that sticks out of the pipette. Denoting by P_v the pressure inside the vesicle, Eq. (6.13) reads

$$P_v - P_e = \frac{2\sigma}{R}. \tag{6.14}$$

We also apply Laplace's law to the small spherical cap at the end of the membrane tongue, which has radius R_p:

$$P_v - P_p = \frac{2\sigma}{R_p}. \tag{6.15}$$

Combining these two equations to eliminate the experimentally inaccessible pressure P_v, we obtain

$$\sigma = \frac{P_e - P_p}{2(1/R_p - 1/R)}. \tag{6.16}$$

This equation implies that by changing the pressure difference $P_e - P_p$, the operator can directly set the membrane tension σ to the value of their choosing (R can be directly measured over the course of the experiment to determine the proportionality factor, and in practice varies little over its course).

We now take a closer look at the tube, which has the shape of a cylinder of radius r and length L. Its total curvature is therefore equal to $C = 1/r$. Considering the vesicle as a membrane reservoir imposing an almost-constant tension given by Eq. (6.16) and using Eqs. (6.1) and (6.2), the tube energy reads

$$H_{\text{tube}} = 2\pi r L \left(\frac{\kappa}{2r^2} + \sigma\right) - fL, \tag{6.17}$$

where the last term denotes the work of the force exerted by the optical tweezer. Minimizing this energy with respect to the tube radius yields

$$0 = -\frac{\pi\kappa L}{r^2} + 2\pi L\sigma \qquad \Rightarrow \qquad r = r_b = \sqrt{\frac{\kappa}{2\sigma}}, \tag{6.18}$$

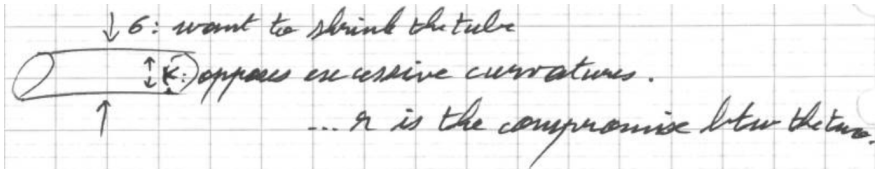

where the index b denotes a bare tube, as opposed to the protein-covered tube of the next subsection. This radius is of the order of the length scale discussed at the end of Sec. 6.1. This is easily understood from the physics of the tube: membrane tension tends to pull membrane area away from the tube and into the reservoir, reducing its radius. When the radius become too small, its curvature energy increases rapidly and prevents further shrinkage. The length scale at which these two effects balance each other is that set by the competition of tension and bending modulus.

Plugging the tube radius from Eq. (6.18) into Eq. (6.17) we find

$$H_{\text{tube}} = \left(2\pi\sqrt{2\kappa\sigma} - f\right) L. \tag{6.19}$$

If $2\pi\sqrt{2\kappa\sigma} - f$ is positive, then the minimum of this function is at $L = 0$. If it is negative, then it is at $L = \infty$. Therefore a finite length tube can only be obtained for

$$f = f_b = 2\pi\sqrt{2\kappa\sigma}, \tag{6.20}$$

and the pulling of the tube from the vesicle happens at constant force. For cell membranes, this force is of the order of 10 pN, on par with typical intracellular forces. Indeed, in many cases molecular motors as well as self-assembling protein constructs pull tubes inside the cell.

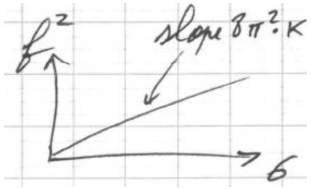

Equation Eq. (6.20) provides the operator with a convenient way to elucidate the characteristics of the membrane itself. Indeed standard optical tweezers setup are able to measure the deviation of the bead relative to the center of the optical trap. Provided we know the effective spring constant of the trap (which can be determined by measuring the amplitude of the thermal fluctuations inside the trap), this enables a measurement of the pulling force of the tube. Plotting the square of this force as a function of the membrane tension as shown in the illustration, one can thus read out the bending rigidity of the membrane from the slope of the resulting linear curve.

Tubes and proteins

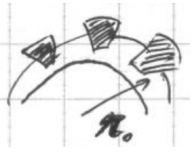

Measuring tube forces can actually yield much information not only about the membrane, but also about the objects that interact with it. Here we consider a simple case where a membrane inserts into the outer leaflet of the membrane, pushing the lipids aside and inducing a spontaneous curvature $C_0 = 1/r_0$, where the spontaneous radius of curvature r_0 is shown in the illustration. We are looking for an experimental protocol to measure this curvature.

In the presence of a spontaneous curvature, the total curvature term $C^2 = (c_1 + c_2)^2$ in the Helfrich Hamiltonian of Eq. (6.2) is replaced by $(C - C_0)^2$, and the energy of the membrane reads

$$H = \iint \left[\frac{\kappa}{2}(C - C_0)^2 + \sigma\right] \mathrm{d}A \tag{6.21}$$

and so the energy of a tube is given by

$$H = 2\pi r L \times \frac{\kappa}{2}\left(\frac{1}{r} - \frac{1}{r_0}\right)^2 + 2\pi r\sigma L - fL. \tag{6.22}$$

Minimizing with respect to r yields

$$r = \sqrt{\frac{\kappa}{2\sigma + \kappa/r_0^2}} \qquad \Rightarrow \qquad \frac{r}{r_b} = \frac{1}{\sqrt{1 + (r_b/r_0)^2}} \tag{6.23}$$

Inserting this expression into the Hamiltonian yields

$$H = \left\{ 2\pi \left[\sqrt{\kappa \left(2\sigma + \frac{\kappa}{r_0^2} \right)} - \frac{\kappa}{r_0} \right] - f \right\} L, \tag{6.24}$$

which as in Eq. (6.20) impose the force required to obtain a tube at mechanical equilibrium:

$$\frac{f}{f_b} = \sqrt{1 + x^{-2}} - x^{-1} \qquad \text{where} \qquad x = \frac{2\sigma r_0^2}{\kappa} \tag{6.25}$$

As shown in the illustration, this form implies that the ratio f/f_b starts to saturate when the tension reaches a typical value κ/r_0^2 corresponding to $x \approx 1$. By fitting Eq. (6.25) to the experimental data, we can precisely determine this value and thus characterize the nanometer-scale interaction between the protein and the membrane through micrometer-scale measurements. This basic strategy has been very successful in elucidating the mechanisms of many membrane-related processes, from the machinery involved in intracellular and extracellular transport to the action of the venom of some bee species and toxins linked to dysentery and cholera.

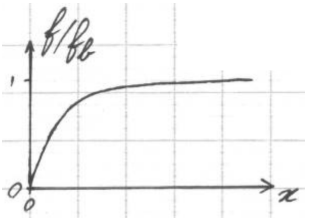

Appendices

Optional exercises

1. Rederive all the symmetry reasonings leading up to Eq. (6.5) with the methodology of Eqs. (5.6) and (5.14) (*i.e.*, writing the Hamiltonian with the primed coordinates, expressing these coordinates as a function of the original one, then subtracting the original Hamiltonian).

2. Compute the Gaussian curvature energy cost associated with cutting the neck of the evaginated structure shown just above Eq. (6.1). This operation turns a flat-ish membrane into a flat-ish membrane plus a closed vesicle.

3. Show that all terms in Eqs. (6.6) containing an ϵ are forbidden in a chiral membrane, *i.e.*, a membrane invariant under the $(x, y, h) \to (x, -y, h)$ transformation.

4. Consider a surface described in the Monge gauge by

$$h(\mathbf{r}) = \frac{1}{2}\mathbf{r}^T \cdot \mathbf{M} \cdot \mathbf{r}, \tag{6.26}$$

   where $\mathbf{M}$ is an arbitrary real symmetrical matrix. To identify the principal curvatures c_1 and c_2 of the membrane as written in Eq. (6.2), we have to identify an orthonormal basis of the horizontal plane with coordinates x', y' such that

$$h(\mathbf{r}) = \frac{c_1}{2}x'^2 + \frac{c_2}{2}y'^2 + \text{a polynomial of order 1 in } x',\, y'. \tag{6.27}$$

   Explain why this is always possible and relate the principal curvatures to the eigenvalues of $\mathbf{M}$. Conclude that the total and Gaussian curvature of the membrane can be expressed as functions of the rotational invariants of M, namely its trace and determinant. Remembering that any membrane shape can be locally Taylor-expanded as

$$h(\mathbf{r}_0 + \delta\mathbf{r}) = h(\mathbf{r}_0) + \partial_i h(\mathbf{r}_0)\delta r_i + \frac{1}{2}\partial_i\partial_j h(\mathbf{r}_0)\delta r_i \delta r_j + \mathcal{O}(\delta r^3), \tag{6.28}$$

   express the local total and Gaussian curvatures of the membrane as functions of the rotational invariants of the local Hessian matrix $\partial_i\partial_j h(\mathbf{r}_0)$.

5. Compute the modified Laplace law for a vesicle whose radius is close to $\sqrt{\kappa/\sigma}$. What is the equilibrium radius of a membrane sphere with tension σ and modulus κ but no pressure difference between the inside and the outside? Does this surprise you?

6. Revisit our discussion of the proteins and membrane tube mechanics for a protein that binds not only to the membrane tube, but also to the vesicle and tongue, thereby modifying the relationship between tension and pressure difference. Derive the new relationship between the tube force and the "apparent membrane tension" $\sigma_{\text{app}} = (P_e - P_p)/(2/R_p - 2/R)$. Do not forget that both R and R_p are much larger than r_b and r_0, or face significant complications.

Learning goals for this chapter

- Know the term"Helfrich Hamiltonian".
- Be able to write the general expression for the free energy of a membrane as a function of its area and curvature.
- Be able to compute this energy for simple membrane shapes.
- Be able to explain why the Gauss-Bonnet theorem often allows us to disregard the Gaussian curvature energy of a membrane. Be able to identify situations where this energy must be taken into account.
- Be able to derive Eq. (6.5) from symmetry considerations.
- Be able to write the free energy of a membrane in the Monge gauge.
- Be able to discuss the significance of the characteristic length scale $\sqrt{\kappa/\sigma}$.
- Be able to quote and rederive Laplace's law.
- Be able to explain the tube pulling setup studied in Sec. 6.2.
- Be able to derive the expression of the membrane tube radius and force in the absence of proteins and in simple membrane-protein interactions models.

Tutorial 3: Membrane-filament interactions

Physics of Complex Systems M2 – Biophysics

1 Membrane fluctuations

Here we consider a membrane whose average position is within the $z = 0$ plane. Let $u(\mathbf{r})$ be the vertical fluctuation of the membrane at a point with horizontal coordinates $\mathbf{r} = (x, y)$. The membrane does not have a spontaneous curvature, but is endowed with a bending modulus κ and a tension γ.

1.1 Write the Helfrich Hamiltonian $\mathcal{H}$ describing the energy of the membrane as the sum of a curvature energy and a tension energy. You may start by writing is as a surface integral involving the membrane's total curvature. Assuming a small membrane deformation, write $\mathcal{H}$ as an integral over the coordinates x, y that only involves κ, γ and the spatial derivatives of $u(\mathbf{r})$. Finally, express $\mathcal{H}$ in Fourier space, that is as a function of $\tilde{u}(\mathbf{q})$, the Fourier transform of $u(\mathbf{r})$. We will define the Fourier transform through:

$$u(\mathbf{r}) = \int \tilde{u}(\mathbf{q}) e^{i\mathbf{q}.\mathbf{r}} \frac{\mathrm{d}^2\mathbf{q}}{(2\pi)^2}, \quad \tilde{u}(\mathbf{q}) = \int u(\mathbf{r}) e^{-i\mathbf{q}.\mathbf{r}} \mathrm{d}^2\mathbf{r}. \tag{1}$$

1.2 Compute the mean square displacement in Fourier space $\langle \tilde{u}(\mathbf{q})\tilde{u}(\mathbf{q}')\rangle$. Deduce that the real-space mean-square displacement of the membrane fluctuations is $\delta^2 = \langle u(\mathbf{r})^2\rangle = \frac{kT}{4\pi\gamma} \ln \frac{q_{\min}^2 + q_c^2}{q_{\min}^2}$, where $q_{\min}$ is a small-wavevector cutoff that you will specify as a function of the system size, and q_c is to be expressed as a function of the parameters of the problem.

1.3 How does the mean square displacement δ^2 depend on the system size if the membrane tension is large? How about the $\gamma \to 0$ limit? Can you cite and experiment allowing to measure this amplitude?

2 Membrane going through a fixed point

2.1 We impose a fixed displacement $u(\mathbf{0}) = a$ on the membrane at the origin of coordinates $\mathbf{r} = \mathbf{0}$. Thus the membrane always goes through the point $(x = 0, y = 0, z = a)$. Explain why the partition function reads

$$Z_p = \int \mathcal{D}u[.]\delta(u(\mathbf{0}) - a) e^{-\mathcal{H}/kT}$$

where δ is a Dirac distribution. The symbol $\mathcal{D}u[.]$ indicates a sum over all possible states of the membrane, and thus over all possible fluctuations $u(\mathbf{r})$. In practice, this boils down to summing over all Fourier components $\tilde{u}(\mathbf{q})$. By replacing the Dirac delta by its Fourier transform $\delta(x) = \int_{-\infty}^{+\infty} e^{i\lambda x}\mathrm{d}\lambda/(2\pi)$, write the partition function as

$$Z_p = \int_{-\infty}^{+\infty} \frac{\mathrm{d}\lambda}{2\pi} \int \mathcal{D}\tilde{u}[.] \exp\left[\int \frac{\mathrm{d}^2\mathbf{q}}{(2\pi)^2}\left(-|\tilde{u}|^2 \frac{\kappa q^4 + \gamma q^2}{2kT} + i\lambda\tilde{u}\right)\right] e^{-i\lambda a}$$

Compute the Gaussian integrals over $\tilde{u}$ by going to discrete q modes and by pretending that $\tilde{u}$ is real. We recall that $\int_{-\infty}^{+\infty} e^{-\alpha x^2}\mathrm{d}x = \sqrt{\pi/\alpha}$. Deduce that

$$\begin{aligned} Z_p &= Z_0 \int_{-\infty}^{+\infty} \frac{\mathrm{d}\lambda}{2\pi} e^{-\frac{\lambda^2\delta^2}{2} - i\lambda a} \\ &= Z_0' \exp\left(-\frac{a^2}{2\delta^2}\right) \end{aligned}$$

where Z_0 and Z_0' are constants which we will not seek to determine.

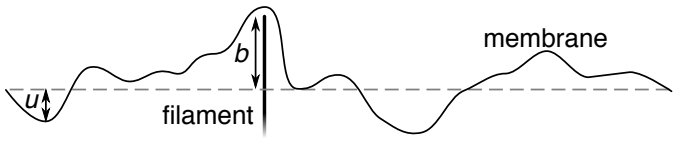

Figure 1: Illustration of the problem studied in Sec. 3.

2.2 Can you assign a physical meaning to Z_0'? What is the membrane's free energy under the constraint that we impose on it?

2.3 What force $f(a)$ must we impose on the membrane to impose a deformation of magnitude a at the location $\mathbf{r} = \mathbf{0}$?

3 Interaction between a filament and the membrane

We now study the interaction between the membrane and a filament—a microtubule for instance. The experiment is schematized in Fig. 1. The filament has a fixed length and is maintained at a constant position so that its tip is at an altitude b above the average plane of the membrane. The filament cannot go through the membrane.

3.1 Explain why the filament exerts a force on the membrane.

3.2 Show that if the filament is fixed, the membrane's partition function is $Z_f = \int_b^{+\infty} Z_p(a)\,\mathrm{d}a$. Compute the free energy of the membrane and the force exerted on the filament. We will introduce the function $\mathrm{erfc}(x) = \frac{2}{\sqrt{\pi}} \int_x^{+\infty} e^{-y^2} \mathrm{d}y$ which is such that $\mathrm{erfc}(0) = 1$ and that for large x we have $\mathrm{erfc(x)} \sim \frac{1}{\sqrt{\pi}x} e^{-x^2}$.

3.3 Compute an order of magnitude for the force at $b = 0$ if the tension is $\gamma = 5.10^{-5}$ N.m^{-1} and the bending modulus $\kappa = 20 k_B T$. We will assume that the membrane has a lateral size $L = 5\,\mu$m.

3.4 The filament is now a biological polymer regarded as fixed at its lower extremity. This filament grows through monomer addition at its upper tip. What are the three possible outcomes of such an experiment? Discuss the conditions under which each of them is observed. You are welcome to draw inspiration from the treatment of Ref. [1]; see also Fig. 2. We recall that when a rigid filament of length l is compressed, it buckles provided that the force is larger than the critical force $f_c = k_B T \ell_p \pi^2 / l^2$, where ℓ_p is its persistence length.

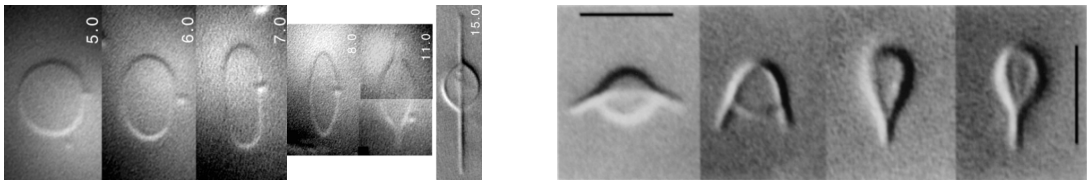

Figure 2: (left) A phospholipid vesicle deformed by 1 to 3 vertical microtubules. (right) Spontaneous buckling of microtubules inside a ϕ-shaped vesicle. In the final image, the microtubules are bent completely and continue to grow with both ends sheathed in a single membrane sleeve. Scale bar: 5 μm [2].

References

[1] D R Daniels, D Marenduzzo, and M S Turner. Stall, spiculate, or run away: The fate of fibers growing towards fluctuating membranes. *Phys. Rev. Lett.*, 97:098101, September 2006.

[2] Deborah Kuchnir Fygenson, John F. Marko, and Albert Libchaber. Mechanics of microtubule-based membrane extension. *Phys. Rev. Lett.*, 79(22):4497–4500, December 1997.

‘

References

[1] Bruce Alberts, Alexander Johnson, Julian Lewis, David Morgan, Martin Raff, Keith Roberts, and Peter Walter. *Molecular biology of the cell*. Garland Science, 6th edition, 2015.

[2] Rob Phillips, Jane Kondev, and Julie Theriot. *Physical Biology of the Cell*. Garland Science, New York, 2009.

[3] Ron Milo and Rob Phillips. *Cell biology by the numbers*. Garland Science, 2015.

[4] James C Maxwell. On the calculation of the equilibrium and stiffness of frames. *Philos. Mag.*, 27:294–299, 1864.

[5] S Feng, M F Thorpe, and E Garboczi. Effective-medium theory of percolation on central-force elastic networks. *Phys. Rev. B*, 31(1):276–280, January 1985.

[6] C R Calladine. Buckminster Fuller's "tensegrity" structures and Clerk Maxwell's rules for the construction of stiff frames. *Int. J. Solids Structures*, 14(2):161–172, 1978.

[7] Martin van Hecke. Jamming of soft particles: geometry, mechanics, scaling and isostaticity. *J. Phys.: Condens. Matter*, 22(3):033101, January 2010.

[8] C P Broedersz and F C MacKintosh. Modeling semiflexible polymer networks. *Rev. Mod. Phys.*, 86:995–1036, July-September 2014.

[9] Shlomo Alexander. Amorphous solids: their structure, lattice dynamics and elasticity. *Phys. Rep.-Rev. Sec. Phys. Lett.*, 296(2–4):65–236, March 1998.

[10] L D Landau and E M Lifshitz. *Theory of Elasticity*, volume 7 of *Course of Theoretical Physics*. Butterworth Heinemann, Oxford, third edition, 1986.

[11] Rutherford Aris. *Vectors, Tensors, and the Basic Equations of Fluid Mechanics*. Dover, New York, 1989.

[12] C S Peskin, G M Odell, and G F Oster. Cellular motions and thermal fluctuations: the brownian ratchet. *Biophys. J.*, 65(1):316–324, July 1993.

[13] Fabien Montel, Morgan Delarue, Jens Elgeti, Laurent Malaquin, Markus Basan, Thomas Risler, Bernard Cabane, Danijela Vignjevic, Jacques Prost, Giovanni Cappello, and Jean-François Joanny. Stress clamp experiments on multicellular tumor spheroids. *Phys. Rev. Lett.*, 107(18):188102, October 2011.

[14] M. C. Marchetti, J. F. Joanny, S. Ramaswamy, T. B. Liverpool, J. Prost, Madan Rao, and R. Aditi Simha. Hydrodynamics of soft active matter. *Rev. Mod. Phys.*, 85:1143, July 2013.